AD-A131 266 FORBIDDEN LINE RADIATION COOLING OF HIGH ALTITUDE PLASMAS(U) MISSION RESEARCH CORP SANTA BARBARA CA W W WHITE 19 FEB 82 MRC-R-687 DNA-6125T 1/2

UNCLASSIFIED DNA001-80-C-0096 F/G 18/3 NL

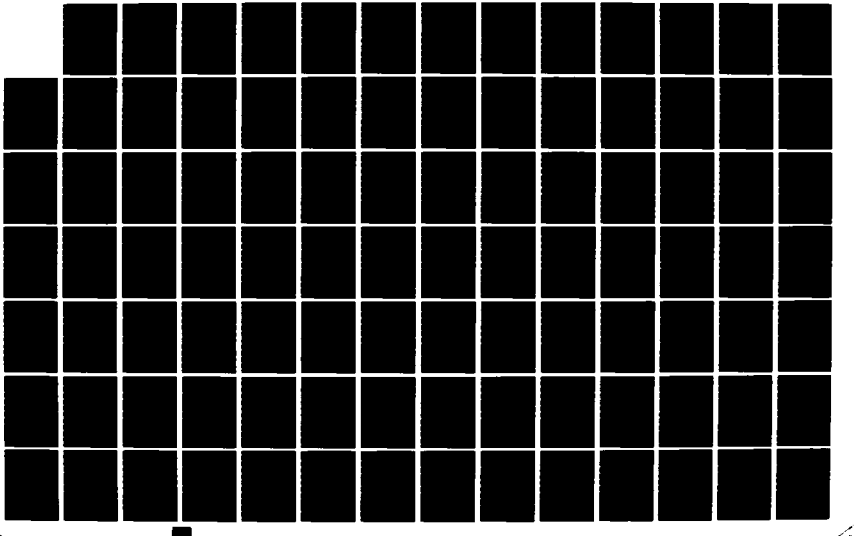

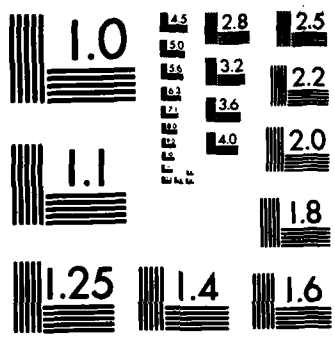

MICROCOPY RESOLUTION TEST CHART
NATIONAL BUREAU OF STANDARDS-1963-A

(12)

DNA 6125T

FORBIDDEN LINE RADIATION COOLING OF HIGH ALTITUDE PLASMAS

W. W. White
Mission Research Corporation
P.O. Drawer 719
Santa Barbara, California 93102

19 February 1982

Topical Report for Period 1 February 1981—1 February 1982

CONTRACT No. DNA 001-80-C-0096

THIS WORK WAS SPONSORED BY THE DEFENSE NUCLEAR AGENCY
UNDER RDT&E RMSS CODE B322081466 S99QAXHC00024 H2590D.

Prepared for
Director
DEFENSE NUCLEAR AGENCY
Washington, DC 20305

Destroy this report when it is no longer needed. Do not return to sender.

PLEASE NOTIFY THE DEFENSE NUCLEAR AGENCY, ATTN: STTI, WASHINGTON, D.C. 20305, IF YOUR ADDRESS IS INCORRECT, IF YOU WISH TO BE DELETED FROM THE DISTRIBUTION LIST, OR IF THE ADDRESSEE IS NO LONGER EMPLOYED BY YOUR ORGANIZATION.

UNCLASSIFIED

SECURITY CLASSIFICATION OF THIS PAGE *(When Data Entered)*

REPORT DOCUMENTATION PAGE	READ INSTRUCTIONS BEFORE COMPLETING FORM
1. REPORT NUMBER: DNA 6125T	2. GOVT ACCESSION NO.: AD-A131 266
3. RECIPIENT'S CATALOG NUMBER:	
4. TITLE *(and Subtitle)*: FORBIDDEN LINE RADIATION COOLING OF HIGH ALTITUDE PLASMAS	5. TYPE OF REPORT & PERIOD COVERED: Topical Report for Period 1 Feb 81—1 Feb 82
	6. PERFORMING ORG. REPORT NUMBER: MRC-R-687
7. AUTHOR(s): W. W. White	8. CONTRACT OR GRANT NUMBER(s): DNA 001-80-C-0096
9. PERFORMING ORGANIZATION NAME AND ADDRESS: Mission Research Corporation, P.O. Drawer 719, Santa Barbara, California 93102	10. PROGRAM ELEMENT, PROJECT, TASK AREA & WORK UNIT NUMBERS: Subtask S99QAXHC000-24
11. CONTROLLING OFFICE NAME AND ADDRESS: Director, Defense Nuclear Agency, Washington, DC 20305	12. REPORT DATE: 19 February 1982
	13. NUMBER OF PAGES: 112
14. MONITORING AGENCY NAME & ADDRESS*(if different from Controlling Office)*	15. SECURITY CLASS *(of this report)*: UNCLASSIFIED
	15a. DECLASSIFICATION/DOWNGRADING SCHEDULE: N/A since UNCLASSIFIED

16. DISTRIBUTION STATEMENT *(of this Report)*

Approved for public release; Distribution unlimited.

17. DISTRIBUTION STATEMENT *(of the abstract entered in Block 20, if different from Report)*

18. SUPPLEMENTARY NOTES

This work was sponsored by the Defense Nuclear Agency under RDT&E RMSS Code B322081466 S99QAXHC00024 H2590D.

19. KEY WORDS *(Continue on reverse side if necessary and identify by block number)*

High Altitude Nuclear Explosions
Metastable States
Forbidden Line Radiation
Ionospheric Plasma
Electron Impact Excitation

20. ABSTRACT *(Continue on reverse side if necessary and identify by block number)*

Time dependent rate equations describing electron impact excitation (and De-excitation) of and forbidden line radiation from ionospheric constituents have been integrated to obtain excited state population densities, radiation rates, ion and electron temperatures, and energy partitions as a function of time. Radiations from low-lying metastable states of oxygen and nitrogen ions, oxygen and nitrogen atoms, and molecular oxygen excited by electrons in the one eV energy range have been computed for plasma compositions characteristic of selected high altitude nuclear explosions.

DD FORM 1 JAN 73 1473 EDITION OF 1 NOV 65 IS OBSOLETE

UNCLASSIFIED

SECURITY CLASSIFICATION OF THIS PAGE *(When Data Entered)*

PREFACE

The author wishes to acknowledge helpful discussions and criticisms from D. H. Archer, F. E. Fajen, R. W. Kilb, and D. S. Sappenfield.

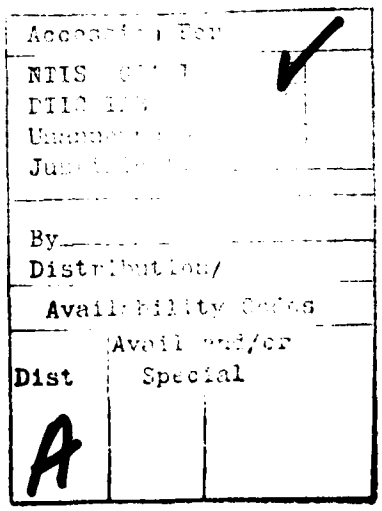

TABLE OF CONTENTS

LIST OF ILLUSTRATIONS

LIST OF ILLUSTRATIONS (Continued)

LIST OF TABLES

SECTION 1

INTRODUCTION

It is well known that optical emissions resulting from deposition of energy in the upper atmosphere by natural and man-made events (e.g., aurora and high altitude nuclear explosions) can serve as useful diagnostics to aid in understanding the detailed physics and chemistry which are operative. It is also well known that hot plasmas (temperatures of several eV to tens of eV or more) which are formed by nuclear explosions may cool quite effectively by emission of electromagnetic radiation via allowed electronic transitions. (Hydrodynamic expansion, of course, produces a great deal of cooling also.) However, once the temperature, or more precisely the electron temperature of such a plasma, has dropped to about an electron volt or so, electron impact excitation of atmospheric constituents effectively is limited to low lying electronic states (and vibrational states in molecules). For the dominant atmospheric species, these states are metastable, so "rapid" radiation cooling is shut off. At this point, interest in radiation as a plasma cooling mechanism traditionally has diminished quite rapidly, although spectroscopic interest remained strong.

The purpose of this paper is to illustrate that warm plasmas (~1 eV temperature) at high altitudes (where interactions with the neutral atmosphere are minimal) can rid themselves over a period of hours of considerable excess energy by forbidden radiation. Such slow but steady cooling turns out to be significant in the case of nuclear explosion produced plasma. In addition, the partition of energy between thermal and excited metastable states is explored.

Spectroscopic and other studies of emissions from the upper atmosphere have aided understanding of a variety of physical phenomena. For example, thermospheric temperatures and neutral winds have been inferred from Doppler measurements of OI 6300 A radiations [1-3], precipitating electron energetics in the auroral region have been deduced from airglows at ionospheric altitudes[4], and F-region plasma depletions[5] and propagating waves[6,7] have been observed by OI 6300 A emissions. A recent review of optical processes as they apply to the F-region, particularly at high latitudes, is available[8].

In the realm of nuclear weapons effects, optical phenomena induced by high altitude nuclear detonations have produced both dazzling displays and scientific diagnostic information. In 1962, a 1.4 megaton nuclear device (Starfish) was detonated at 400 km altitude near Johnston Island in the Pacific. As this was an announced test with both scientific and military objectives, numerous groups stationed equipment at a variety of locations across the Pacific. Spectroscopic observations[9,10] of optical radiation both immediately following and several minutes after detonation confirmed the presence of allowed and forbidden radiation from atmospheric species in the immediate vicinity of the burst point and in regions of optical activity ("artifical" aurora, etc.) well removed from the burst point. A review article by Hoerlin[11] contains color photos of Starfish which illustrate some of the striking optical features which produced the spectroscopic records of references 9 and 10.

This report attempts to provide reasonable estimates of radiation cooling processes which operate over extended periods (i.e., hours) in such high altitude plasmas. Forbidden radiations arising from radiative decay of low-lying metastable states of O^+, O, N^+, N, and O_2 have been computed under the assumption that the low-lying states have been populated by electron impact. Quenching of excited states by electron collisions has been included, but heavy particle quenching has been

ignored. Time dependent rate equations for the ground and excited states of the five emitting species have been numerically integrated to obtain self-consistent solutions free from assumptions of equilibrium excited state populations. Section 2 of the report describes the radiating systems of interest and presents the relevant equations. Section 3 contains the results of detailed calculations which span radiation periods of several hours, and Section 4 presents a discussion of results and some conclusions.

SECTION 2

RADIATION COOLING EQUATIONS

Each of the atmospheric species of interest here (O^+, O, N^+, N, and O_2) possesses a series of low-lying metastable states which can be populated by electron impact. These states are displayed schematically in Figure 1. In order to simplify the calculations a bit, each set of closely spaced (doublet or triplet) states, shown in the figure, has been lumped together into a composite state.† Thus, for the calculations described here, each of the species is modelled as a system with two excited states above the ground state.

These excited states can be populated (and de-populated) by collisions with electrons, processes for which the cross-sections seem to be reasonably well known. (Collisions with other particles also can alter excited state populations. More about this later.) For the present work, it has been assumed that radiation emitted from a plasma volume element is not reabsorbed and that the total radiation field is sufficiently weak that stimulated emission is insignificant. Under these conditions, the rate equations describing the excited state populations of a generic three level system are

$$\frac{dn_0}{dt} = -k_{01}n_0n_e - k_{02}n_0n_e + A_{10}n_1 + k_{10}n_1n_e + k_{20}n_2n_e + A_{20}n_2 \qquad (1)$$

---

† Present use of the word "state" is somewhat unprecise. In precise spectroscopic terminology, "levels" are being combined into "terms." See page 122 of E. U. Condon and G. H. Shortley, The Theory of Atomic Spectra, Cambridge University Press (1964).

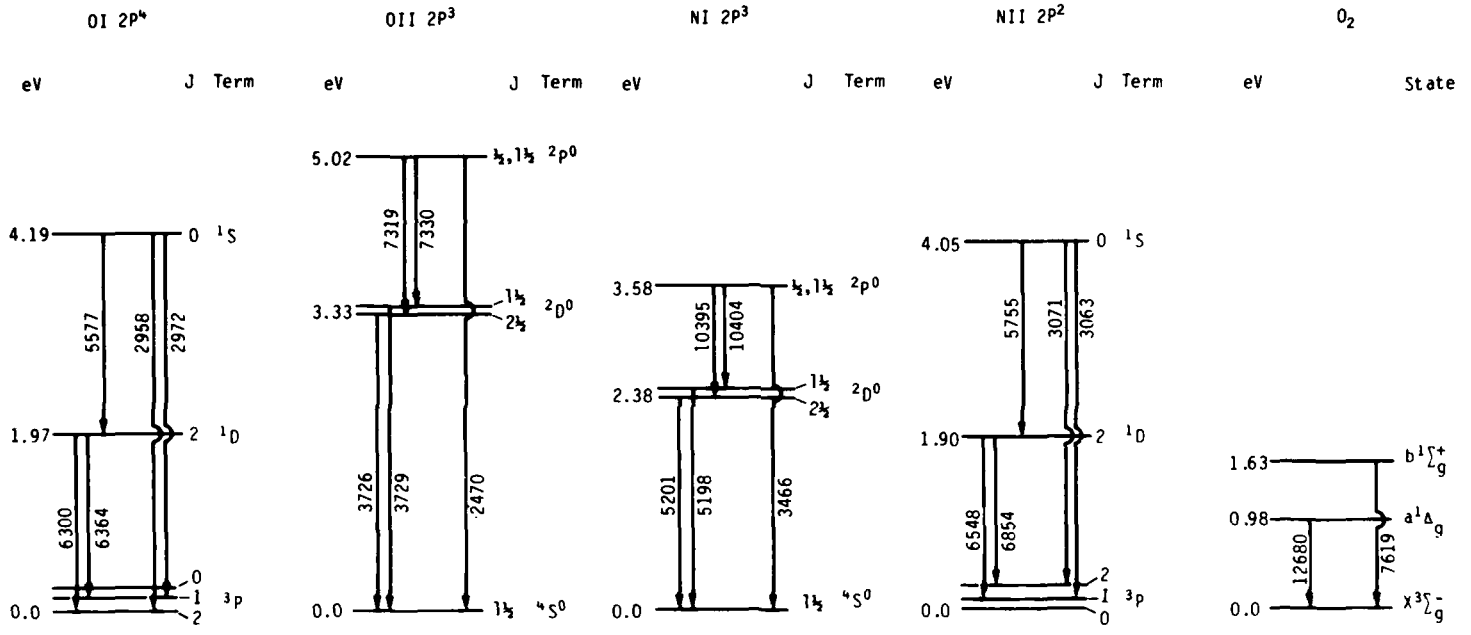

Figure 1. Schematic of metastable states of interest.

$$\frac{dn_1}{dt} = k_{01}n_0n_e - k_{10}n_1n_e - A_{10}n_1 + k_{21}n_2n_e - k_{12}n_1n_e + A_{21}n_2 \qquad (2)$$

$$\frac{dn_2}{dt} = k_{02}n_0n_e - k_{20}n_2n_e - A_{20}n_2 + k_{12}n_1n_e - k_{21}n_2n_e - A_{21}n_2 \qquad (3)$$

In this notation, k_{ij} is the collisional excitation (or deexcitation) rate coefficient from state i to state j, A_{ij} is the Einstein coefficient for spontaneous emission, n_i is the number density of particles in state i, and n_e is the electron density. The ground state, first excited state, and second excited state are denoted by subscripts 0, 1, and 2, respectively. Because photon absorption and stimulated emission are assumed insignificant in the present work, terms containing the Einstein B coefficient are absent from these rate equations.

The electron impact excitation and deexcitation rate coefficients used for O^+, O, N^+, and N were from Ali[12] and Ali, et al[13]. These coefficients were obtained by integrating cross-section data with an electron Boltzmann distribution. (Other rate coefficients or cross-sections that one might want to consider are available.)[14-16] Note that the excitation rate coefficient, k_{ij}, is related by detailed balance to the deexcitation rate coefficient, k_{ji}, by

$$g_i k_{ij} = g_j k_{ji} e^{-\Delta E_{ij}/kT} \qquad (4)$$

where the g's are statistical weights[17], ΔE_{ij} is the i-j energy level spacing, k is the Boltzmann constant, and T is the electron temperature.

Excitation rate coefficients for transitions from the ground state ($X^3\Sigma_g^-$) to the first excited ($a^1\Delta_g$) and second excited ($b^1\Sigma_g^+$) states of O_2 were computed by integrating excitation cross-sections multiplied by

electron velocity over a Boltzmann energy distribution:

$$k_{excit} = \frac{2}{m} \frac{2\pi}{(\pi kT)^{3/2}} \int_0^\infty E\, \sigma(E)\, e^{-E/kt} dE \tag{5}$$

where m is the electron mass. The cross section for ground to first excited state transitions was assumed to be

$$\sigma = 3.5 \times 10^{-14} \left(\frac{0.98}{E}\right)^3 \left[1-\left(\frac{0.98}{E}\right)^{0.1}\right]^3 + 8.0 \times 10^{-13} \left(\frac{2.2}{E}\right)^{2.5} \left[1-\left(\frac{2.2}{E}\right)^{0.05}\right]^3 \quad (cm^2) \tag{6}$$

The cross-section for ground to second excited state transitions was assumed to be

$$\sigma = 3.09 \times 10^{-17} \left(\frac{1.63}{E}\right)^{2.5} \left[1-\left(\frac{1.63}{E}\right)\right]^3 + 4.67 \times 10^{-16} \left(\frac{2.3}{E}\right)^{2.1398} \left[1-\left(\frac{2.3}{E}\right)^{0.4}\right]^3 \quad (cm^2) \tag{7}$$

In Equations 6 and 7, the energy, E, has units of electron volts. The square bracketed terms are to be interpreted as

$$\left[1-\frac{E_o}{E}\right] = \begin{cases} 1 - \frac{E_o}{E} & , E > E_o \\ 0 & , E < E_o \end{cases} \tag{8}$$

These cross sections are due to Archer[18] and result from his analytic fit to cross-section data of Trajmar, et al.[19] Deexcitation rate coefficients for these transitions were computed with the aid of Equation 4. Unfortunately, no suitable cross-sections or excitation rate coefficients for first to second excited state transitions appear to be available. Therefore, the rate coefficients for excitation and deexcitation through this transition are assumed to be zero.

The probabilities (Einstein A coefficients) used for radiative decay of the metastable states of O^+, O, N^+, and N are due to Wiese, et al[17]. The reader's attention is called to Appendix B of that publication wherein rules are given for combining transition probabilities for members of a multiplet into a composite transition probability. Transition probabilities for O_2 (0-0 band) are due to Bader, et al[20] ($a^1\Delta_g \rightarrow X^3\Sigma_g^-$ transition), and from the life time data assembled by McGowan, et al[2] ($b^1\Sigma_g^- \rightarrow X^3\Sigma_g^-$ transition).

Transition probabilities, statistical weights, etc., for the five systems of interest are summarized in Table 1. Electron impact excitation and deexcitation rate coefficients are summarized in the Appendix.

Once the excited state populations have been determined, the instantaneous radiation rates can be computed as the products of the state densities and the transition probabilities. Thus, the rate at which energy is lost from the plasma is obtained.

If electron thermal energy were the only energy reservoir to be tapped, then our model for radiation cooling would be reasonably complete. However, at the plasma densities of interest here, ion-electron collisions are sufficiently frequent to insure some measure of thermal energy transfer, with the result that radiation cooling indirectly removes at least some of the ion thermal energy. In order to compute this process, collisional heat transfer between ions and electrons was assumed to obey

$$\frac{\partial}{\partial t}\left(\frac{3}{2} N_e kT_e\right) = N_i N_e h_{ie}(kT_i - kT_e) \tag{9}$$

where

$$h_{ie} = 3.6 \times 10^{-9} (kT_e)^{-1.5} \quad cm^3/sec. \tag{10}$$

TABLE 1
TRANSITION PARAMETERS

Species	Transition	g_{upper}	g_{lower}	A(sec^{-1})	Approximate Transition Energy (eV)	λ(A)
O	$^1D \rightarrow {}^3P$	5	9	0.00677	1.96	6300 6364
	$^1S \rightarrow {}^3P$	1	9	0.0674	4.17	2958 2972
	$^1S \rightarrow {}^1D$	1	5	1.34	2.22	5577
O^+	$^2D^O \rightarrow {}^4S^O$	10	4	0.000097	3.33	3726 3729
	$^2P^O \rightarrow {}^4S^O$	6	4	0.0479	5.02	2470
	$^2P^O \rightarrow {}^2D^O$	6	10	0.173	1.69	7319 7330
N	$^2D^O \rightarrow {}^4S^O$	10	4	0.0000107	2.38	5198 5201
	$^2P^O \rightarrow {}^4S^O$	6	4	0.00496	3.58	3466
	$^2P^O \rightarrow {}^2D^O$	6	10	0.0790	1.19	10395 10404
N^+	$^1D \rightarrow {}^3P$	5	9	0.00407	1.89	6548 6584
	$^1S \rightarrow {}^3P$	1	9	0.0342	4.04	3063 3071
	$^1S \rightarrow {}^1D$	1	5	1.08	2.15	5755
O_2	$^1\Delta \rightarrow {}^3\Sigma$	2	3	0.000258	0.98	12680
	$^1\Sigma \rightarrow {}^3\Sigma$	1	3	0.085	1.63	7619

Here the subscripts refer to ions and electrons; the N's are number densities (cm^{-3}); kT_i and kT_e are in eV. The heat transfer coefficient, h_{ie}, is due to Kilb, Stagat, and Stoeckly[22].

In principle, ion-neutral, electron-neutral, and electron-vibrational mode (of neutral molecules) heat transfers also should be computed. Processes involving ion-neutral and electron-neutral collisions can be evaluated with the aid of heat transfer coefficients from reference 22. For the purpose of estimating relative rates, a 700°K Jacchia atmosphere[23] has been used. For altitudes above 200 km, electron-neutral heat transfer is negligible. In the 300 km altitude regime, and at the densities considered here, ion-neutral transfer roughly is on a par with ion-electron transfer. With increasing altitude, heat transfer involving neutrals diminishes as the neutral density decreases exponentially. Energy transfer between electrons and the vibrational modes of nitrogen molecules can be computed also. If we assume the vibrational state distribution can be characterized by a temperature T_v, then Equation 9 (with T_i replaced by T_v) can be used provided we adjust the rate coefficient. Thus, instead of h_{ie}, we have used an electron - N_2 vibrational modes heat transfer coefficient which is based on vibrational excitation cross sections due to Schulz.[24] This coefficient is

$$h_{ev} = 2.0 \times 10^{-10} (kT_e + 0.3) \exp(-0.3/kT_e) + 8.3 \times 10^{-9} (kT_e + 2.3) \exp(-x) \quad (cm^3/sec) \tag{11}$$

where

$$x = \begin{cases} -2.3/kT_e , & T_e > T_v \\ -2.0/kT_v , & T_e \leqslant T_v \end{cases} \tag{12}$$

with kT_e and kT_v in electron volts. One finds that below about 350 km (again using the neutral atmosphere of reference 13) electron - N_2 collisions can be quite significant.

For the present work, the effects of ion-electron heat transfer collisions as prescribed by Equations 9 and 10 have been included. The other collisional energy transfer processes have been ignored, in order to avoid undue complexity. It must be recognized that a complete calculation of a high altitude plasma must include hydrodynamics, chemistry, etc., processes which we are not prepared to include in the present work. We leave that to full blown nuclear burst simulation which should include radiation cooling equations and all the relevant energy transfer processes.

Electron impact collisions are not the only means by which metastable state populations may be changed. Excited state populations also can be altered (quenched) by collisions with heavy particles, but results of such collisions may depend strongly on the initial and final states of *the heavy particle.* Given the large variety of potential target particle state and quenching heavy particle state combinations which are possible, one should not be surprised that cross-section or rate coefficient data for heavy particle quenching are rather spotty and tend to be fairly uncertain. If one uses the limited set of quenching rate coefficients suggested by Gerard[8] or Ali, et al,[13] and a nominal neutral atmosphere,[23] and if one looks for the altitude above which radiative decay of a state exceeds heavy particle quenching, then one finds that the present calculations generally apply above 200-300 km altitude, the precise altitude depending on the particular excited species - quenchant combination.

For the present, heavy particle quenching has been ignored also. However, the lack of such quenching is consistent with the decision to ignore heat transfer processes which would tap the neutral thermal and N_2 vibrational energy pools. Quenching collisions involving neutrals would tend to return energy from the metastable states to neutral thermal where, by heat transfer, it could find its way back to the electrons.

SECTION 3

RESULTS

This section contains results from a systematic set of calculations which was designed to illustrate the behavior of the various three level metastable systems under circumstances representative of conditions in the ionosphere/magnetosphere following a high altitude nuclear burst. The results are divided into two categories; the first illustrates single species systems collisionally excited by electrons at densities of 10^4, 10^6, and 10^8 cm^{-3}. The second category represents calculations of multi-species systems based on conditions found in selected, detailed calculations of high altitude nuclear bursts.

Computational results are presented in four types of plots. The first type of plot shows ground and excited state population densities as a function of time. In most cases, the excited state densities remain less than a few percent of the total species density, so the ground state density curve usually appears as a horizontal line across the upper portion of this type of graph. The discerning eye, however, will find that the ground state curve is not simply a constant.

The second type of graph displays radiation cooling rates as a function of time. The third type of graph shows electron and ion temperatures as a function of time. At low ion and electron densities (10^4 cm^{-3}), one frequently finds that collisional thermal energy transfer is slow compared to collisional excitation and radiation, so the ion and electron temperatures can depart significantly from each other.

The relative partition between excited state and thermal energies as a function of time is contained in the fourth type of plot. This class of graph displays the ratio of energy tied up in excited states to available energy. The available energy is defined as the sum of excited state and electron thermal energies, plus ion thermal energy provided that thermal energy transfer (Equation 9) is included in the calculation. (Equation 9 was included in all but two cases which are noted.)

Because the objective of this report was to emphasize energy partition and radiation cooling over extended periods, most calculations covered an interval of 30,000 seconds (8 1/3 hours). In order to insure legibility of plots which might span many decades, most graphs have been limited to no more than six decades. As a result, some curves (e.g., certain excited state densities) of particularly small magnitude rapidly disappear or don't appear at all. This plotting effect usually occurs, if at all, in low electron density calculations.

The calculations presented here are summarized in Table 2. In all cases, initial excited state densities were assumed to be zero. As Table 2 indicates, two categories of calculations were done. The first category is composed of a single species systems with the species and electron densities set equal. Electron densities were set to 10^4, 10^6, or 10^8 cm^{-3} to cover the range of interest in late-time high altitude nuclear burst problems; electron and ion temperatures were initialized to one electron volt.

The second category of cases is composed of multi-species systems which are representative of a range of conditions found in detailed two-fluid numerical simulations of high altitude nuclear bursts. Species densities, electron density, and ion electron temperatures were as indicated in Table 2.

TABLE 2
SUMMARY OF CALCULATIONS

Figure No.	$[O^+]$ (cm^{-3})	$[N^+]$ (cm^{-3})	$[O]$ (cm^{-3})	$[N]$ (cm^{-3})	$[O_2]$ (cm^{-3})	$[n_e]$ (cm^{-3})	Initial T_e(eV)	Initial T_i(eV)
2	10^4					10^4	1.0	--
3	10^8					10^8	↓	--
4	10^4					10^4	↓	1.0
5	10^6					10^6	↓	↓
6	10^8					10^8	↓	↓
7		10^4				10^4	↓	↓
8		10^6				10^6	↓	↓
9		10^8				10^8	↓	↓
10			10^4			10^4	↓	↓
11			10^6			10^6	↓	↓
12			10^8			10^8	↓	↓
13				10^4		10^4	↓	↓
14				10^6		10^6	↓	↓
15				10^8		10^8	↓	↓
16					10^4	10^4	↓	↓
17					10^6	10^6	↓	↓
18					10^8	10^8	↓	↓
19	10^4	7.2×10^6	6.7×10^8	2.9×10^8	2.4×10^6	7.7×10^6	0.85	0.65
20	1.7×10^8	7.6×10^7	2.5×10^8	9.1×10^7	3.7×10^4	2.5×10^8	1.24	1.29
21	4.3×10^7	6.7×10^7	2.7×10^6	2.9×10^6	2.0×10^2	1.1×10^8	0.504	0.504
22	8.2×10^5	1.5×10^6	9.4×10^5	9.2×10^5	6.4×10^2	2.3×10^6	0.393	0.393

It's worthwhile, perhaps, to note that excited state densities and radiation rates are not trivially related to the electron density. If, for example, we assume the quasi-steady state, then Equations 2 and 3 yield the ratio of first to second excited state densities for our generic three level system:

$$\frac{n_1}{n_2} = \frac{k_{01}\left(\left[k_{20} + k_{21}\right] n_e + A_{20} + A_{21}\right) + k_{02}\left(k_{21}\, n_e + A_{21}\right)}{k_{02}\left(\left[k_{10} + k_{12}\right] n_e + A_{10}\right) + k_{01}\, k_{12}\, n_e} \qquad (13)$$

Even in the quasi-steady state, the A's are not negligible in general, so the population ratio and radiation rate ratios depend in a non-trivial manner on the electron density. This is, of course, already well known.

The first series of calculations presented here deals with fully ionized oxygen plasmas. In order to dispense at the outset with questions about the significance of collisional thermal energy transfer between ions and electrons, cases without and with the transfer process are presented in Figures 2, 3 (without) and Figures 4-6 (with). Thus, if one compares Figures 2 and 4 (electron density of 10^4 cm^{-3}), it is seen that the $O^+(^2D^o)$ densities are virtually identical during the first 10,000 seconds and then gradually deviate until the curve in the absence of energy transfer (Figure 2) is about 20% below the curve with the transfer (Figure 4). A comparison of radiation rates in these two figures shows the same trend, e.g., at 30,000 seconds, the $^2D^o \rightarrow {}^4S^o$ transition is cooling about 20% slower in Figure 2 than in Figure 4. Both of these observations are readily understood by comparing the electron temperature curves of Figures 2 and 4. During the first few thousand seconds both curves compare favorably, and the ion temperature curve in Figure 4 indicates very little energy transfer from ions to electrons. At 30,000 seconds, however, the electron temperatures differ by about 10% and the ion temperature (Figure 4) has dropped by about a tenth of an eV.

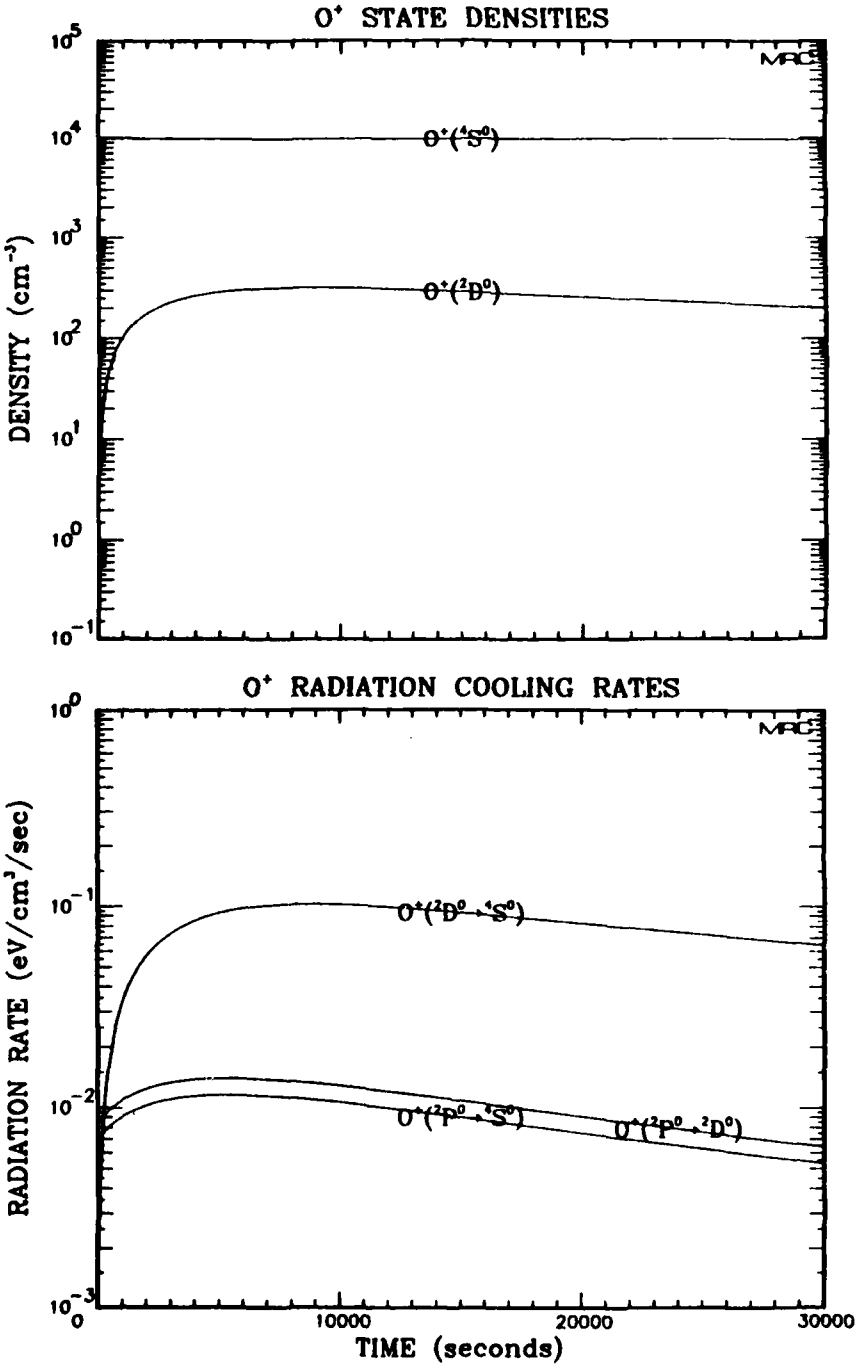

Figure 2. Radiation properties of O^+ at an electron density of 10^4 cm^{-3}. Ion-electron heat transfer (Equation 9) is absent from this calculation.

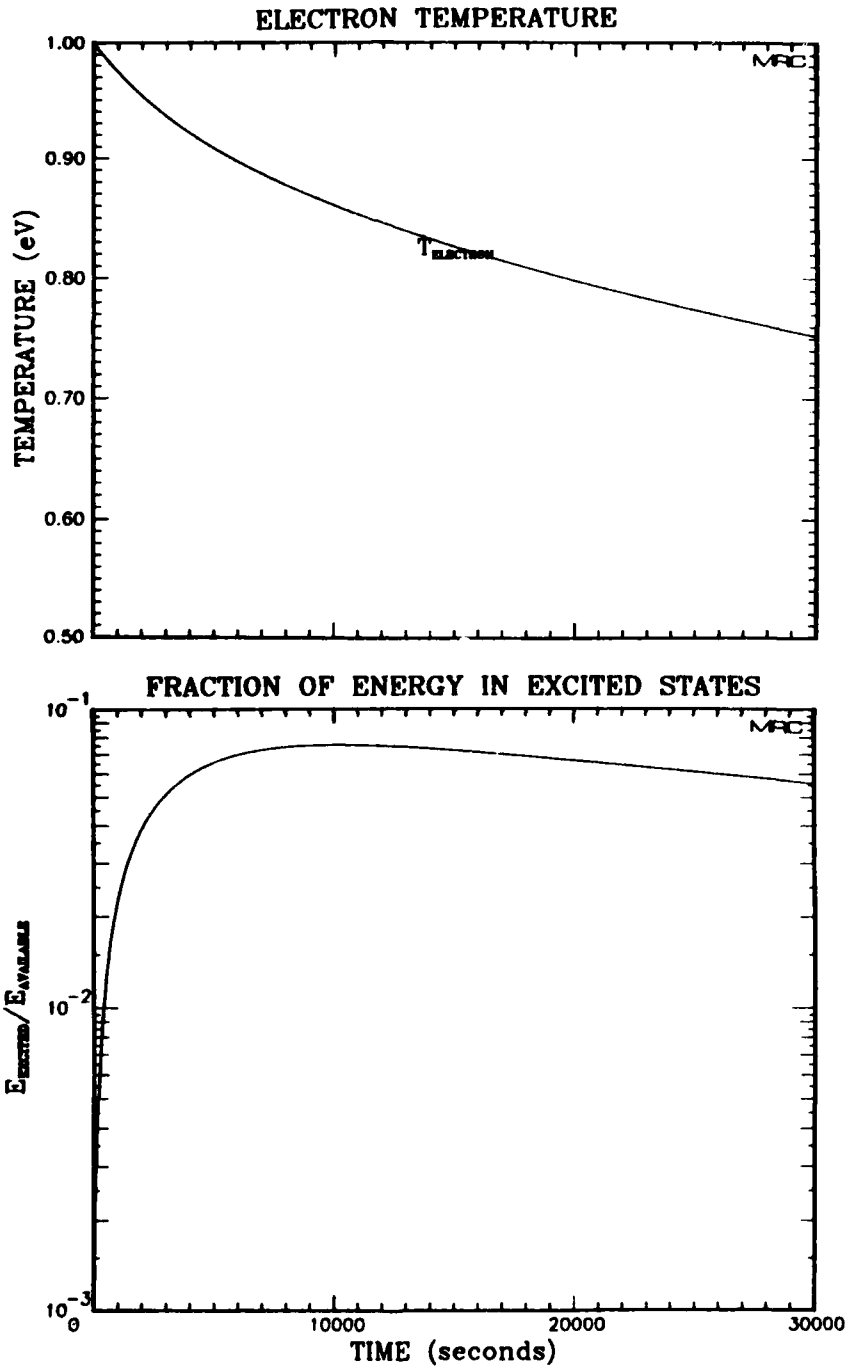

Figure 2 (Continued)

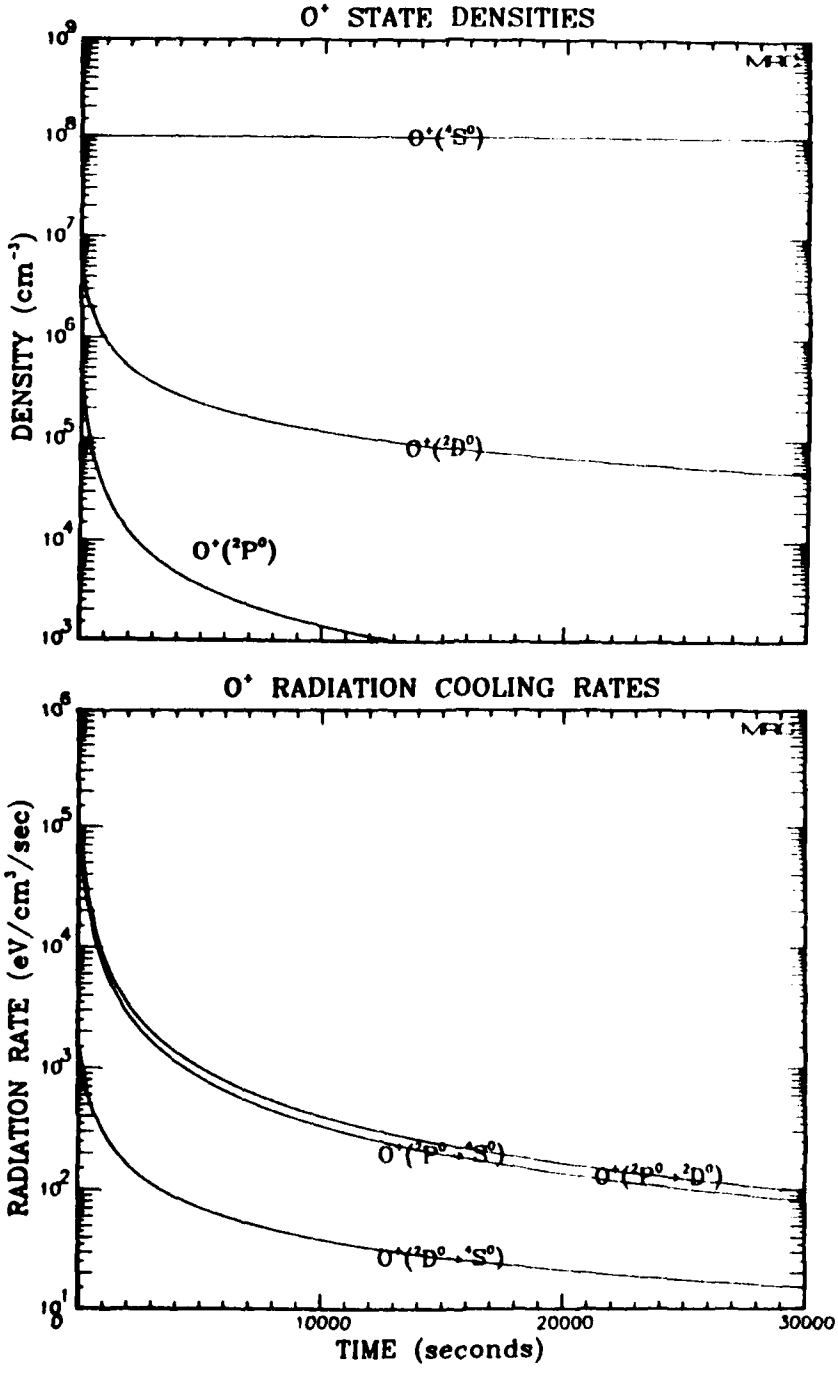

Figure 3. Radiation properties of O^+ at an electron density of 10^8 cm^{-3}. Ion-electron heat transfer (Equation 9) is absent from this calculation.

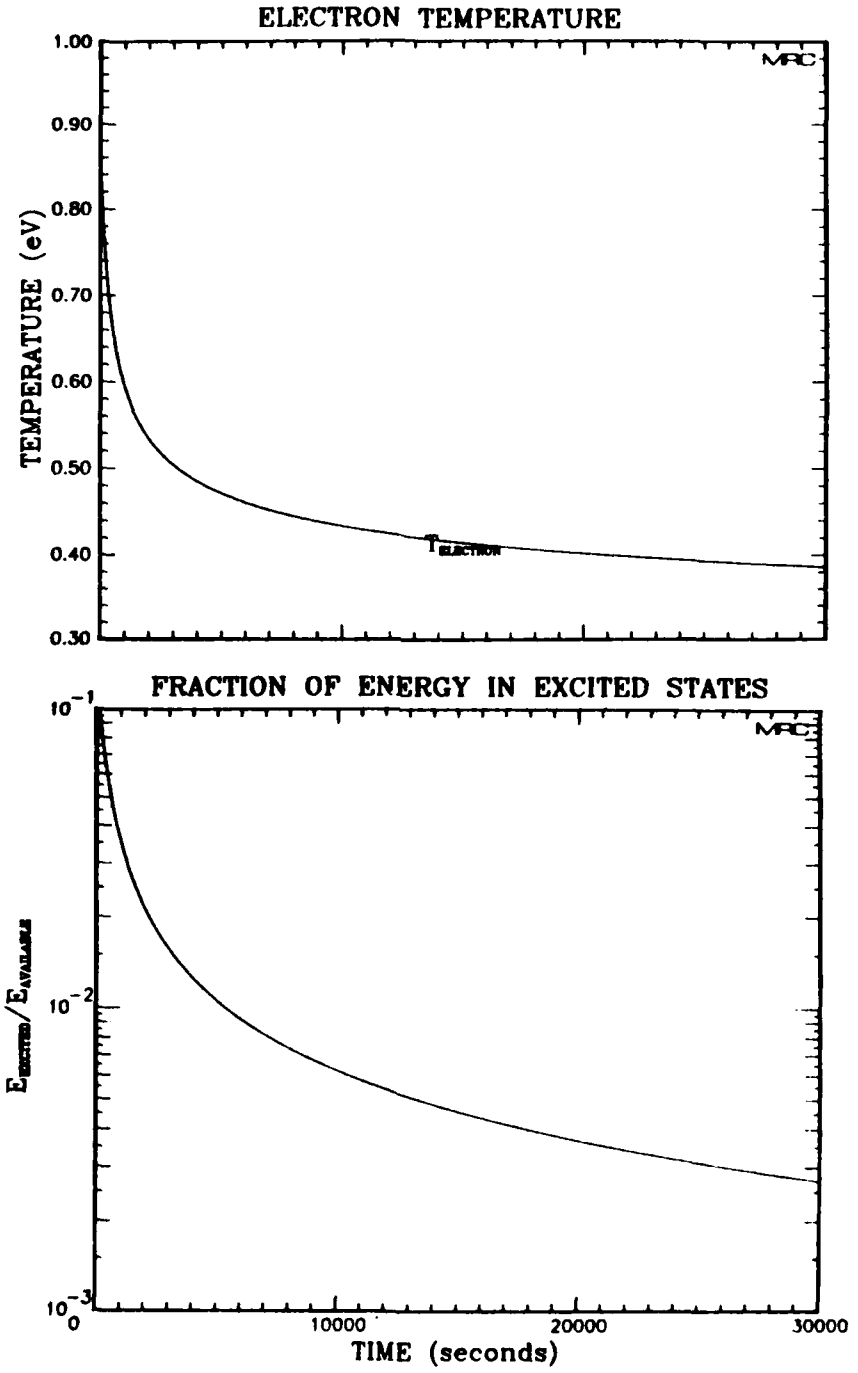

Figure 3 (Continued)

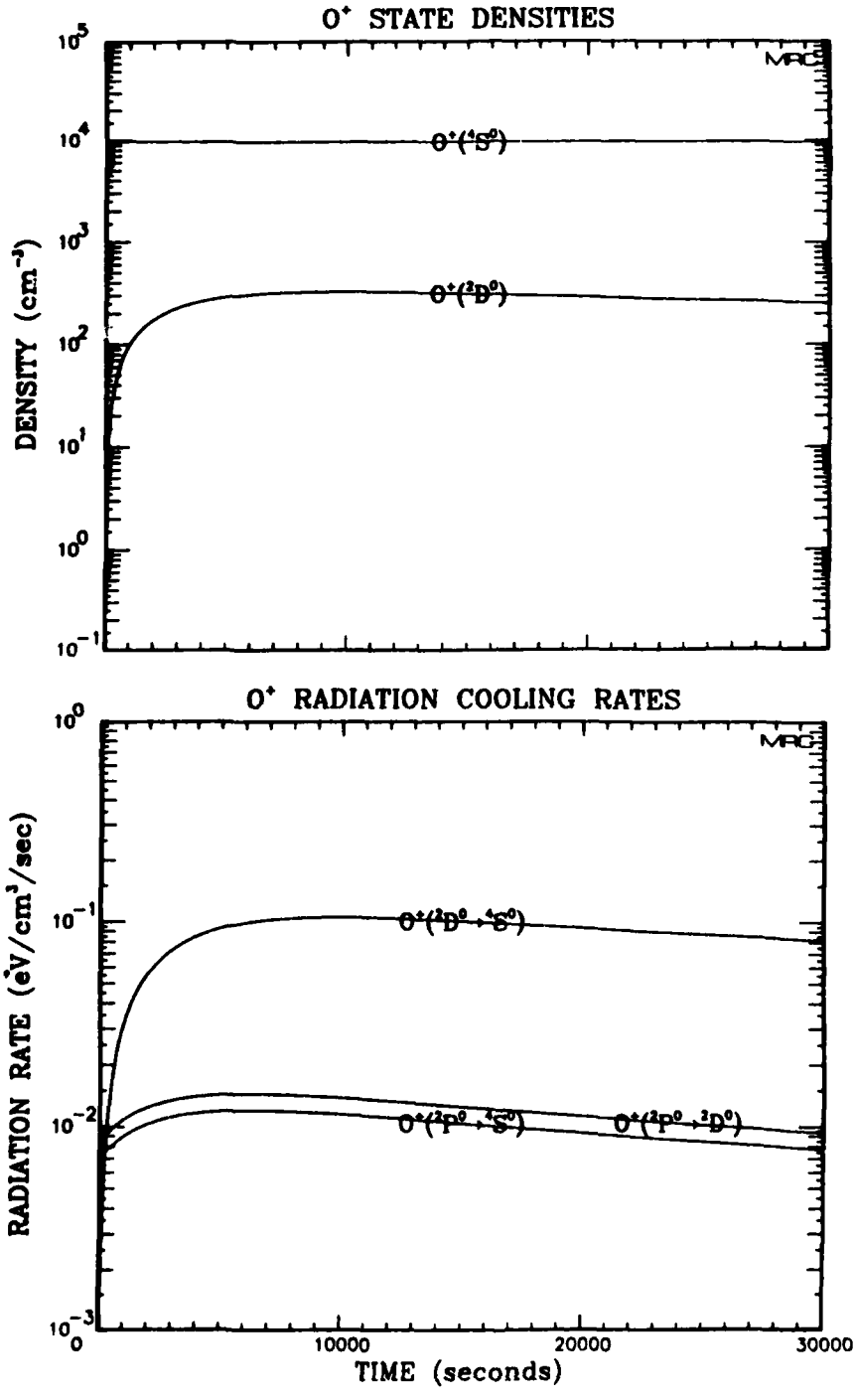

Figure 4. Radiation properties of O^+ at an electron density of 10^4 cm^{-3}.

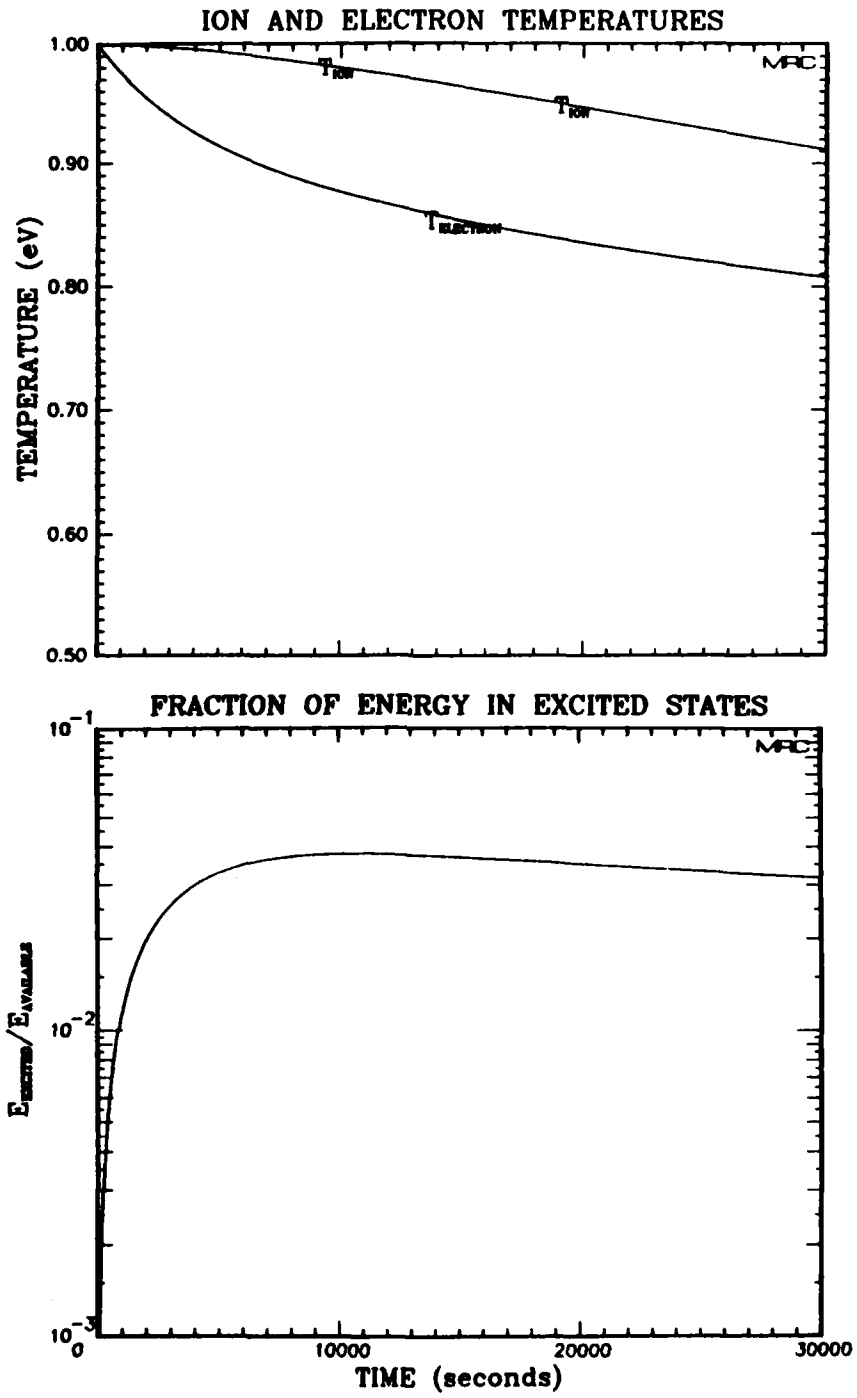

Figure 4 (Continued)

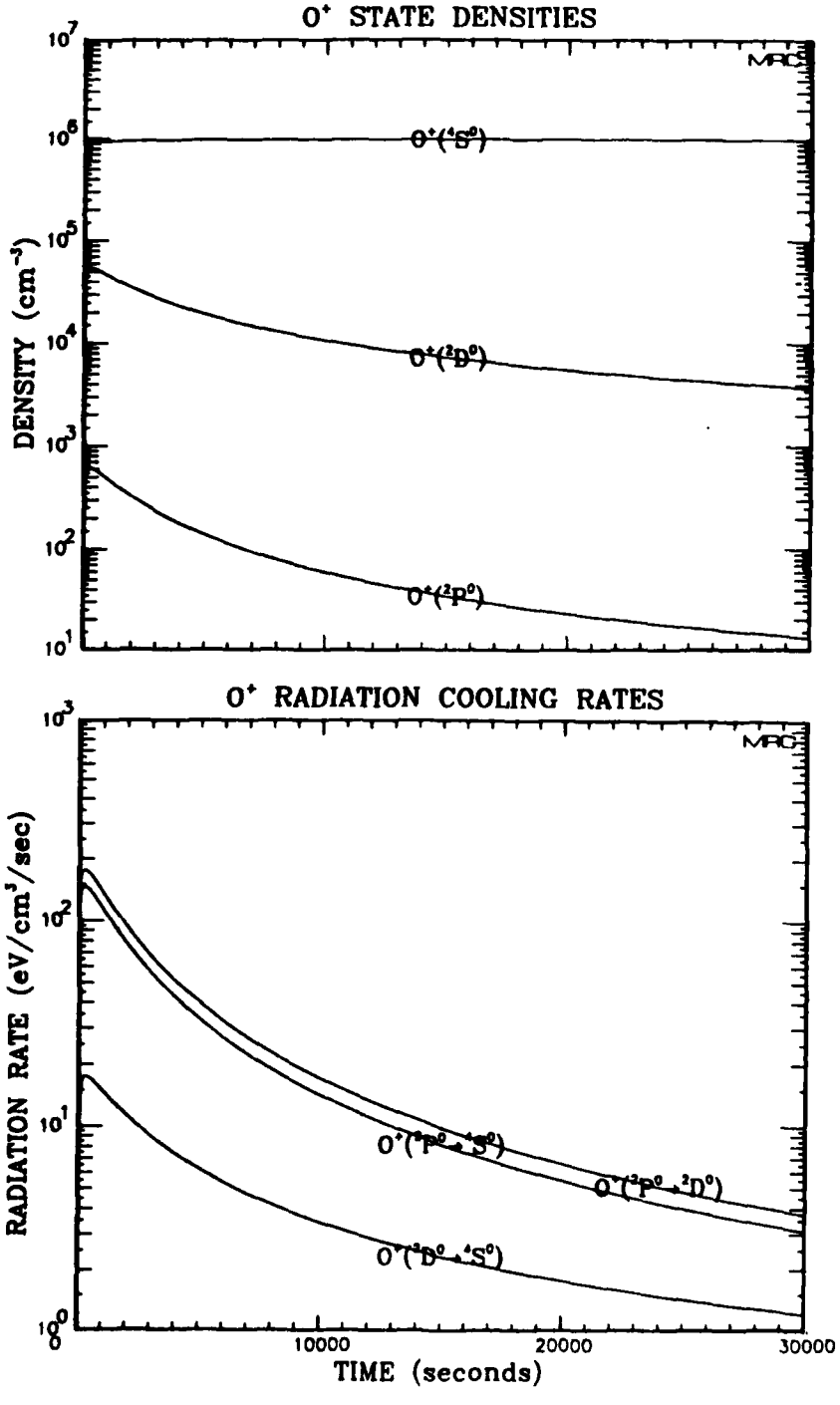

Figure 5. Radiation properties of O^+ at an electron density of 10^6 cm^{-3}.

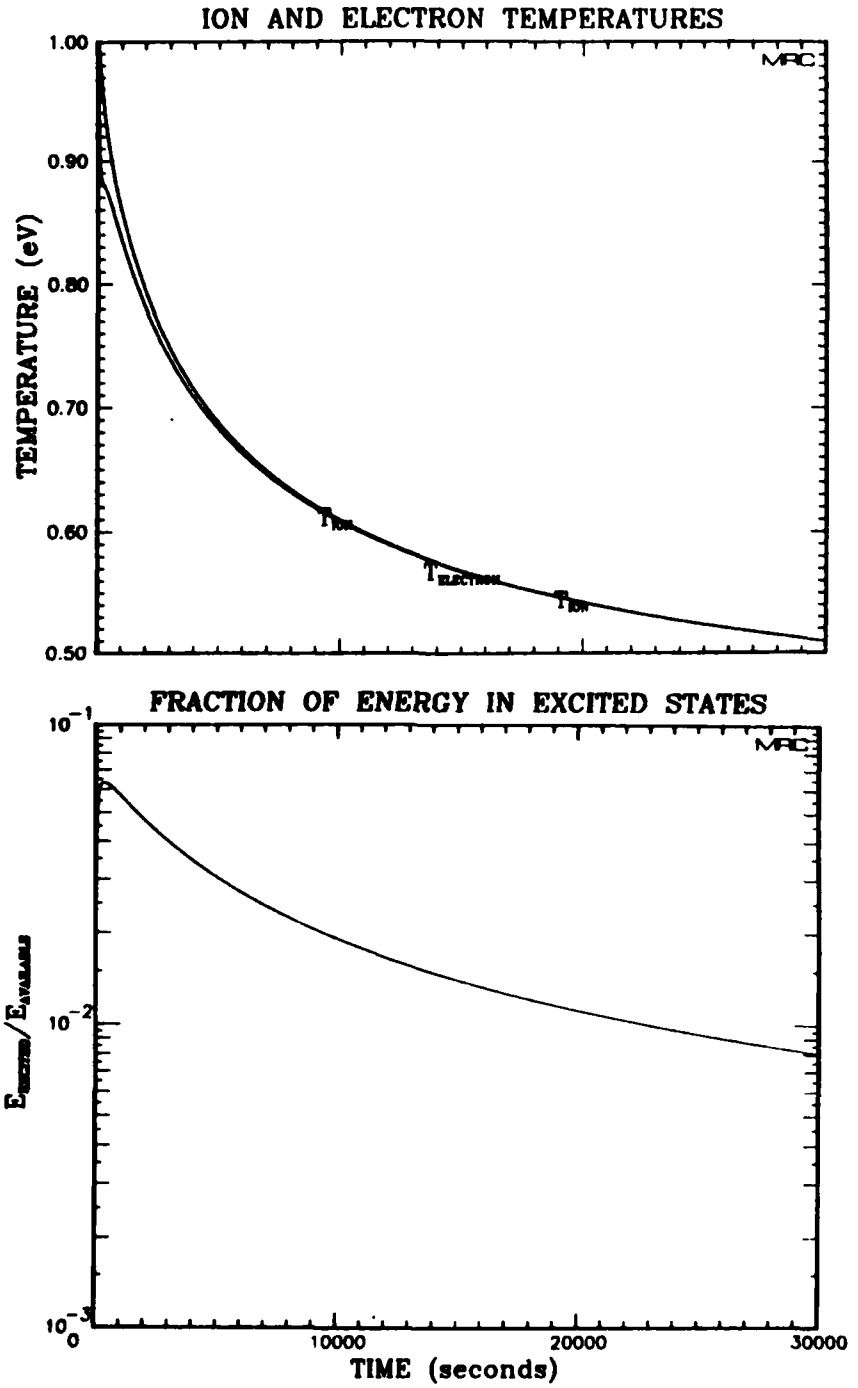

Figure 5 (Continued)

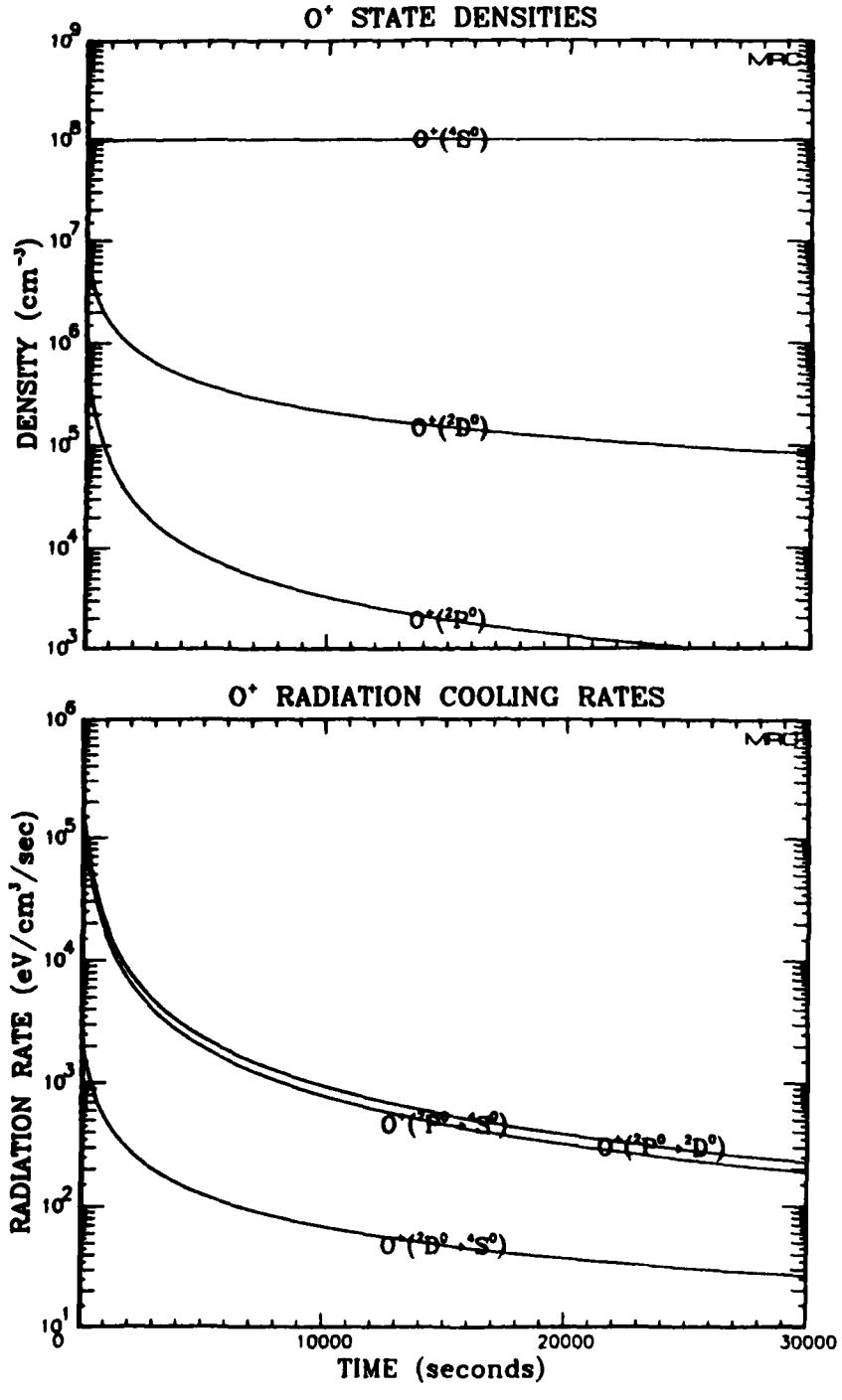

Figure 6. Radiation properties of O^+ at an electron density of 10^8 cm^{-3}.

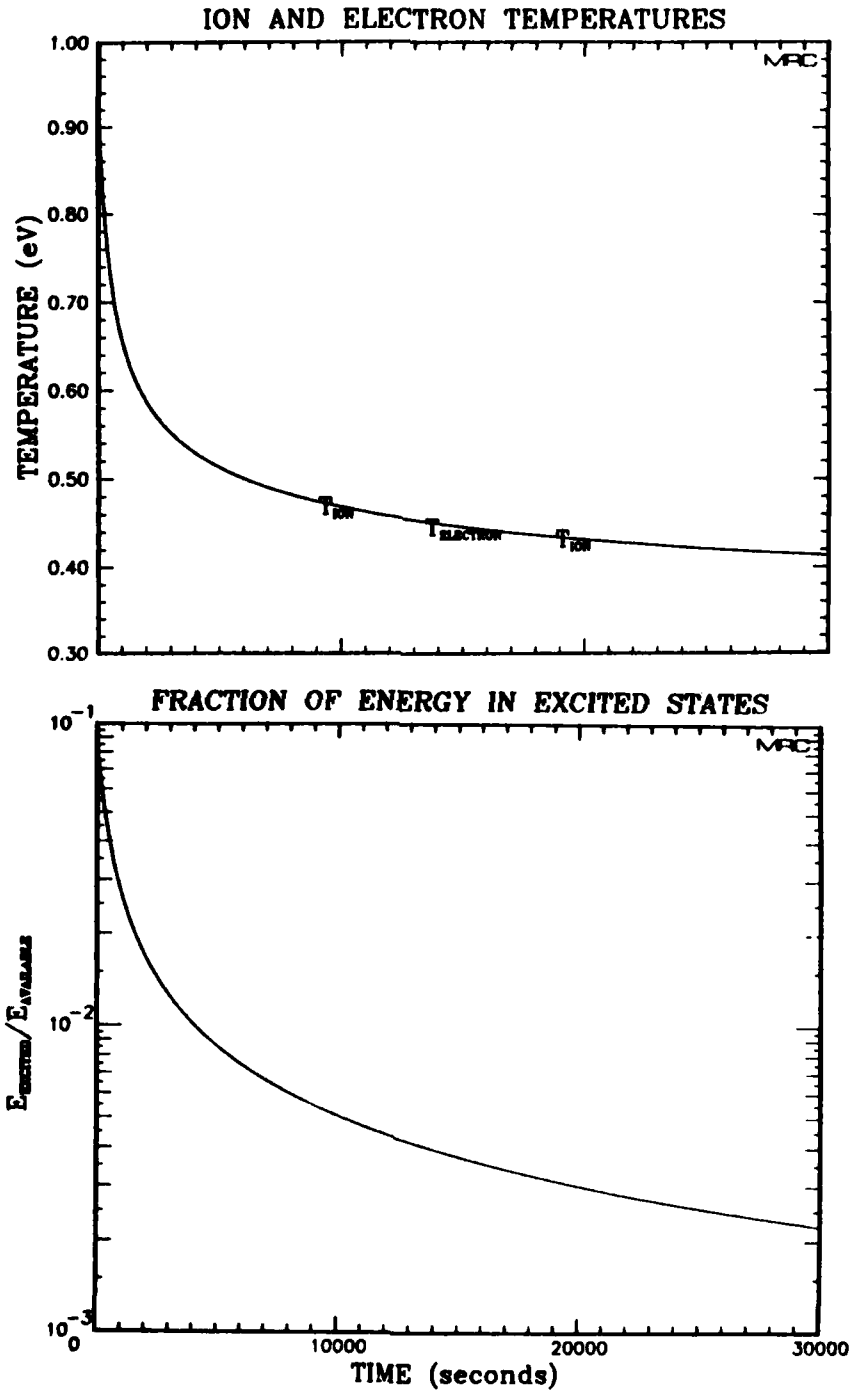

Figure 6 (Continued)

Finally, the curves denoting the fraction of available energy which is tied up in excited states may be compared. Both curves peak at about 10,000 seconds, but the curve in Figure 4 peaks at a lower value (even though the electron temperature and excited state densities are higher than found in Figure 2) because the available energy has been doubled by coupling to the ions. The most significant point here is that in each case the fraction of available energy tied up in excited states is a few percent.

With the aid of Figures 3 and 6 one can make a parallel set of comparisons at the other electron density extreme considered here (10^8 cm^{-3}). As one would expect, the case with ion-electron energy transfer (Figure 6) maintains a slightly (~30%) higher electron temperature than the case without (Figure 4), so exicted state densities and radiation rates are also somewhat larger. Unlike the preceding pair of cases, the ion and electron temperatures are now locked together by collisional coupling which transfers energy to the electrons faster than it can be pumped into excited states and radiated away. In Figure 3, the energy fraction in excited states very rapidly peaks at about 10% while in Figure 6 the corresponding peak is at about 8%.

These comparisons (and similar comparisons, not presented, for the other emitting species) lead us to observe that for the range of electron and species densities considered (where the electron and species densities are equal) failure to couple ion and electron thermal energy reservoirs results at most in a modest alteration of the excited state densities, radiation rates, and energy partition. Now that the magnitude of such coupling has been established, we proceed to the remaining calculations, all of which included the coupling.

One can now consider Figures 4, 5, and 6 as a set of calculations which illustrate the electron density dependence of radiation cooling by the O^+ system. This series of figures shows that at an electron

density of 10^4 cm^{-3} it takes roughly 10,000 seconds to reach a quasi-steady distribution of excited states, radiation rates, etc. At 10^6 cm^{-3} density, the time required to reach the quasi-steady state is about 200 seconds; at 10^8 cm^{-3} density, the quasi-steady state is attained "instantly" as compared to the time scale of the plots. (Note that the ion-electron energy transfer rate can alter the scaling of this time constant because the electron temperature can remain higher for a longer time.) As one would expect, the high ion-electron density case radiates much more rapidly than the lower density cases. In addition note that at the 10^4 cm^{-3} density, the dominant transition is $^2D^0 \rightarrow {}^4S^0$. At higher densities, the $^2p^0 \rightarrow {}^2D^0$ and $^2p^0 \rightarrow {}^4S^0$ transitions dominate. This switch results from the shift in relative populations of the exicted states, as expressed in Equation 13, which occurs as the electron density is altered. It is the interplay of excitation rates and transition probabilities which is primarily responsible for this effect.

As noted earlier, the curves denoting the fraction of available energy tied up in excited states all remain in the range of a few percent or less. Thus, from the ion and electron temperature curves we conclude that the time required to radiate one-half the energy is about 6,000 seconds at 10^8 cm^{-3}, about 30,000 seconds at 10^6 cm^{-3}, and (very) roughly 2×10^5 seconds at 10^4 cm^{-3}.

The excitation and radiation characteristics of nitrogen ions at the electron densities of interest are displayed in Figures 7, 8, and 9. Upon inspection of these figures, one notes that the excited state densities and radiation rates attain a quasi-steady state virtually instantly as compared to the 30,000 second time scale of the plots. Only the case at 10^4 cm^{-3} electron density (Figure 7) shows a perceptible period (a few hundred seconds) when departures from a quasi-steady distribution of states are evident.

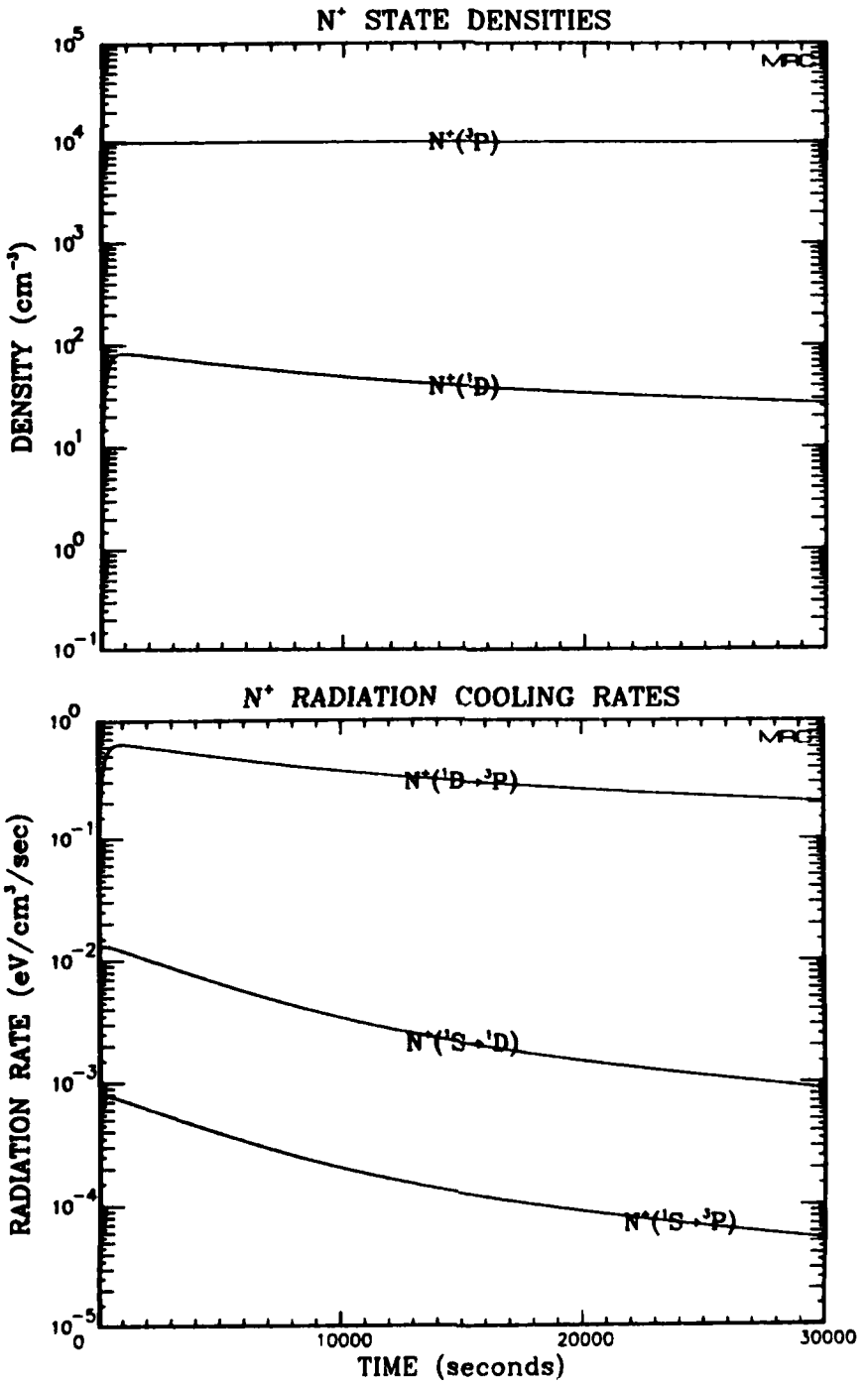

Figure 7. Radiation properties of N^+ at an electron density of 10^4 cm^{-3}.

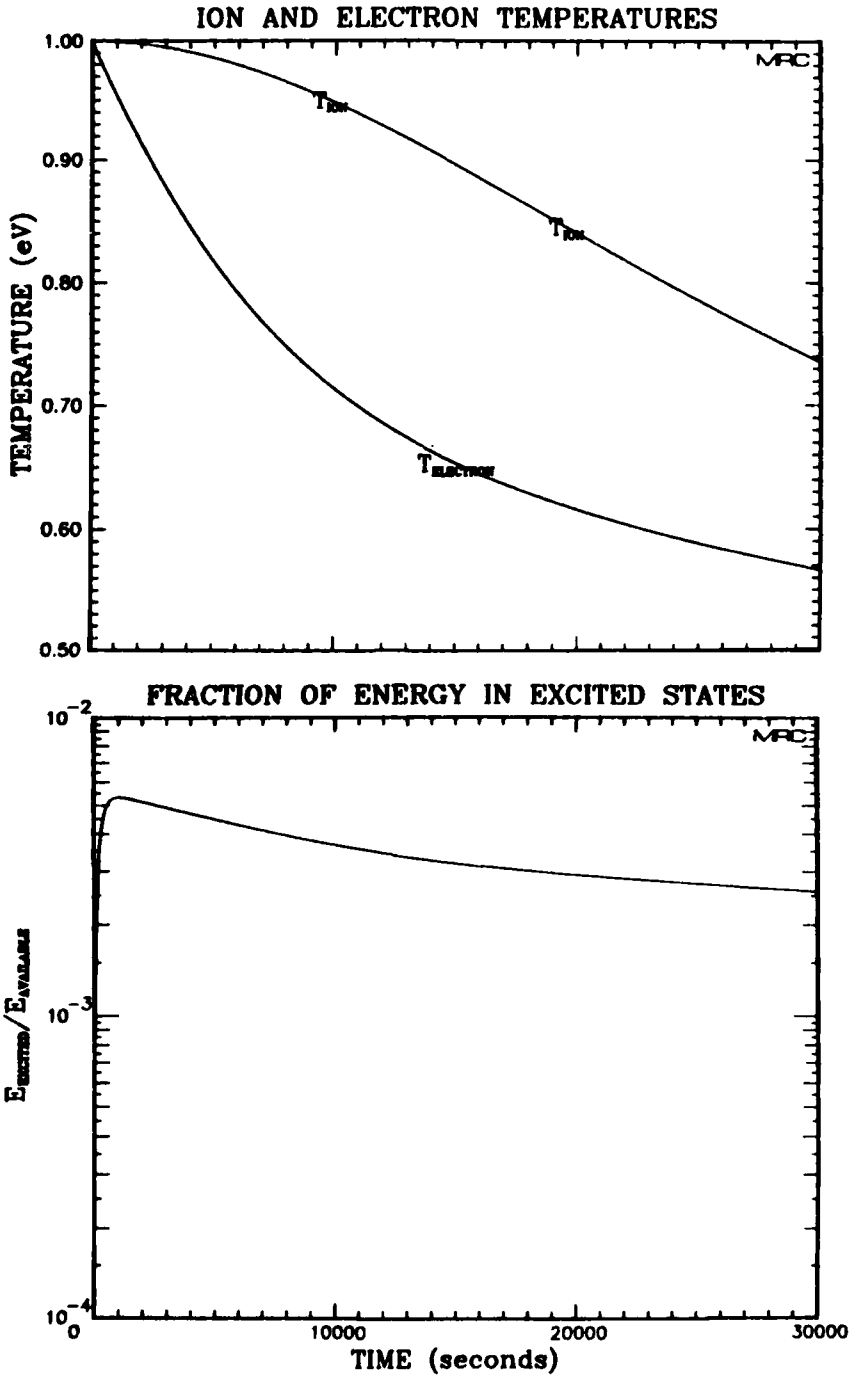

Figure 7 (Continued)

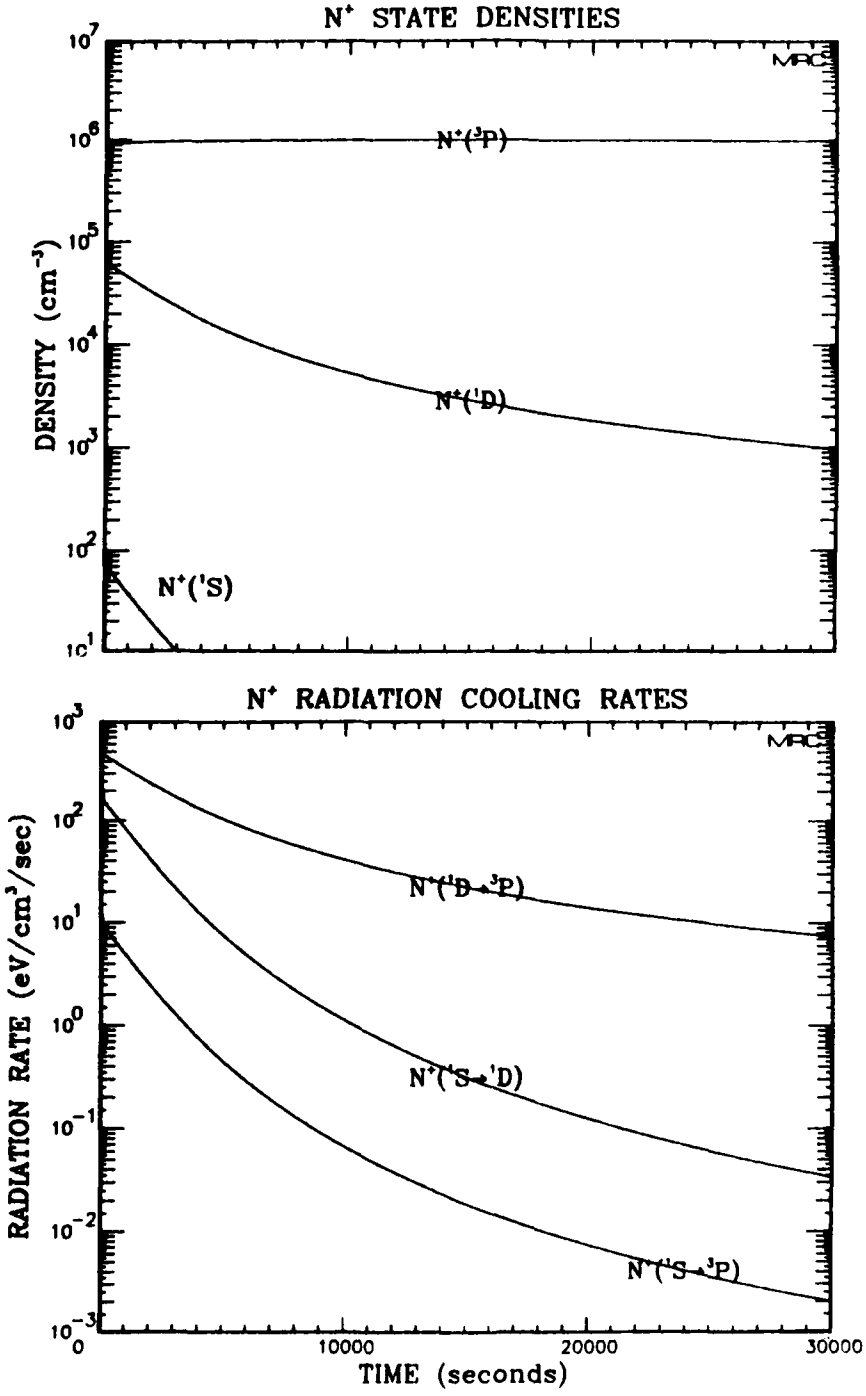

Figure 8. Radiation properties of N^+ at an electron density of 10^6 cm^{-3}.

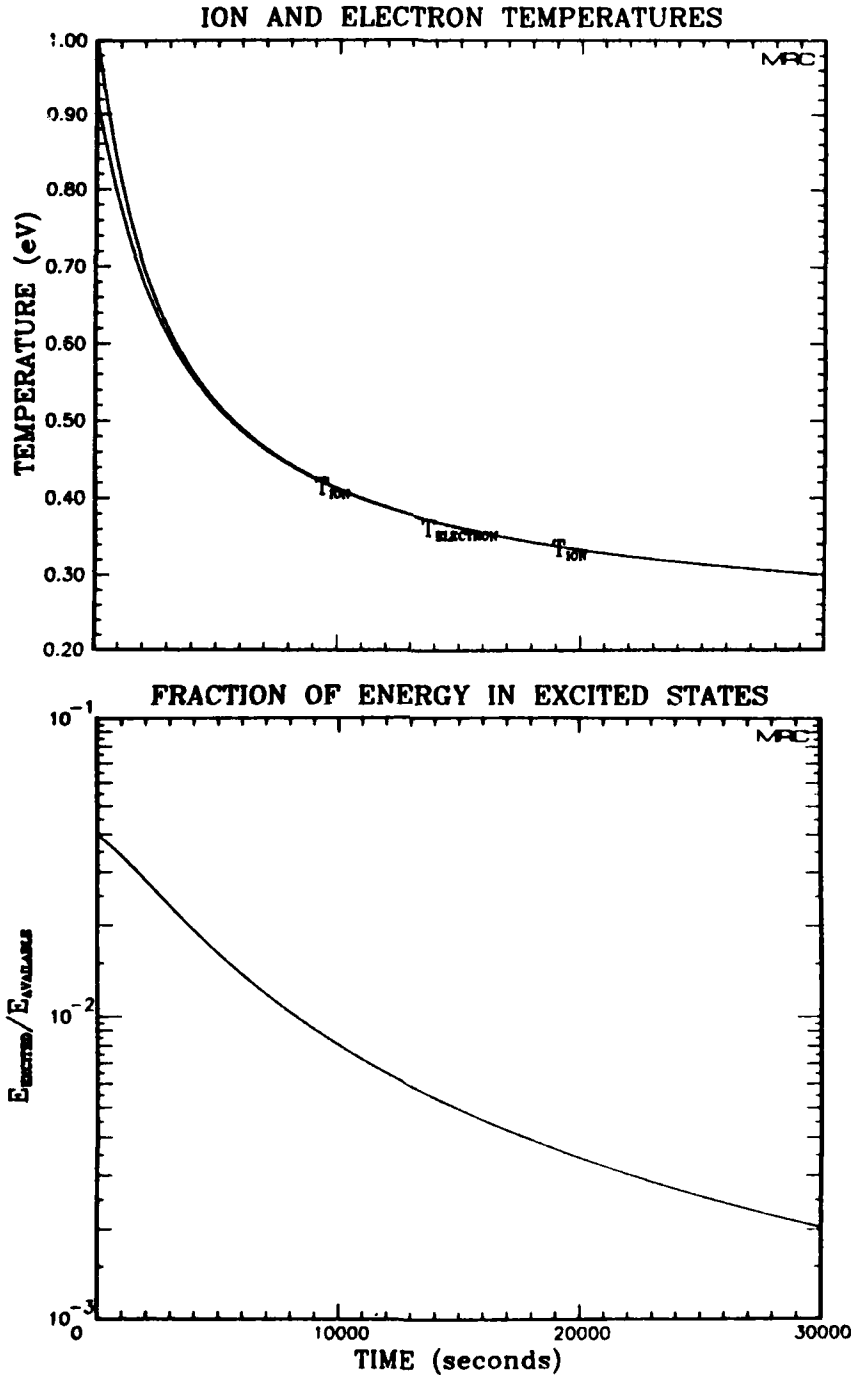

Figure 8 (Continued)

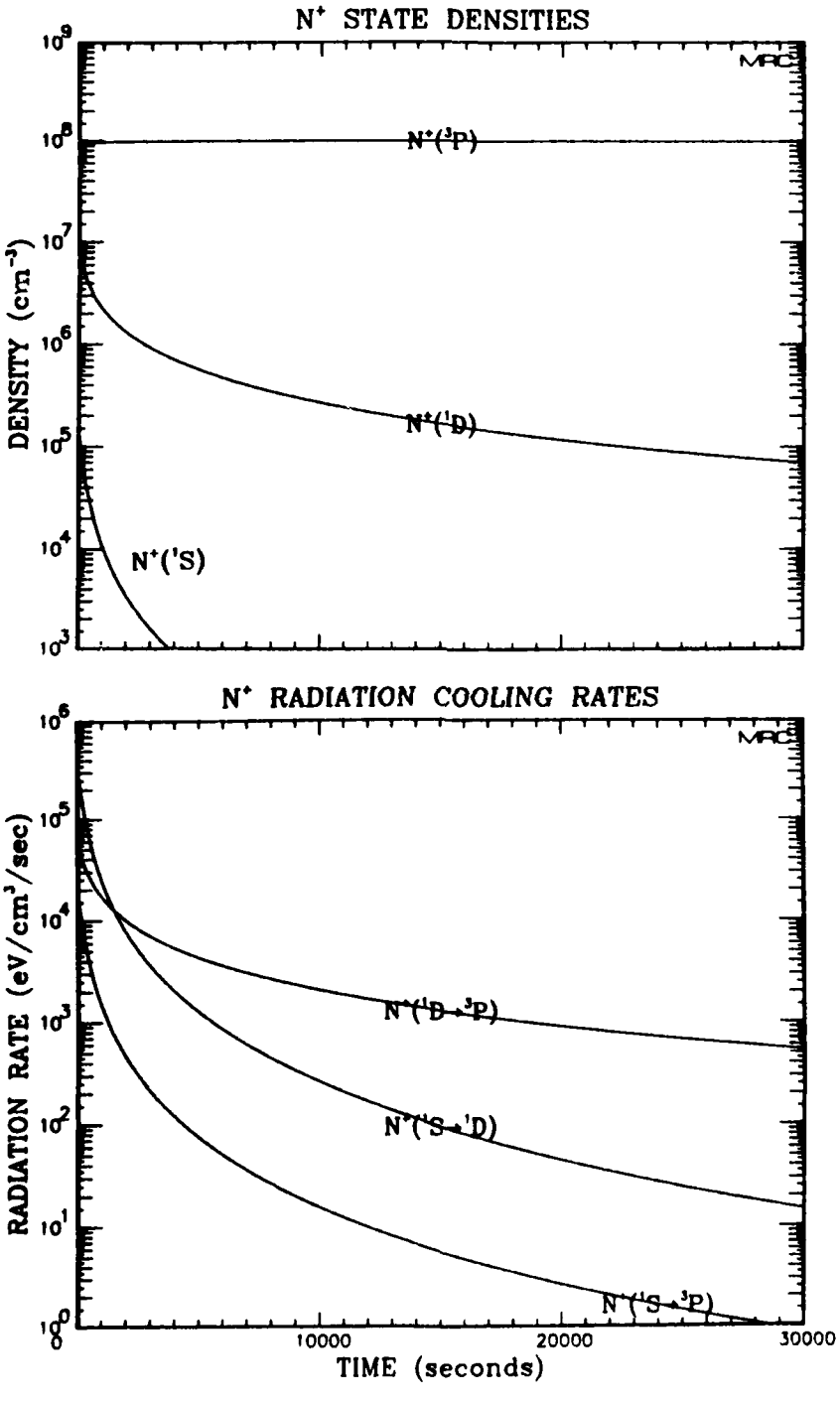

Figure 9. Radiation properties of N^+ at an electron density of 10^8 cm^{-3}.

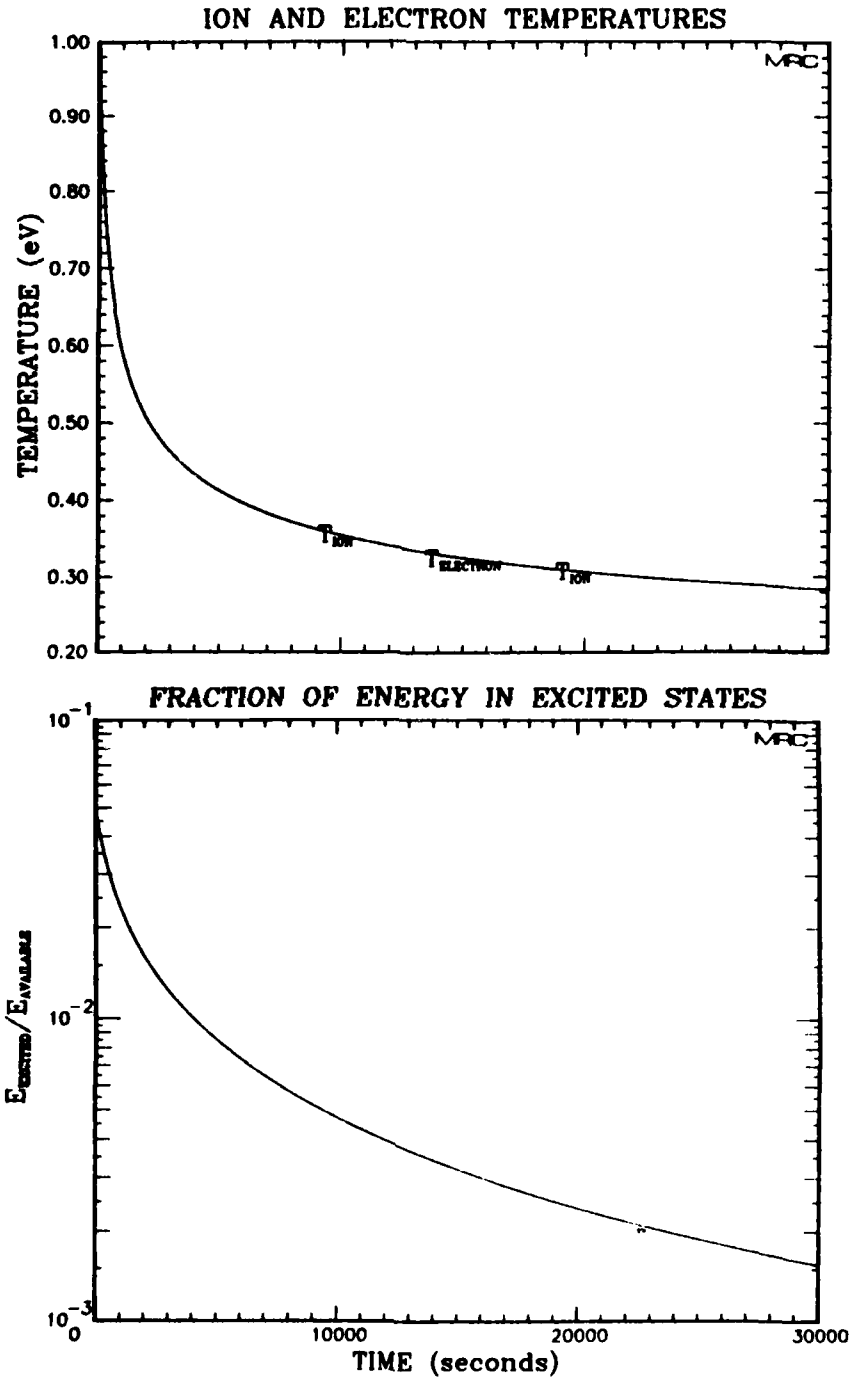

Figure 9 (Continued)

It's worth noting the variation with electron density of the ratio of radiation rates for the $^1D \rightarrow ^3P$ and $^1S \rightarrow ^1D$ transitions. For the 10^4 cm^{-3} and 10^6 cm^{-3} electron density cases, this ratio is always greater than one. At 10^8 cm^{-3} electron density and while the electron temperature is above ~0.53 eV (during the first ~1500 seconds), the ratio is less than one. This behavior can be understood in terms of Equation 13. Based on trasition probabilities and photon energies, one can compute that the ratio of ^1D to ^1S state densities needs to be ~ 233 or less if the radiation rate for the $^1S \rightarrow ^3P$ transition is to dominate. At low electron density, electron empact excitation is insufficient to generate a ratio this small. One observes in Figure 9 (early time) that the ^1D to ^1S state density ratio is about 100 (electron density is 10^8 cm^{-3}), but in Figure 8 the ratio has jumped to roughly 1000 (electron density is 10^6 cm^{-3}).

As in the case for radiation from oxygen ions, the nitrogen ion calculations indicate that energy associated with excited states is at most a few percent of the available energy. Thus, the temperature curves allow us to readily calculate that a bit more than 2000 seconds is required to radiate one-half the available energy at 10^8 cm^{-3}; about 5500 seconds are required at 10^6 cm^{-3}. One also notes that at the 10^4 cm^{-3} electron density, excitation and radiation is able to remove energy from the electrons faster than it can be replaced by transfer from the ions. As the higher electron densities, this is not the case.

The radiating characteristics of oxygen atoms over the electron density range of interest are presented in Figures 10, 11, and 12. The reader is reminded that the radiating species density has been set equal to the electron density (and also to a non-radiating ion density). This rather arbitrary choice influences quite strongly the magnitudes of various results. The particular choice of equal densities was made because it provides a reasonable balance between the heat capacity of the ion-electron gas and energy stored in excited states. From these results

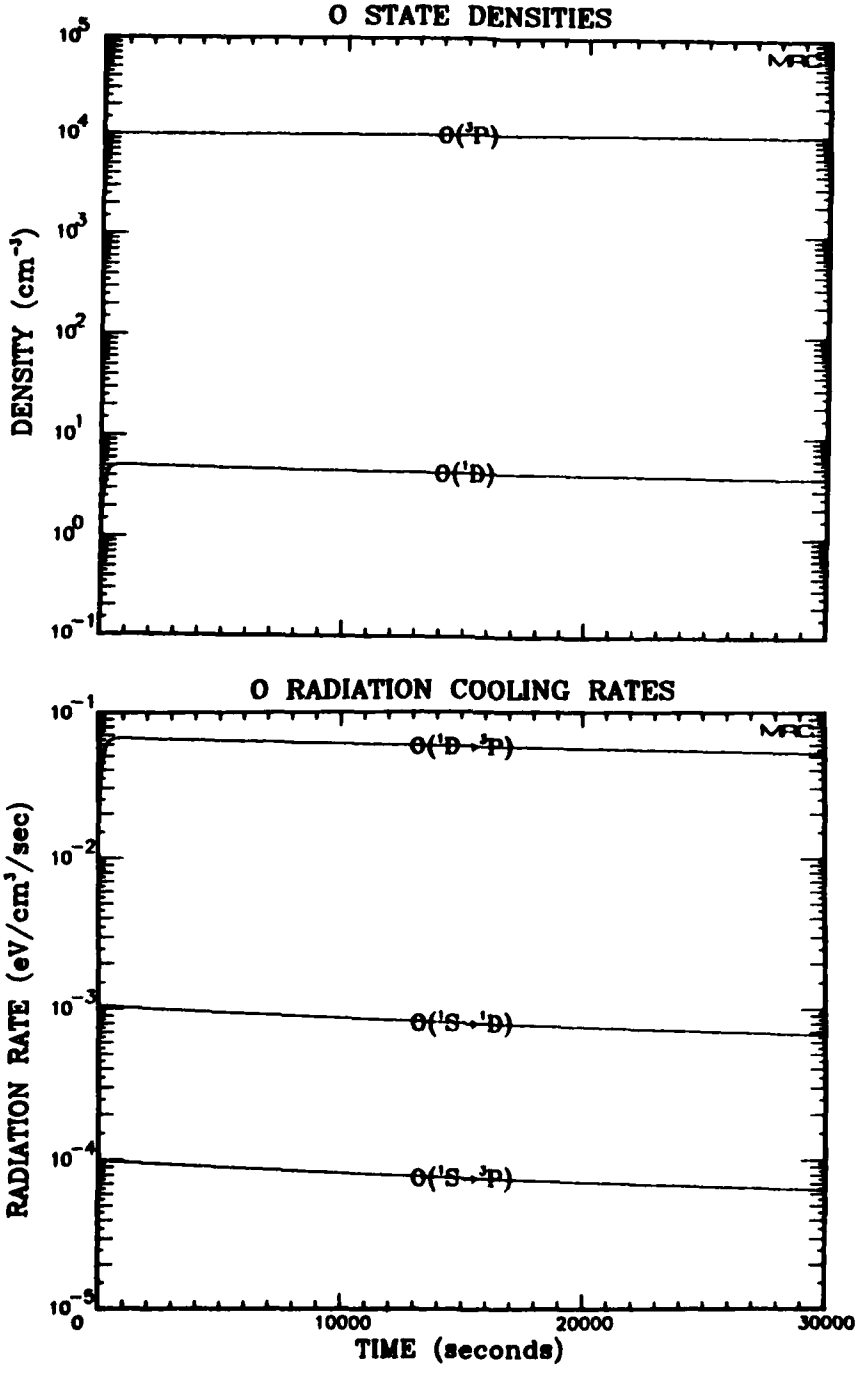

Figure 10. Radiation properties of O atoms at an electron density of 10^4 cm^{-3}.

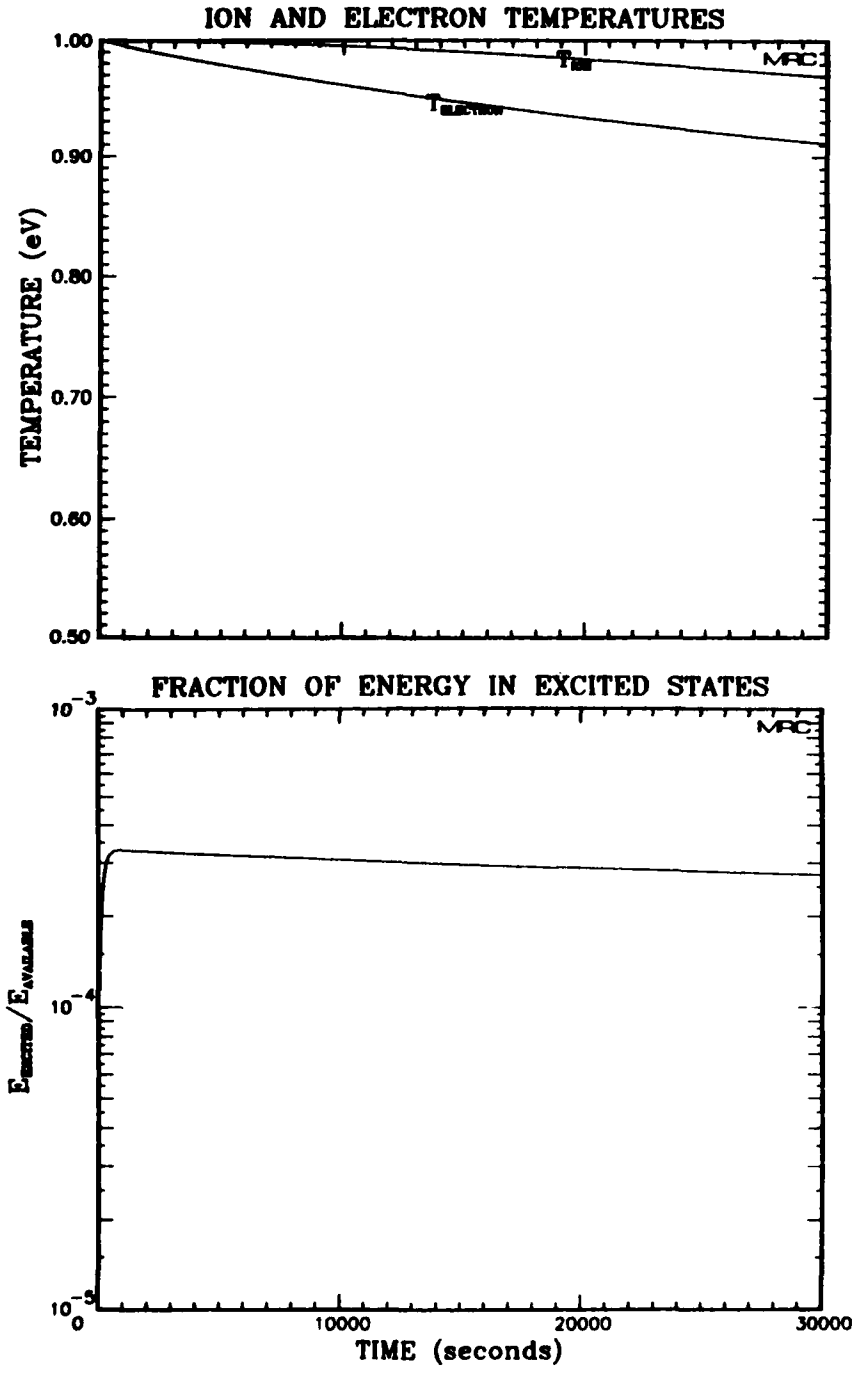

Figure 10 (Continued)

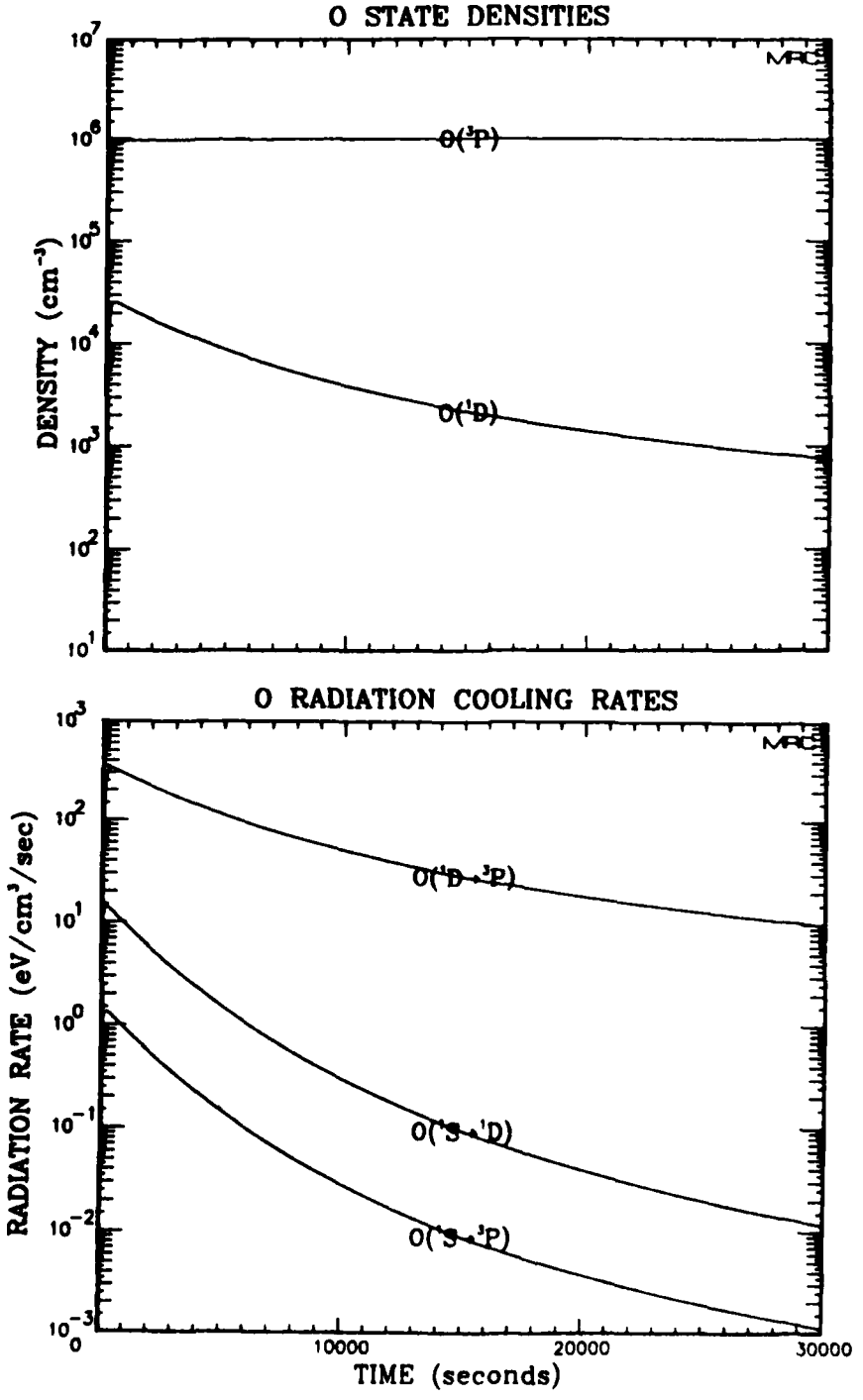

Figure 11. Radiation properties of O atoms at an electron density of 10^6 cm^{-3}.

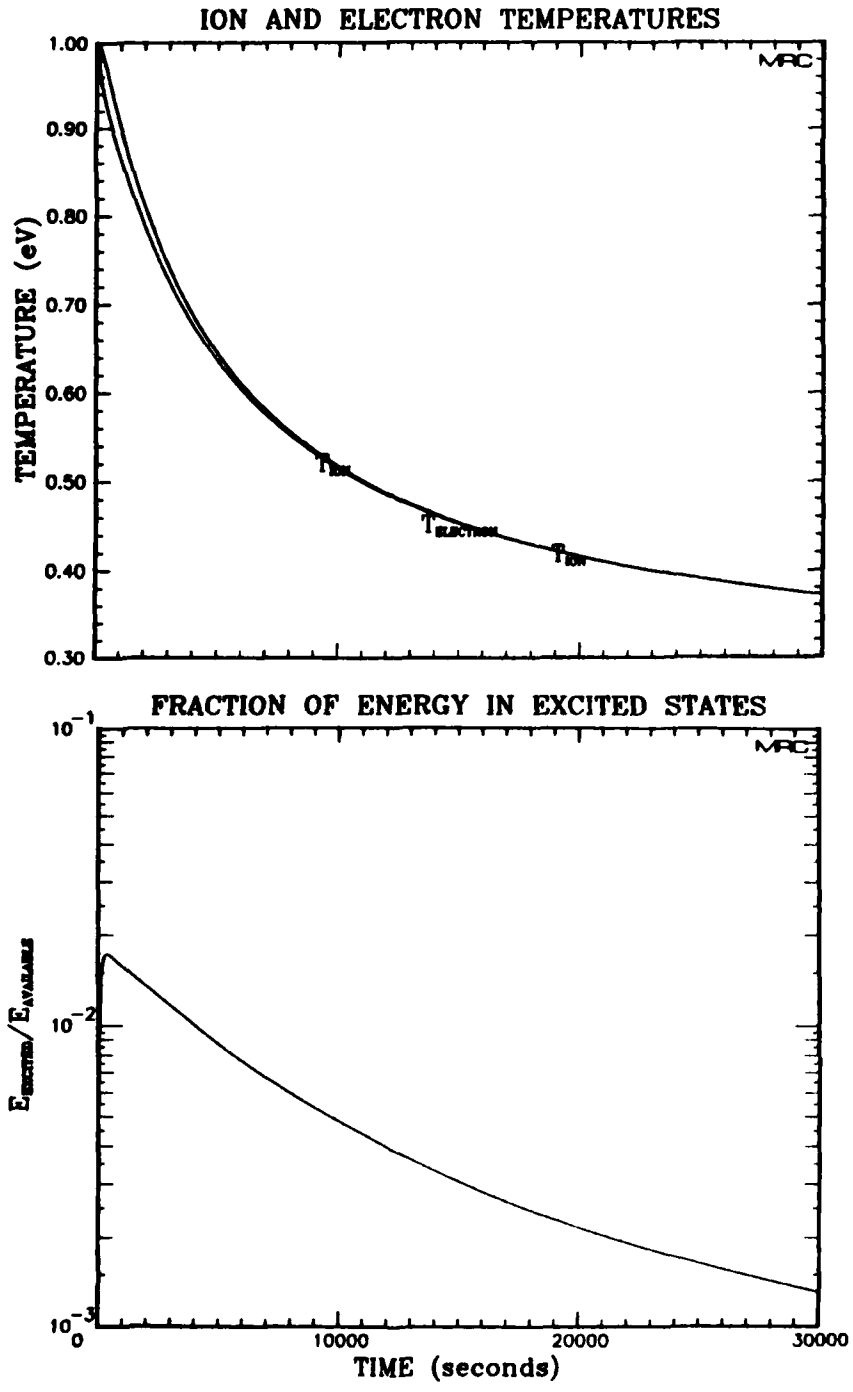

Figure 11 (Continued)

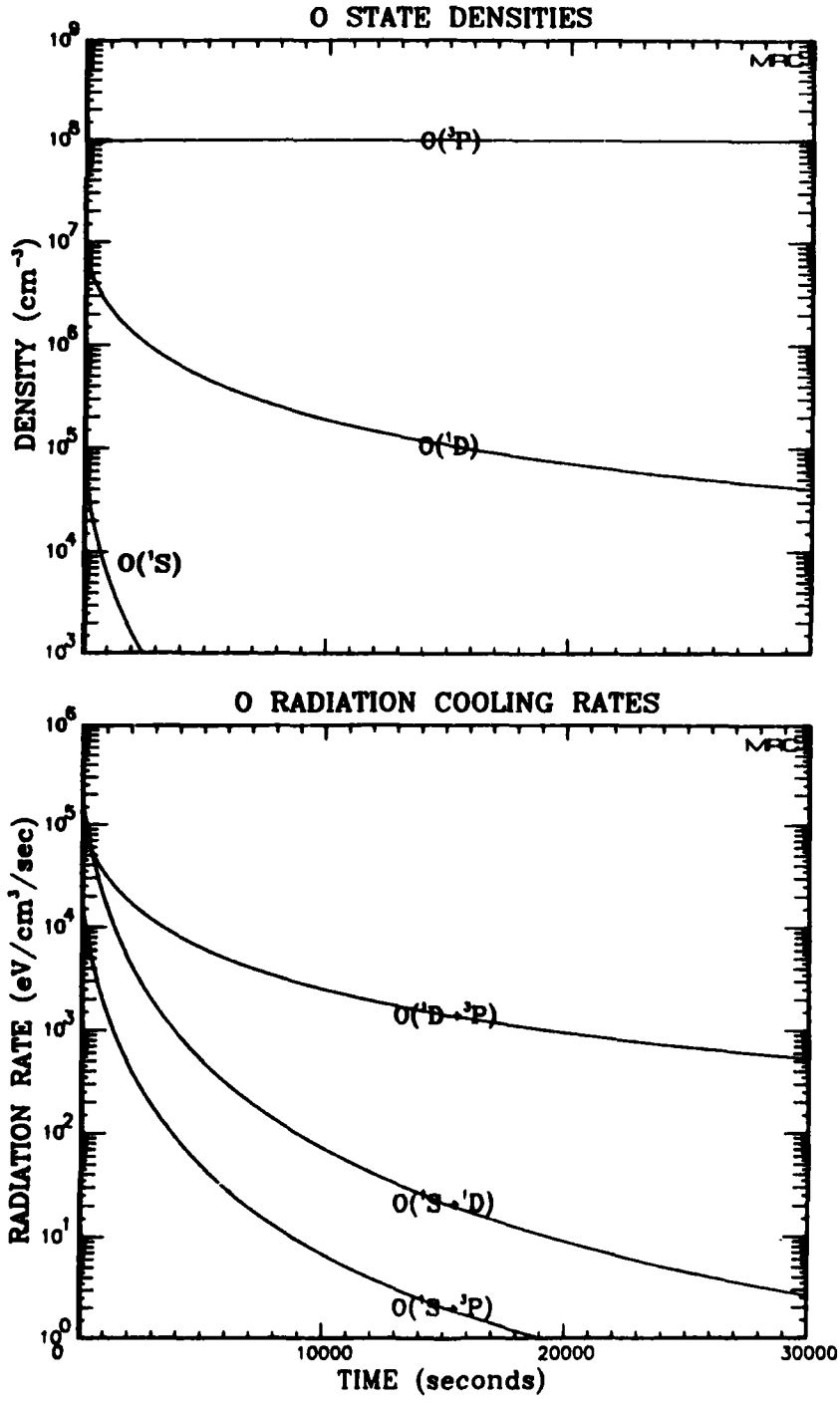

Figure 12. Radiation properties of O atoms at an electron density of 10^8 cm^{-3}.

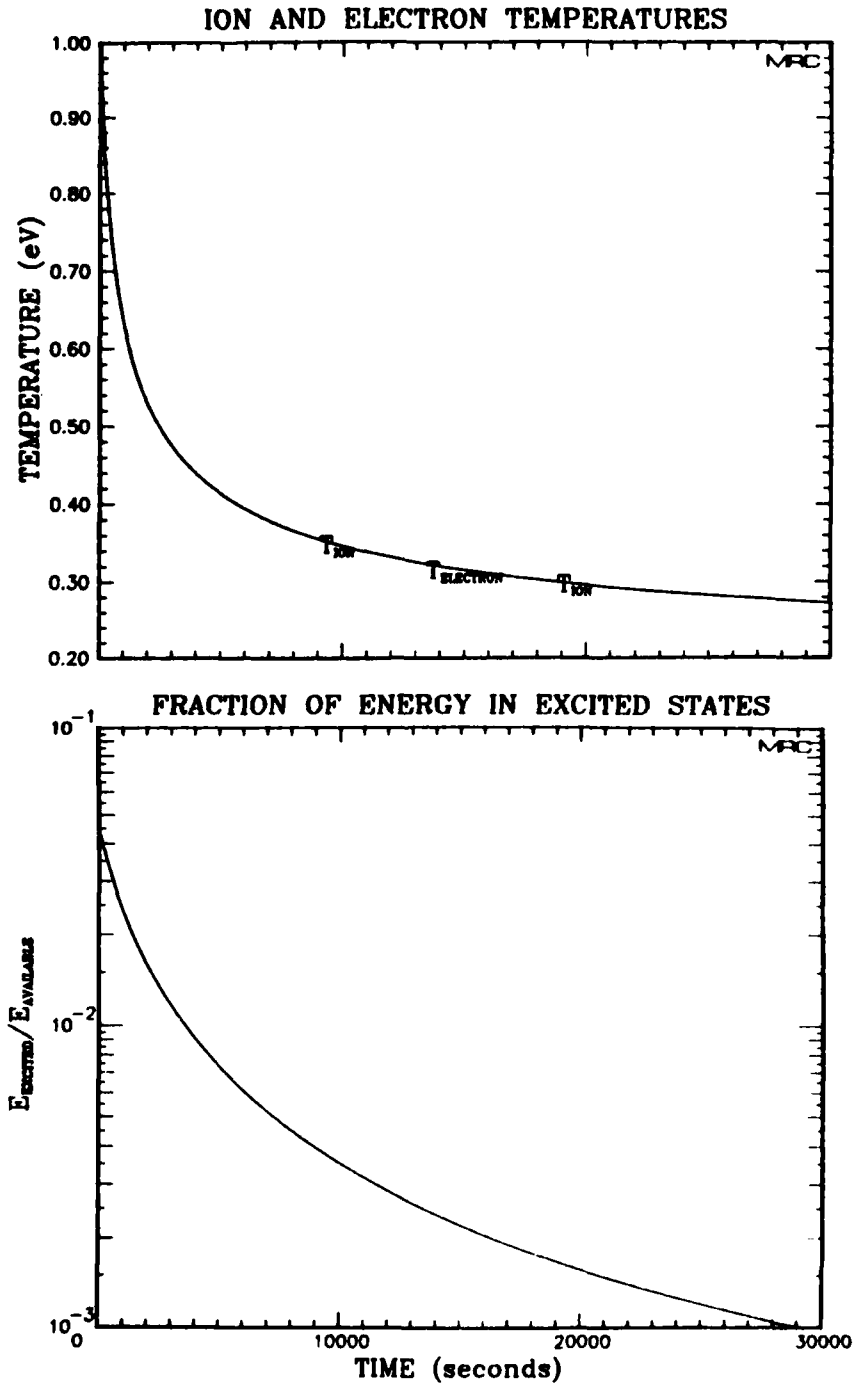

Figure 12 (Continued)

the reader can extrapolate, in a limited sense, to other density combinations. If the oxygen atom density had been substantially larger than the electron and ion densities, then most of the available energy would have gone mainly into the lowest excited state at the same time the electron and ion temperatures dropped to low values. The resultant curves would be relatively flat and uninteresting. (Clearly, the best approach is to compute for the precise conditions of interest in a particular problem.)

The first point to note in this series of three figures is that the quasi-steady state is obtained, even at the lowest electron density, rather quickly as compared to the time scale of the plots. However, at 10^4 cm^{-3} electron density (Figure 10), the radiation cooling and temperature curves are quite flat as a result of relatively low excitation rates. One sees that less than a percent of the available energy is tied up in excited states, so it readily can be inferred from the temperature curves that only about 6 percent of the original energy has been radiated over the 30,000 second period.

The calculation at 10^6 cm^{-3} electron density shows more interesting temporal behavior and achieves substantial cooling over 30,000 seconds. Once again, the fraction of available energy which is tied up in excited states is quite small (< 2%), so we readily estimate from the temperature curves that one-half the initial energy was radiated by about 11,000 seconds. Note that radiation from the long lived $^1D \rightarrow {}^3P$ transition is the dominant loss channel, a result which is not too surprising in light of the fact that the ^1D state has at least three orders of magnitude greater population density than does the ^1S state. One might expect the relatively short lived $^1S \rightarrow {}^1D$ transition to dominate, but the ratio of transition probabilities ($^1S \rightarrow {}^1D$ to $^1D \rightarrow {}^3P$) is only about 200 and can't compensate for the (at least) three orders of magnitude difference in populations (Refer to Table 1).

Inspection of results corresponding to an electron density of 10^8 cm^{-3} (Figure 12) reveals that at early times the ^1S state density is about two orders of magnitude smaller than the ^1D state density. In view of the ratio of transition probabilities, it's not surprising to find that initially the $^1S \rightarrow {}^1D$ transition dominates. Note that the rapid drop in temperature reduces the ^1S state density and the $^1S \rightarrow {}^1D$ radiation rate so that after several hundred seconds the $^1D \rightarrow {}^3P$ transition dominates. This shift from predominantly green to predominantly red radiation is consistent with observations[10] of the Starfish high altitude nuclear explosion. (One should not expect these simplified calculations to accurately reproduce the temporal behavior observed in the actual nuclear burst event because too many relevant aspects of the magnetohydrodynamics, air chemistry, etc. have been omitted here.) Finally, we note that in this calculation one-half the initial energy was radiated during the first 2500 seconds.

We now turn our attention to radiation from atomic nitrogen; Figures 13, 14, and 15 contain computational results at the selected electron densities. The reader is reminded that as in the atomic oxygen calculations, nitrogen atom, electron, and non-radiating ion densities are equal. Figure 13 presents the results for an electron density of 10^4 cm^{-3}. Note that the excited state population densities never really reach a quasi-steady distribution, i.e., the excited state densities continue to increase as the electron temperature falls during the entire 30,000 second interval. Also note that at zero time the $^2p^0$ state density "instantly" jumps to a value near 10^{-1} cm^{-3}, and the radiation rates for transitions which originate from this level similarly jump to finite values. A plot with a greatly expanded time scale shows that the $^2p^0$ state density rises with an e-folding time of about 10 seconds, so the rise appears instantaneous on a 30,000 second time scale. Finally, the fraction of available energy tied up in excited states is seen to reach 7% at 30,000 seconds. If excited state energy and temperature drops are taken together, one can see that only about 3% of the initial energy has been radiated by the end of this calculation.

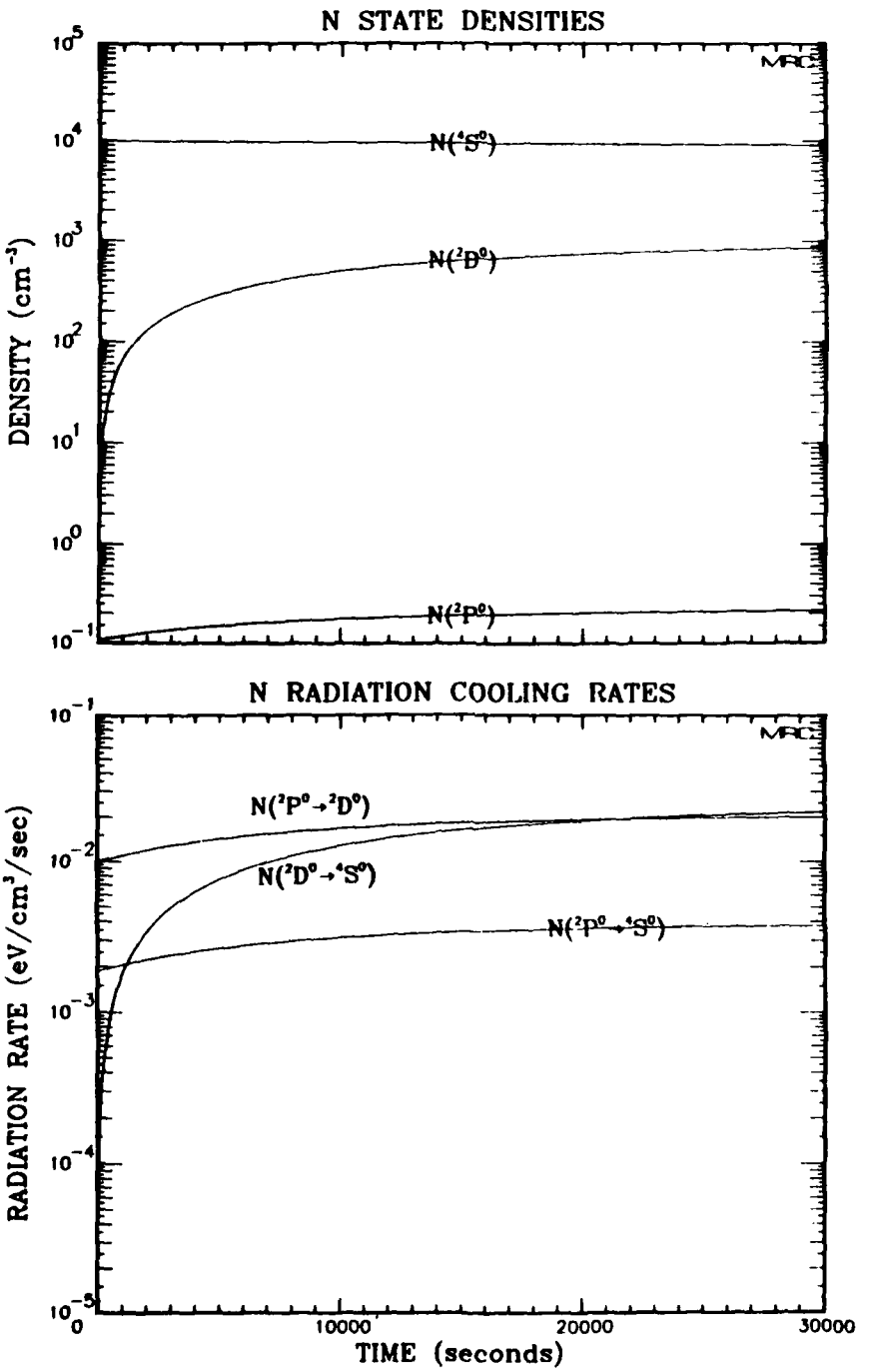

Figure 13. Radiation properties of N atoms at an electron density of 10^4 cm^{-3}.

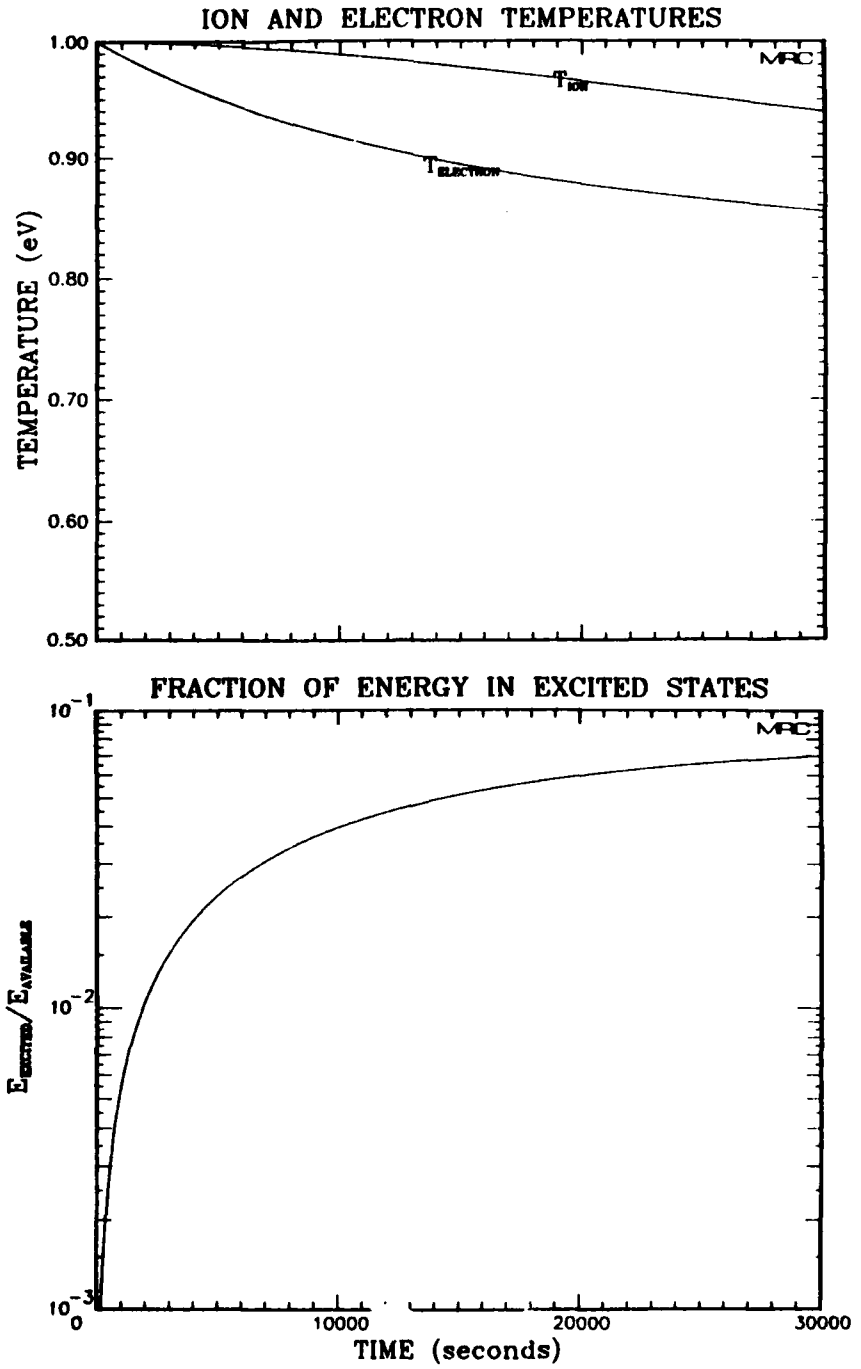

Figure 13 (Continued)

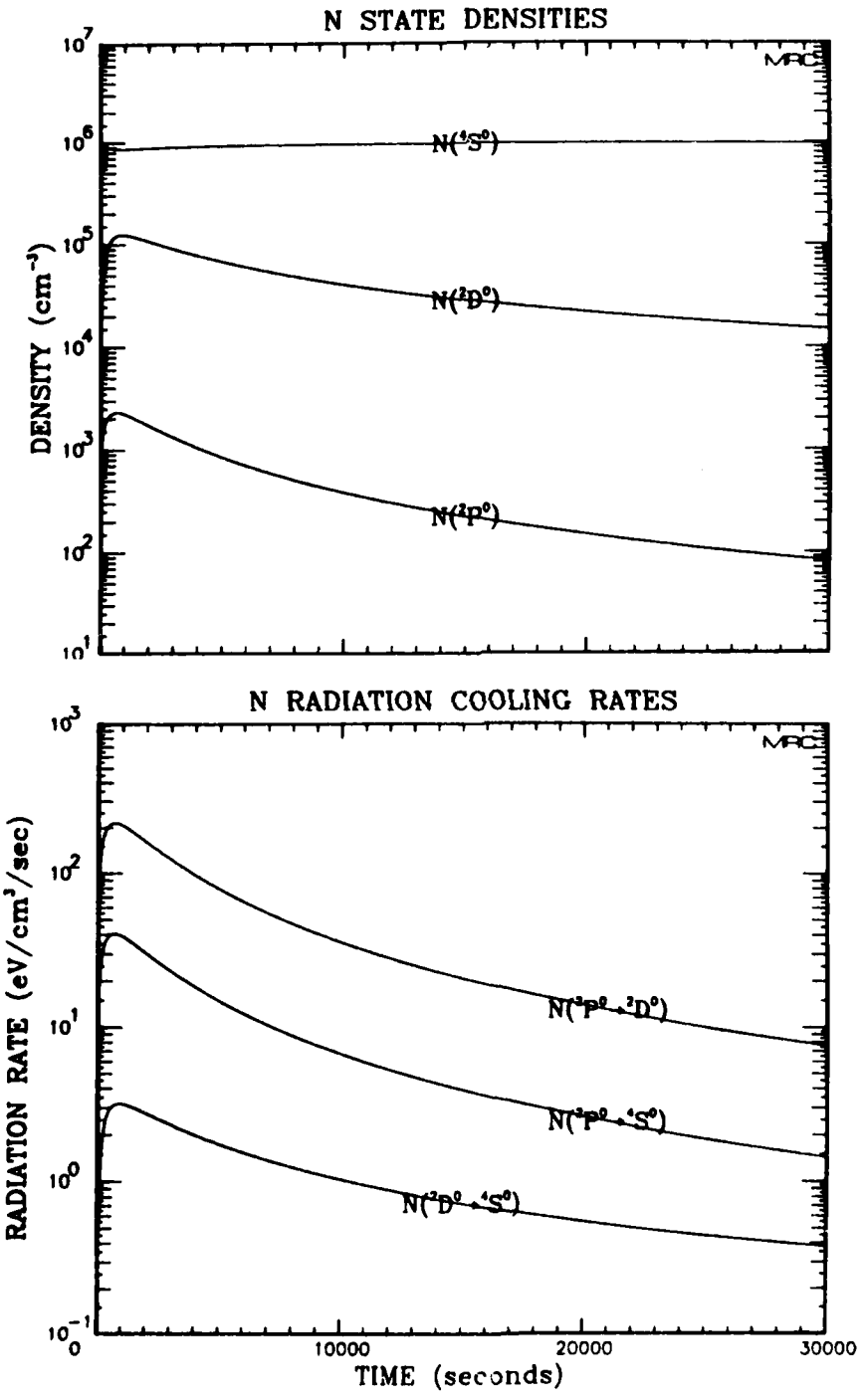

Figure 14. Radiation properties of N atoms at an electron density of 10^6 cm^{-3}.

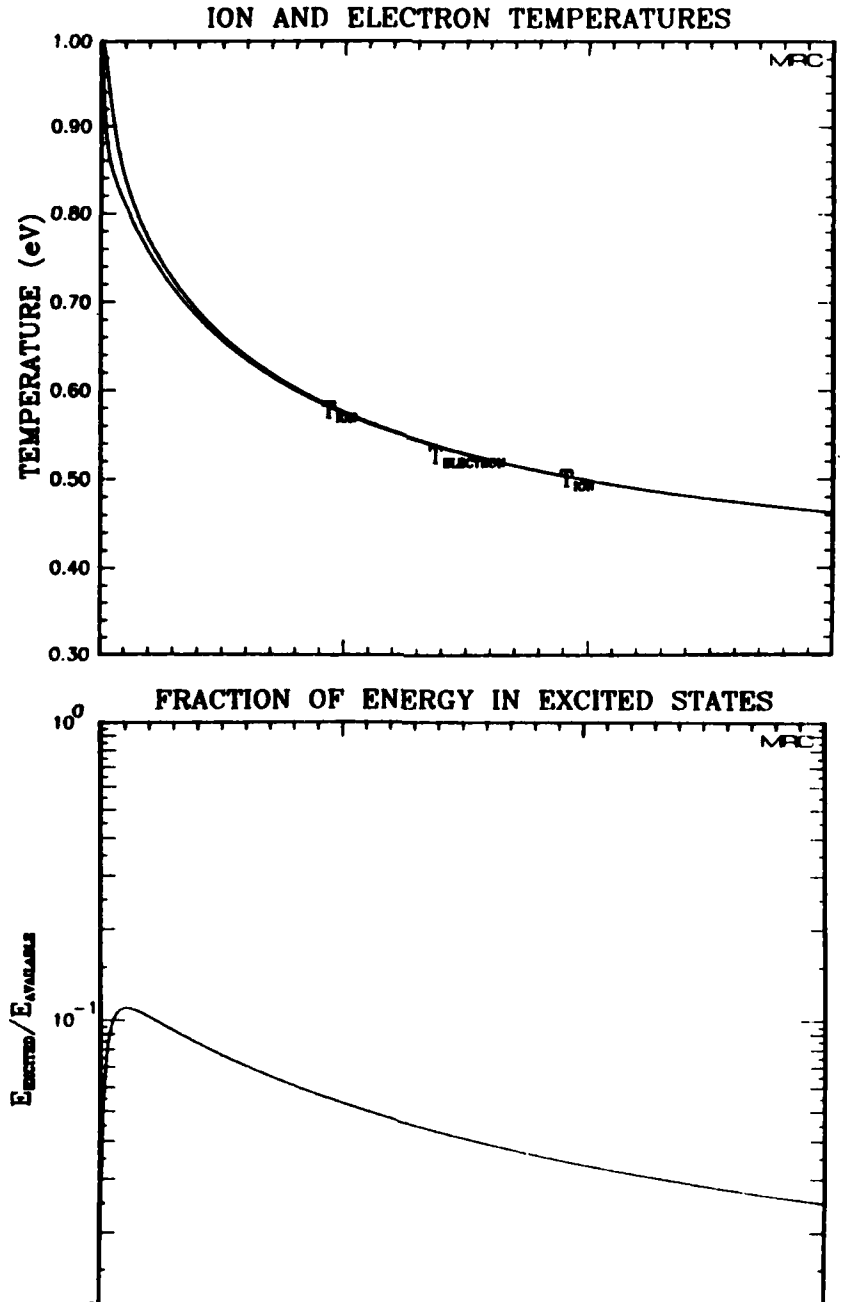

Figure 14 (Continued)

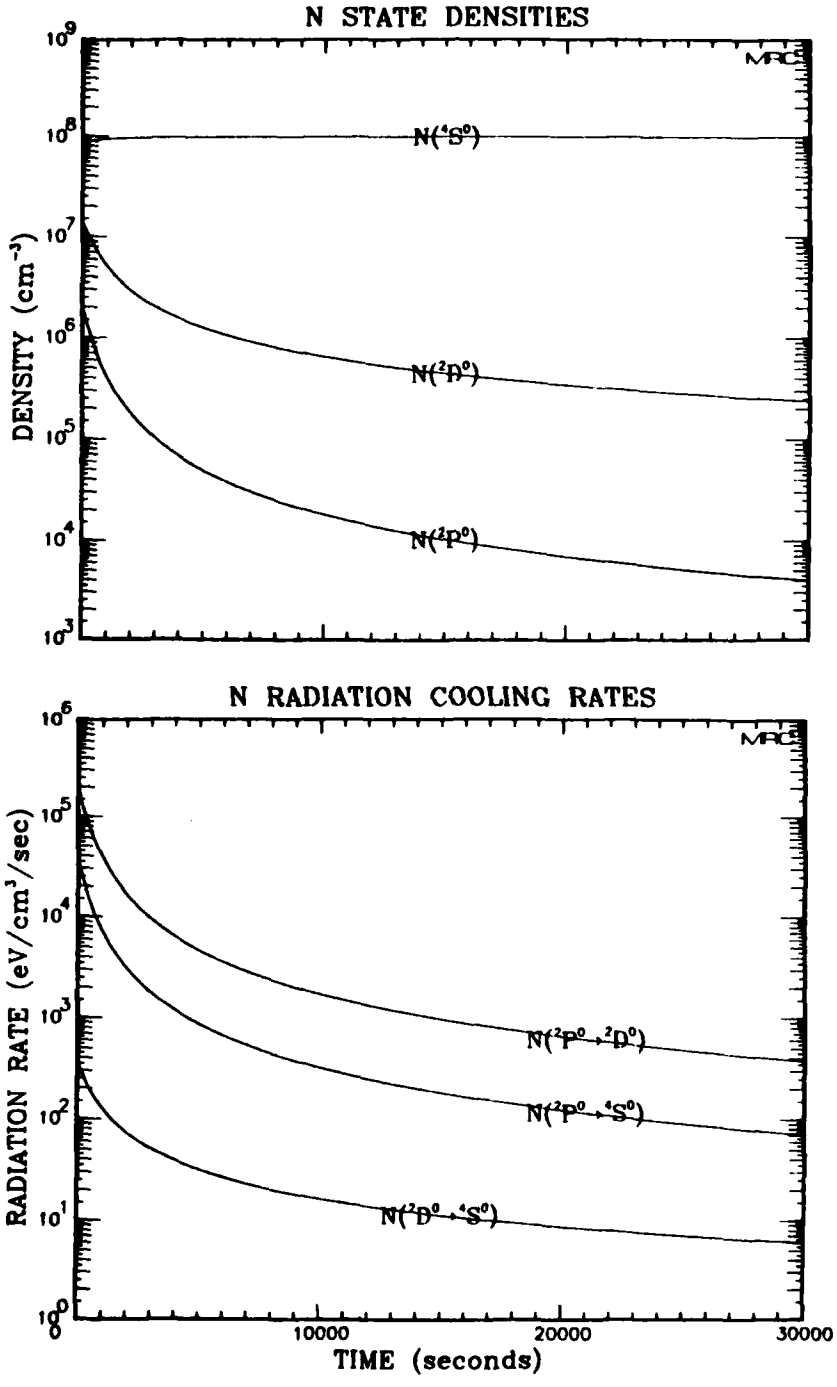

Figure 15. Radiation properties of N atoms at an electron density of 10^8 cm^{-3}.

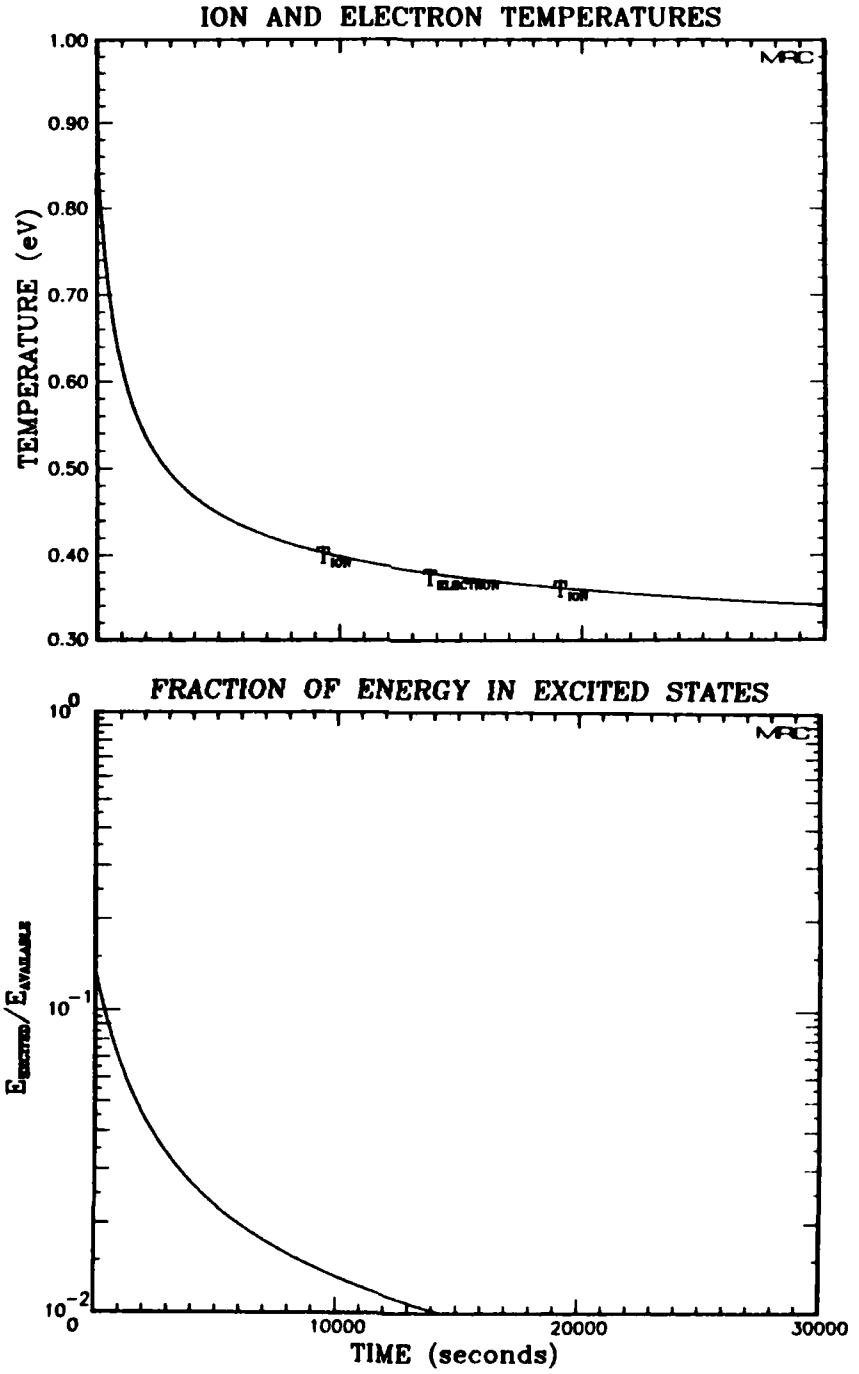

Figure 15 (Continued)

Calculations at electron densities of 10^6 and 10^8 cm^{-3} show quite different behavior. Both of these cases rapidly reach a quasi-steady configuration (less than 1000 seconds required at 10^6 cm^{-3}) and substantial fractions of the initial energy have been radiated. Although the curves denoting the energy fraction in excited states peak a bit above 10%, they decay to about 3.5% by the time one-half the initial energy has been radiated (~20,000 seconds at 10^6 cm^{-3}; ~3000 seconds at 10^8 cm^{-3}). In these cases, the infrared ($^2P^0 \rightarrow {}^2D^0$) transition is responsible for the bulk of the cooling. Observe that in both Figures 14 and 15, the $^2D^0$ state density peaks at about 13% of the total nitrogen atom density. This common feature arises because the radiative transition probability from the state (see Table 1) is quite low, so collisional excitation and deexcitation is responsible for establishing the state density in accord with a Boltzmann distribution, i.e., the ratio of excited state densities in Equation 13 becomes independent of electron density.

Calculations of radiations from O_2 are considered next. Once more, the O_2 density has been equated to the ion and electron densities. Figures 16, 17, and 18 contain the relevant plots. The ground and excited states, $X^3\Sigma_g^-$, $a^1\Delta_g$, and $b^1\Sigma_g^+$, have been abbreviated as $^3\Sigma$, $^1\Delta$, and $^1\Sigma$ in these figures. Also note that the present calculations considered only two optical transitions, as mentioned earlier.

Figure 16 details the excitation and radiation characteristics of O_2 at an electron density of 10^4 cm^{-3}. From the first parts of the figure, it's clear that the $^1\Delta$ state requires about 10,000 seconds to attain a quasi-steady state but the $^1\Sigma$ state is populated virtually instantly as compared to the time scale of these calculations. The radiation rates reflect these excitation characteristics. At this electron density, much less than a percent of the available energy goes into excited states, and only about 2-1/2% of the initial energy is radiated during the calculation time.

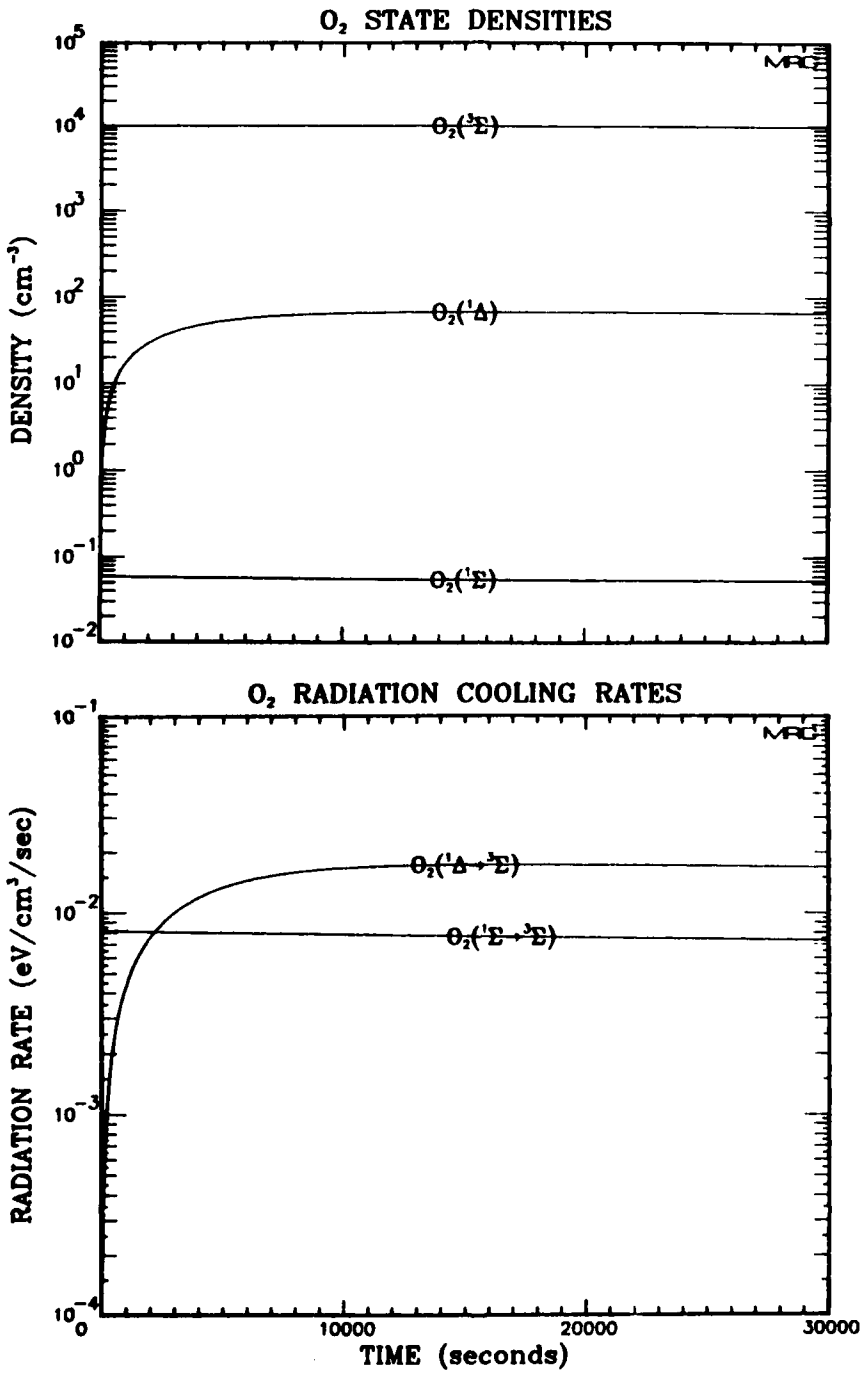

Figure 16. Radiation properties of O_2 at an electron density of 10^4 cm^{-3}.

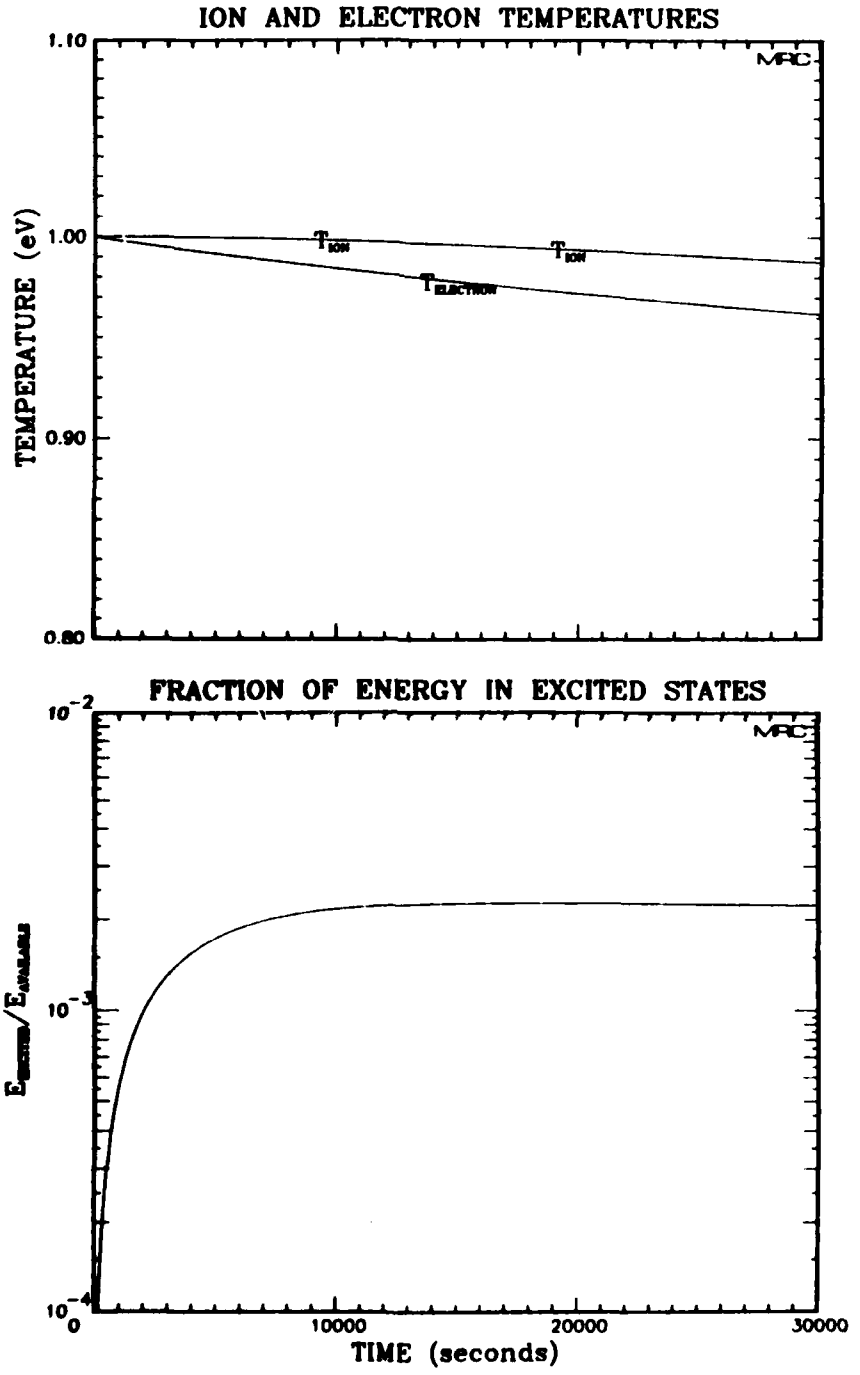

Figure 16 (Continued)

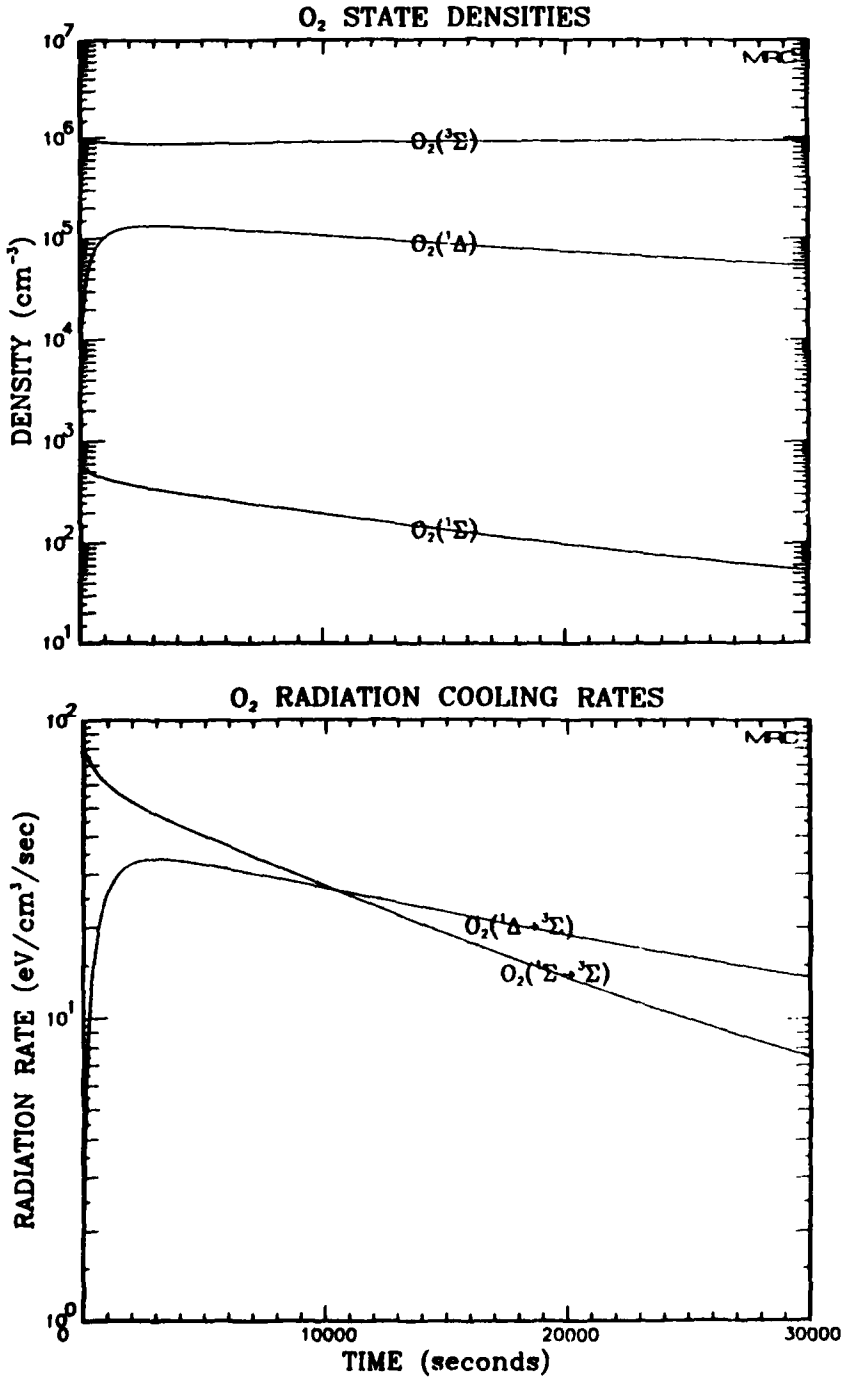

Figure 17. Radiation properties of O_2 at an electron density of 10^6 cm^{-3}.

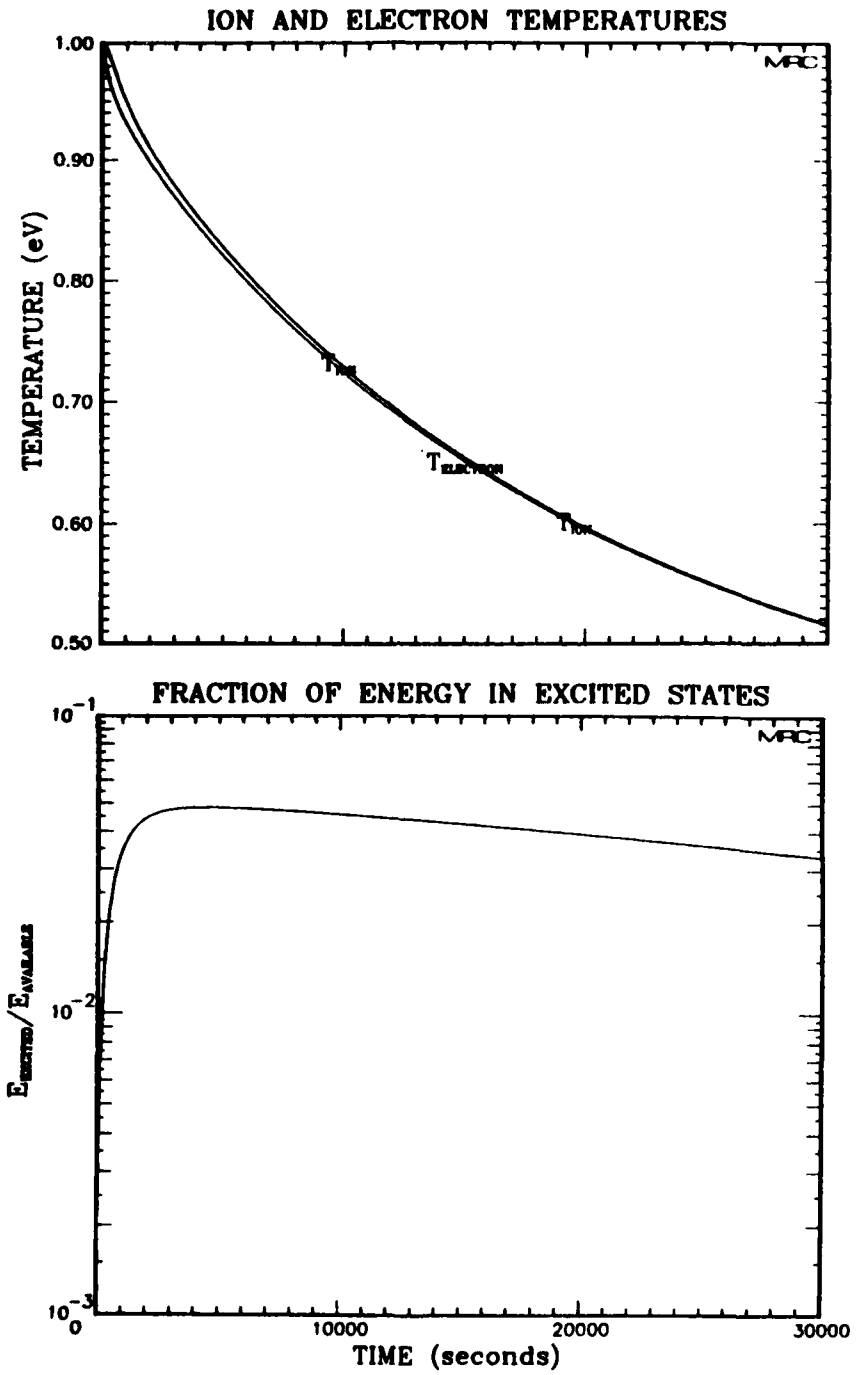

Figure 17 (Continued)

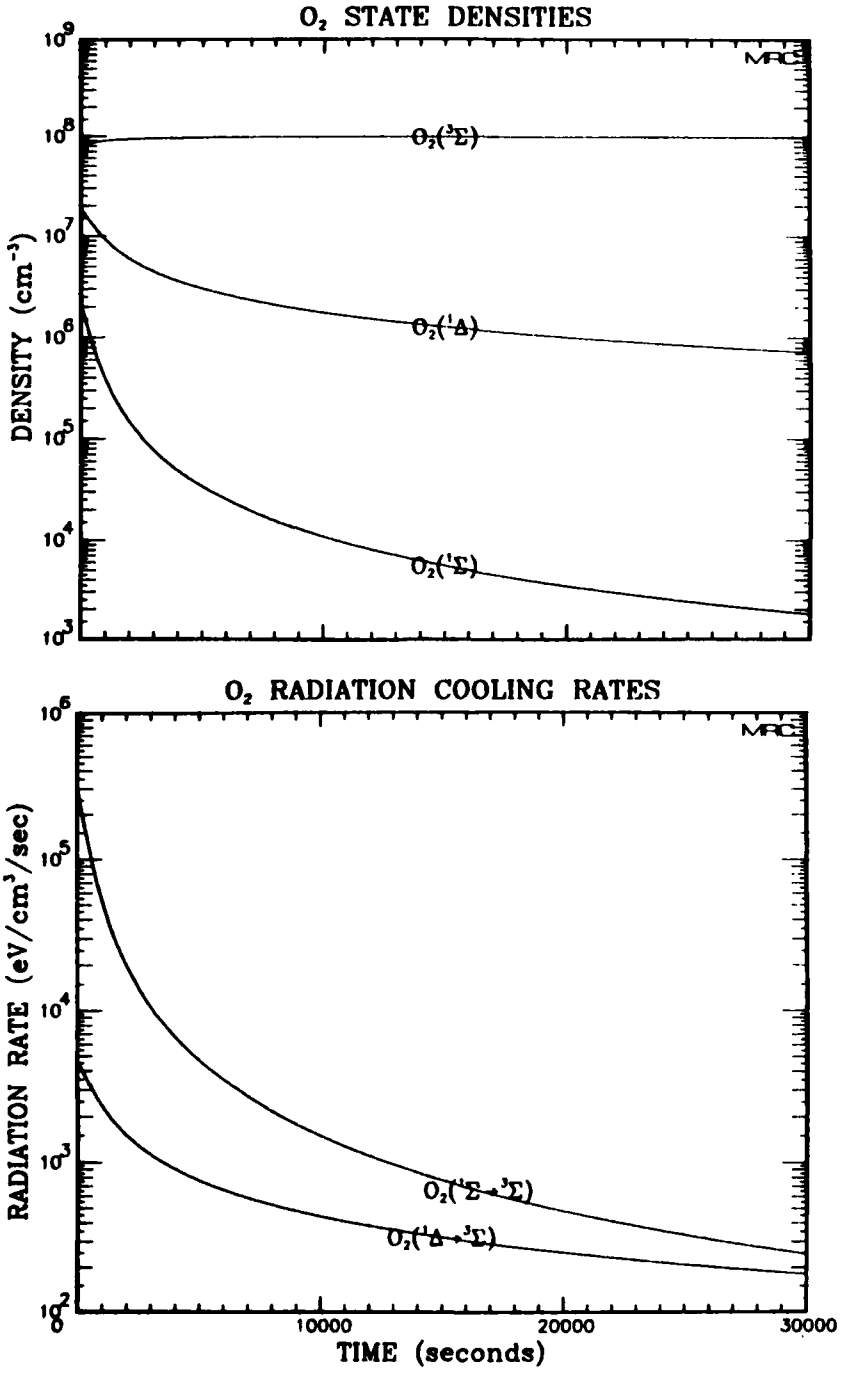

Figure 18. Radiation properties of O_2 at an electron density of 10^8 cm^{-3}.

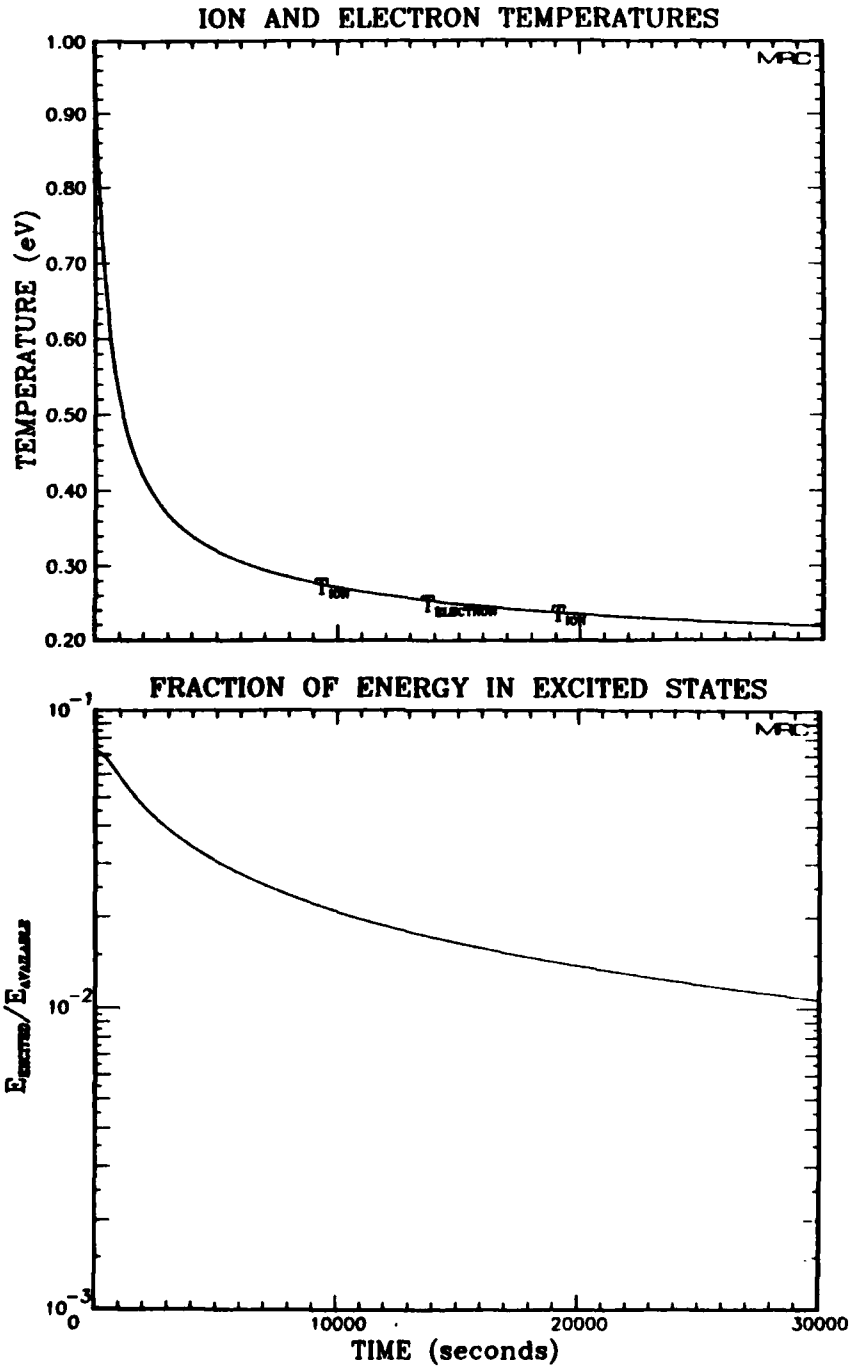

Figure 18 (Continued)

At higher electron densities, the O_2 radiation characteristics are quite different. At 10^6 cm^{-3} (Figure 17), the quasi-steady state is attained in about 2500 seconds, and radiation removes nearly one-half the initial energy, as indicated by the temperature curves. At most, only about 5% of the available energy is tied up in excited states. Note that prior to ~10,000 seconds, radiation from the $^1\sum \rightarrow {}^3\sum$ transition was the dominant cooling mechanism, but afterwards the $^1\Delta \rightarrow {}^3\sum$ transition dominates.

Figure 18 illustrates that at 10^8 cm^{-3} electron density, the quasi-steady state is obtained instantaneously as compared to the computation time span. The $^1\sum \rightarrow {}^3\sum$ transition is seen to be dominant over the full 30,000 second period and is chiefly responsible for the energy loss over the entire computation. About 1500 seconds were required to radiate one-half the initial energy. Note that in this case, radiation cooling lowered both ion and electron temperatures to 0.22 eV after 30,000 seconds. This particularly low temperature could be achieved because the metastable levels of O_2 are quite low as compared to the metastable states of O^+, O, N^+, and N (Refer to Figure 1). Finally, observe that in this calculation the peak fraction of available energy in excited states was about 7%.

To complete the discussion of these three cases, it's worth pointing out the trend as to which of the O_2 transitions dominates. At 10^4 cm^{-3} electron density (Figure 16), the $^1\sum \rightarrow {}^3\sum$ transition is dominant for only the first 2000 seconds; at 10^6 cm^{-3} (Figure 17) it's dominant for the first 10,000 seconds, and at 10^8 cm^{-3} (Figure 18), it dominates for the entire 30,000 seconds. This trend is not a direct temperature effect (lower ultimate temperatures at higher electron densities) because the $^1\Delta$ state is lower energy than is the $^1\sum$ state. Instead, the trend is explained by Equation 13, i.e., it is the play-off between collisional and radiative processes which is important. There is an indirect temperature effect insofar as the collisional excitation and deexcitation rate coefficients are temperature dependent.

The discussion of single species systems is now complete. The remainder of this section will be devoted to calculations based on species densities and initial electron and ion temperatures extracted from detailed high altitude nuclear burst calculations. In these calculations, the time scale has been adjusted to span the most interesting phase of the radiation cooling process.

The Starfish high altitude nuclear test event, conducted on 9 July 1962 during the Fishbowl series, consisted of a 1.4 megaton device detonated at 400 km altitude above Johnston Island in the Pacific. Recently, Fajen[25] has performed a series of detailed two-fluid magneto-hydrodynamic calculations of the Starfish event. The results of his computer simulations contain the best available spatially and temporally resolved estimates of electron and species densities, ion and electron temperatures, and coupled ion-neutral dynamics. Numerical data corresponding to 90 seconds after detonation have been extracted from Fajen's calculations and have been used as the time equals zero initial conditions for radiation cooling calculations which are presented in Figures 19 and 20. The reader may wish to refer to Table 2 for a summary of these data.

Figure 19, which corresponds to an altitude of 395 km, illustrates an element of fireball plasma which is predominantly atomic neutrals (N and O) at a total atom density of 9.6×10^8 cm^{-3}. Oxygen ions are the least populous species (10^4 cm^{-3}); the nitrogen ion density is about 0.75% of the neutral atom density. Molecular oxygen has a density of about 0.25% of the neutral atom density. The plots indicate that with the exception of O_2, the initial transients required to populate the excited states are finished in a few tens of seconds. As one might expect, based on the preponderance of oxygen atoms and the relatively low temperature, radiation in the oxygen red line ($^1D \rightarrow {}^3P$ transition) is the major cooling mechanism; the electron temperature is too low to effectively excite the oxygen green line ($^1S \rightarrow {}^1D$ transition). The second most

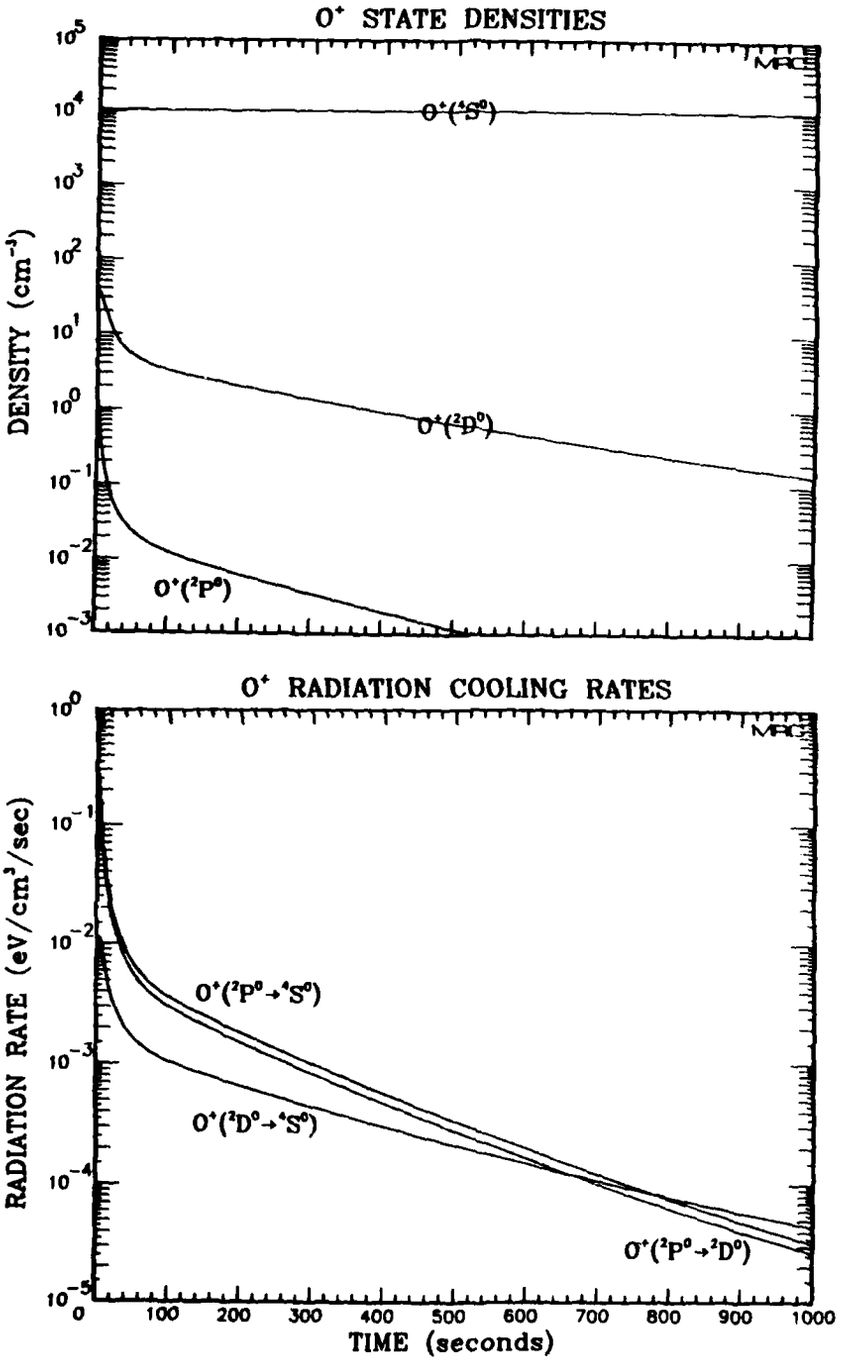

Figure 19. Radiation properties based on the 90 second environment at 395 km altitude in Fajen's Starfish calculation.

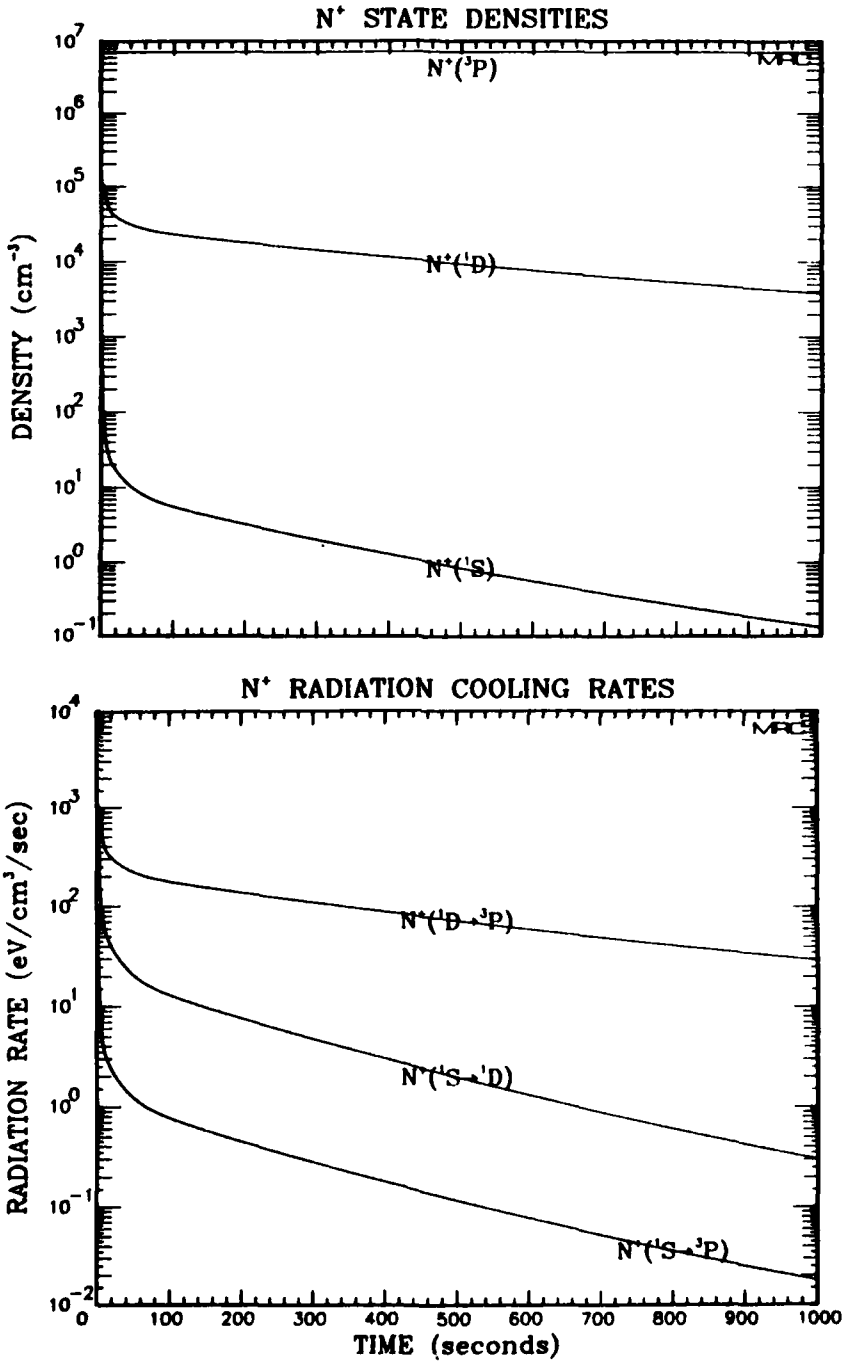

Figure 19 (Continued)

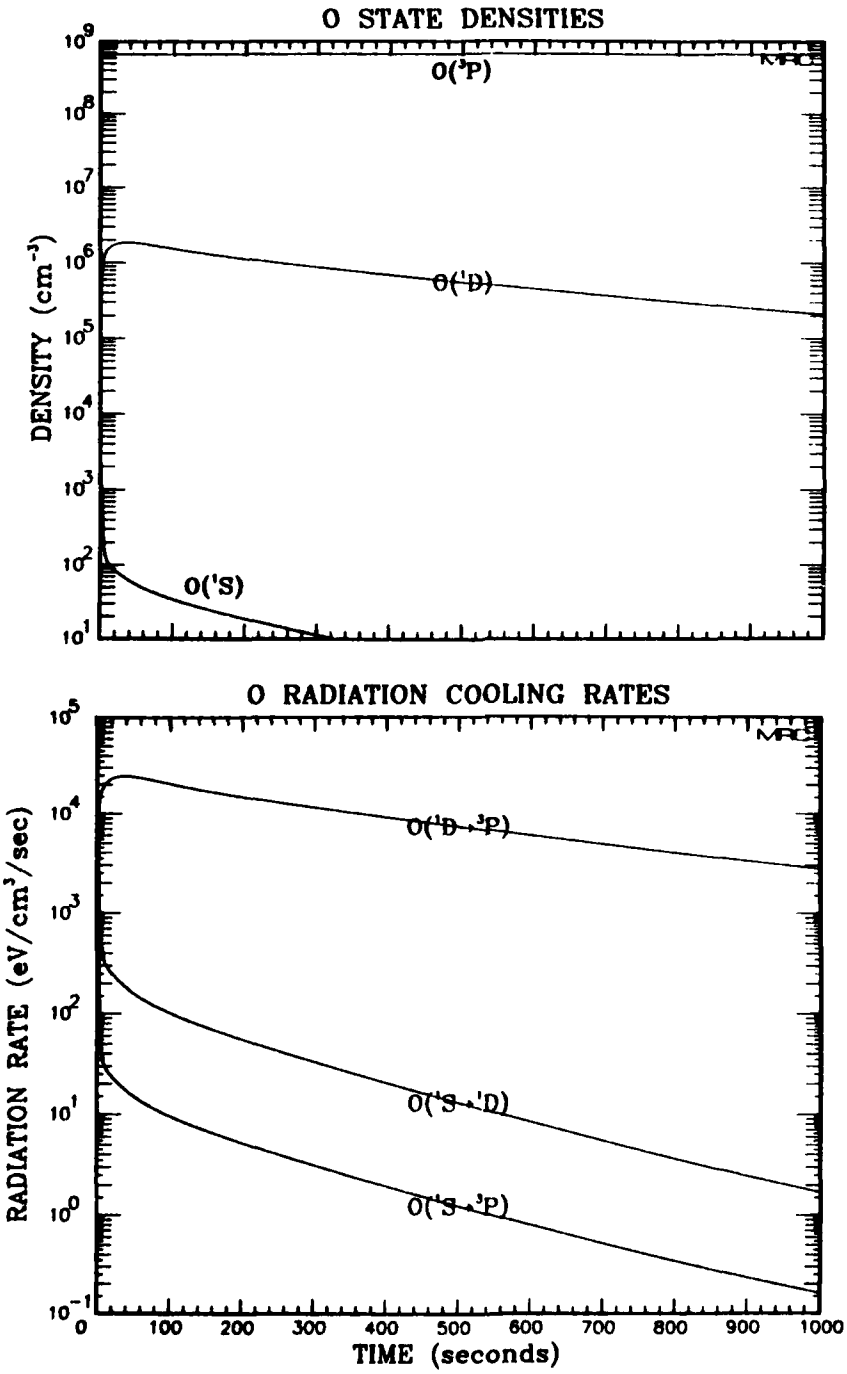

Figure 19 (Continued)

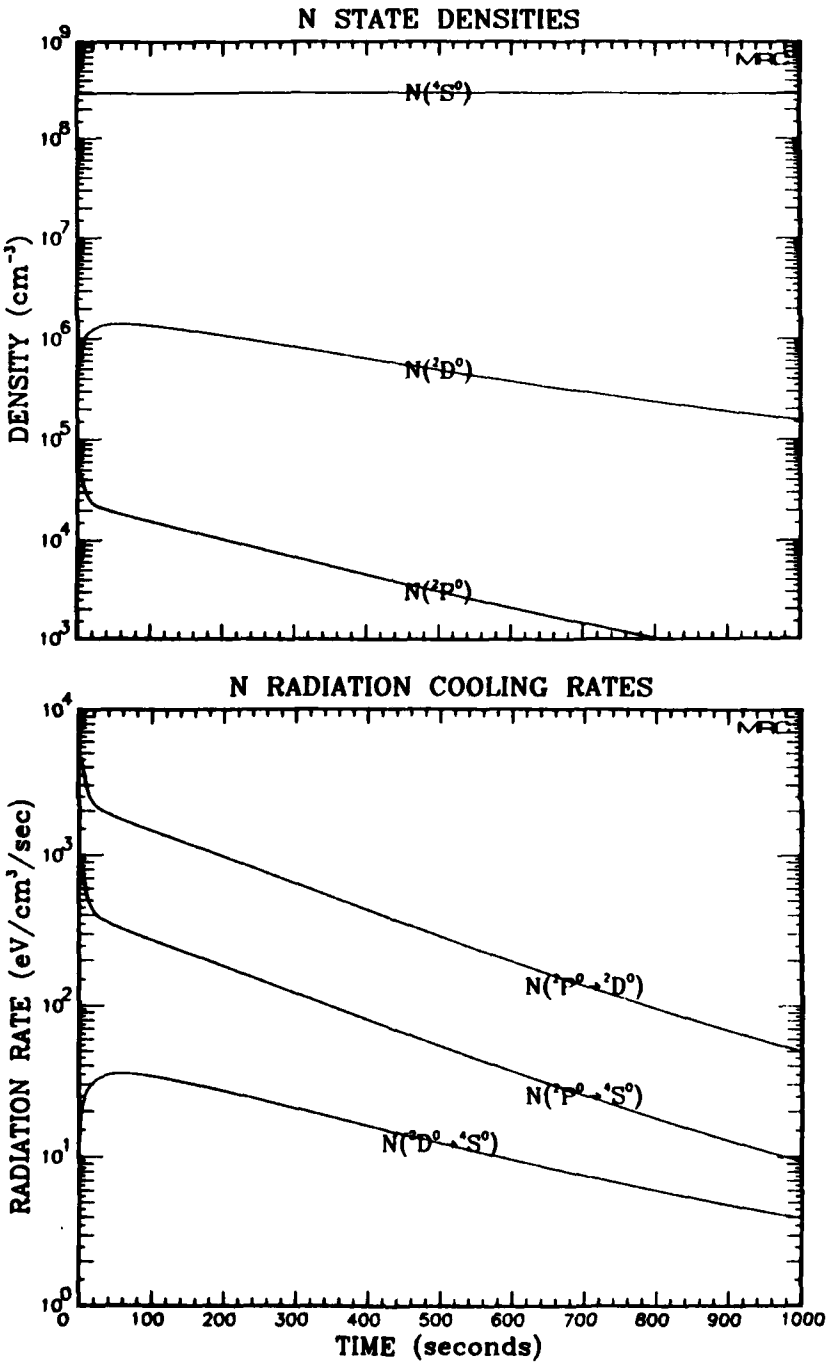

Figure 19 (Continued)

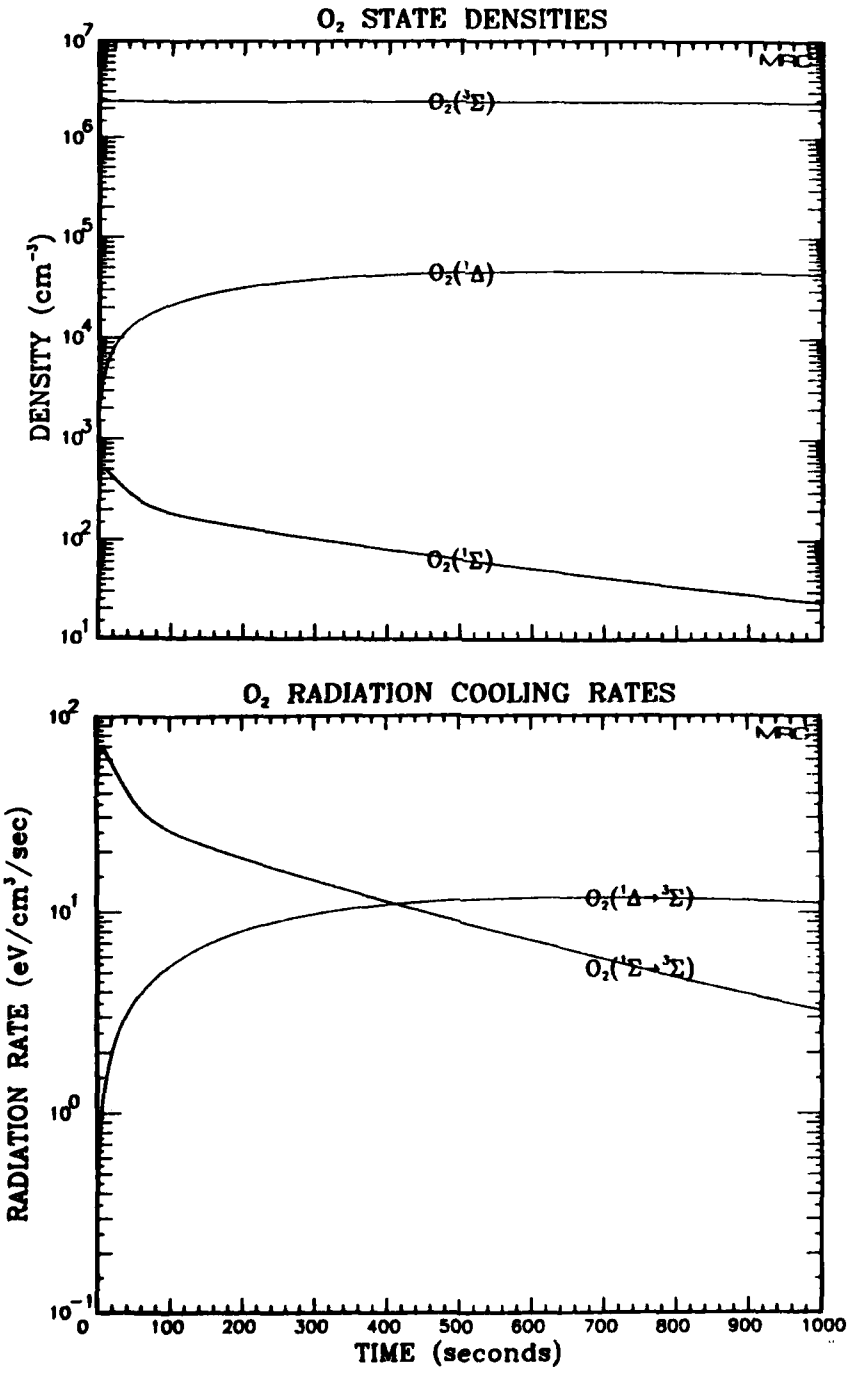

Figure 19 (Continued)

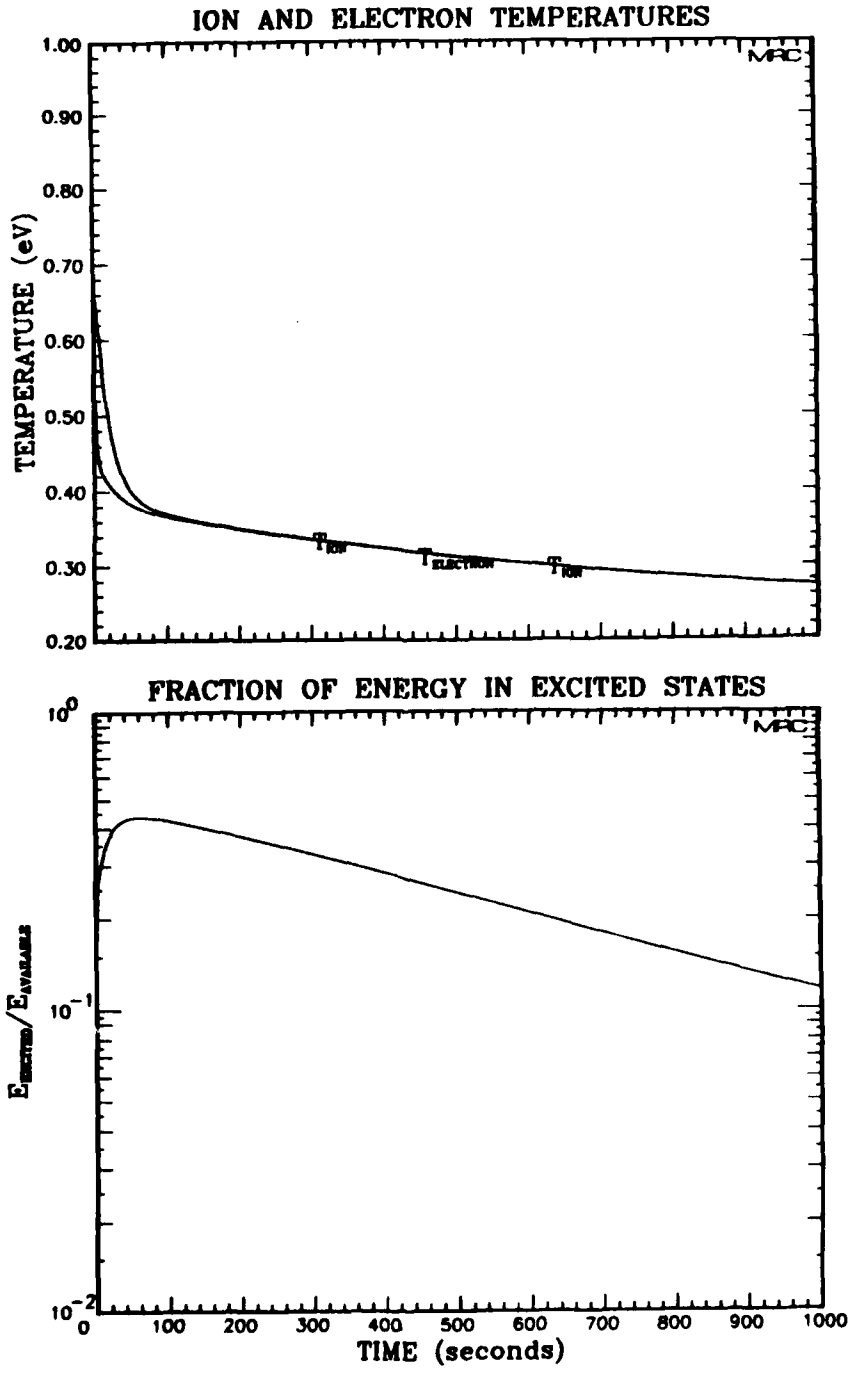

Figure 19 (Continued)

active transition (energy-wise) is the infrared $^2p^0 \rightarrow ^2D^0$ transition in atomic nitrogen, but after about 50 seconds (i.e., 140 seconds after detonation) the energy loss rate is about a factor of ten below that for the oxygen red line. For this particular calculation, other transitions and species are relatively unimportant to the cooling process.

The fraction of available energy tied up in excited states is seen in Figure 19 to peak at about 45%, a value substantially larger than found in previous calculations. This large fraction ocurs because the ratio of atoms to free electrons is large (~100), and the electrons have sufficient thermal energy to populate the excited states. Thus, nearly half the avaialble energy is rapidly stored as excited state energy.

The calculation depicted in Figure 20 corresponds to conditions extracted from Fajen's Starfish simulation at 90 seconds after burst at 550 km altitude. In this case the electron density and neutral atom densities are nearly equal. The O^+ density is about a factor of 2 larger than the N^+ density, while the O density is about a factor of 3 larger than the N density. Molecular oxygen is a minor constituent. Although both ion and electron temperatures were about 1.5 eV initially, very rapid collisional processes caused these temperatures almost instantly to drop to about an eV. In conjunction, we note that the fraction of available energy in excited states peaks at nearly 18% quite early in the calculation. It's also interesting to observe that except for N and O_2, the population densities of the first excited states of the species reach 10% of the density of the respective ground states. For N and O_2, the first excited state populations reach about 25% of the respective ground state densities.

The combined action of the ionic and atomic radiators, all of which are radiating at roughly the same rate, is to remove about 59% of the initial energy over the 1000 second time span. (Keep in mind that

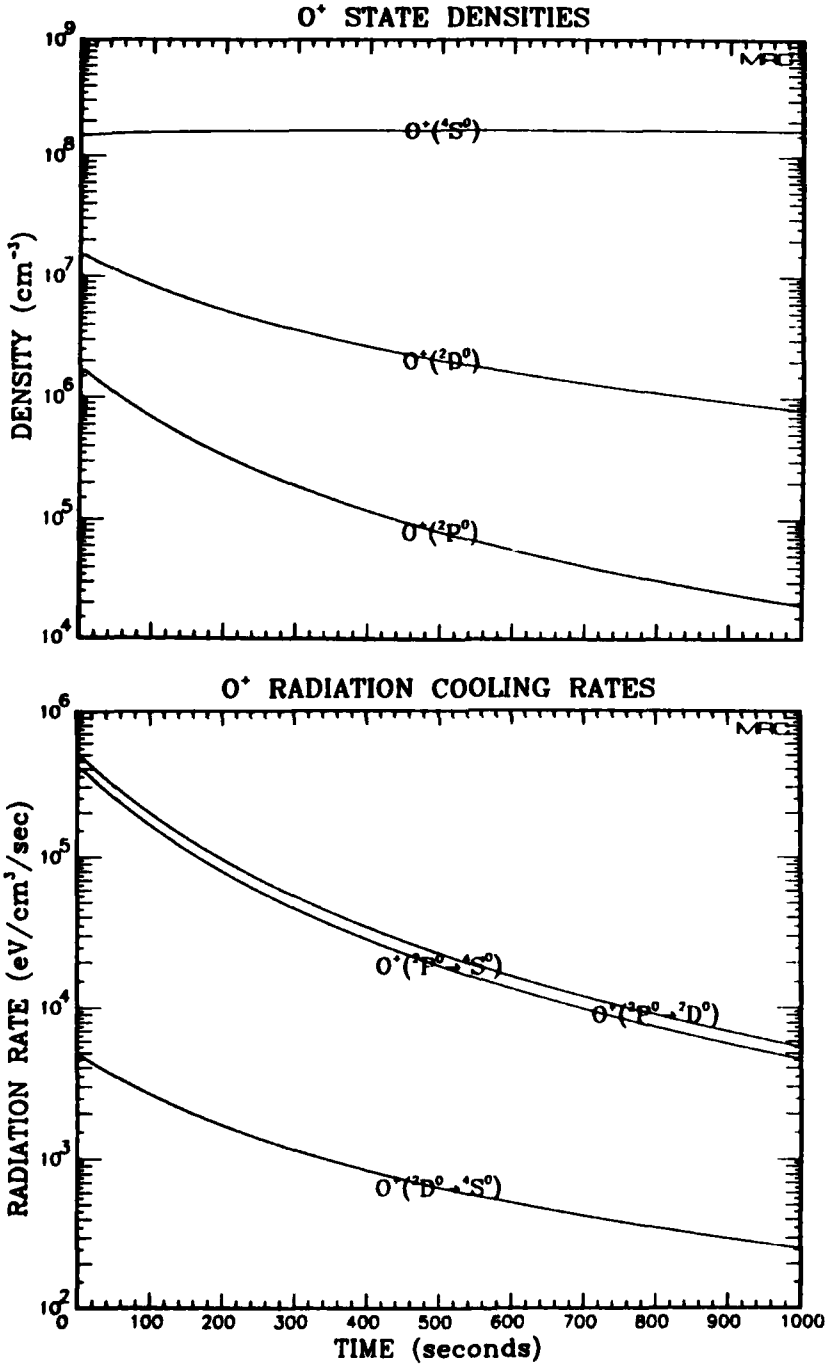

Figure 20. Radiation properties based on the 90 second environment at 550 km altitude in Fajen's Starfish calculation.

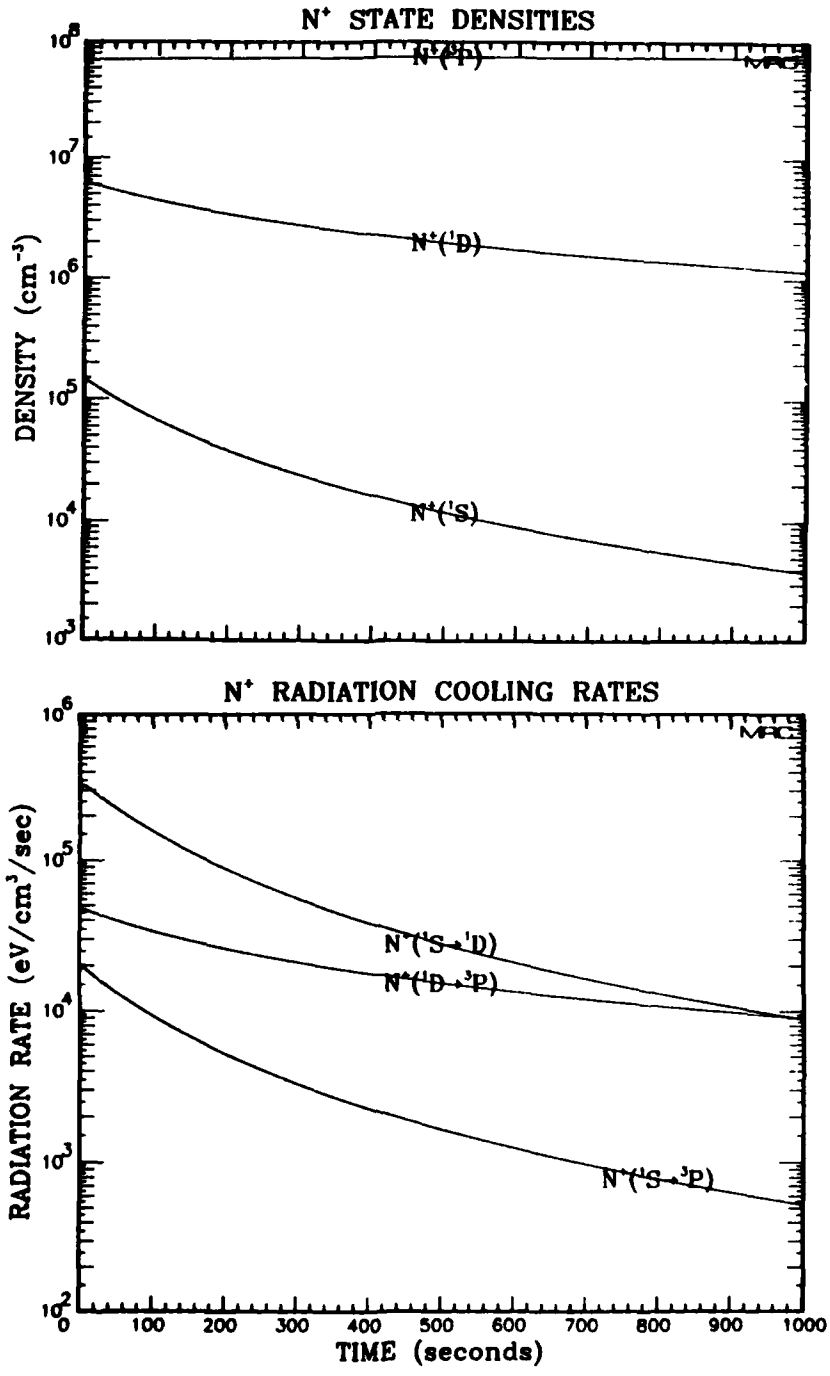

Figure 20 (Continued)

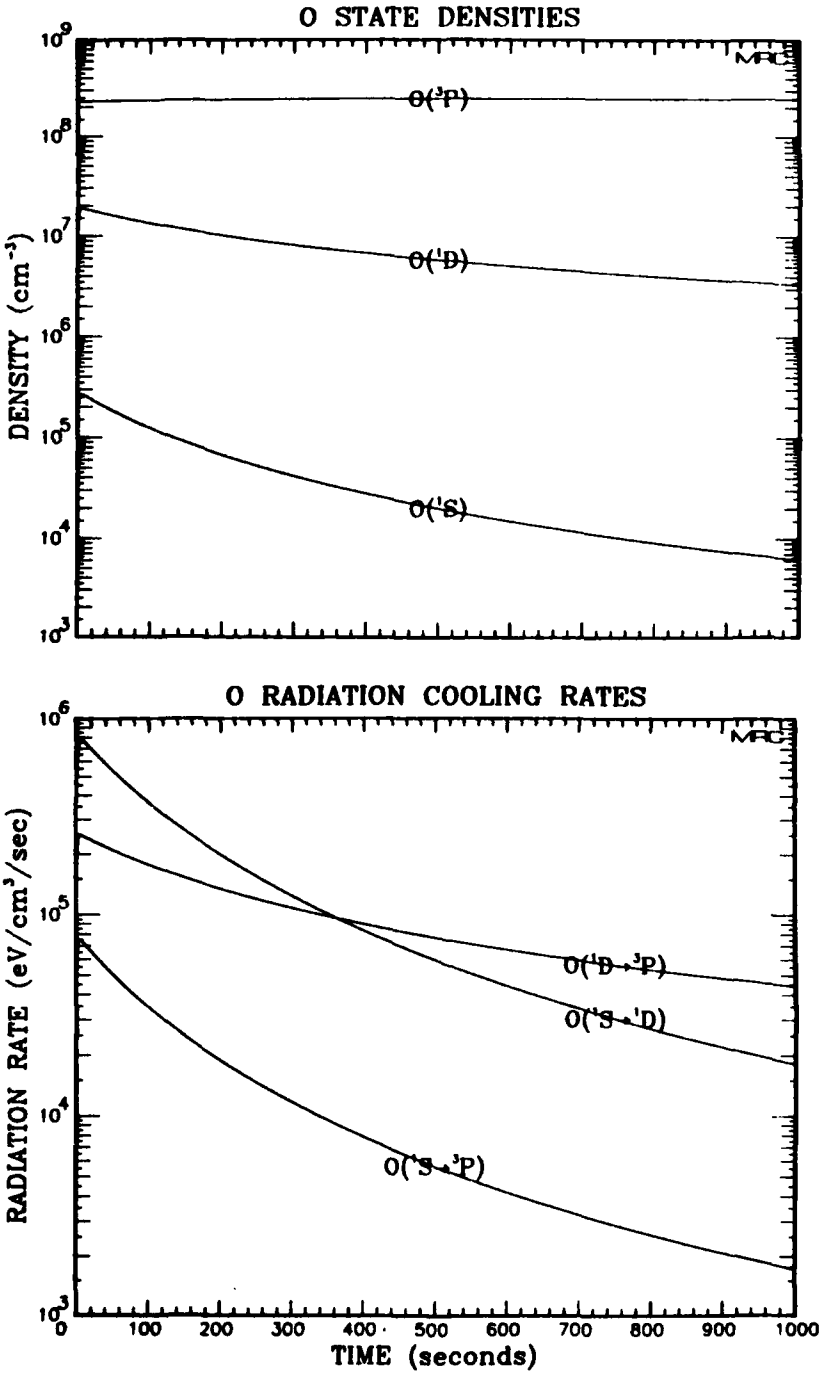

Figure 20 (Continued)

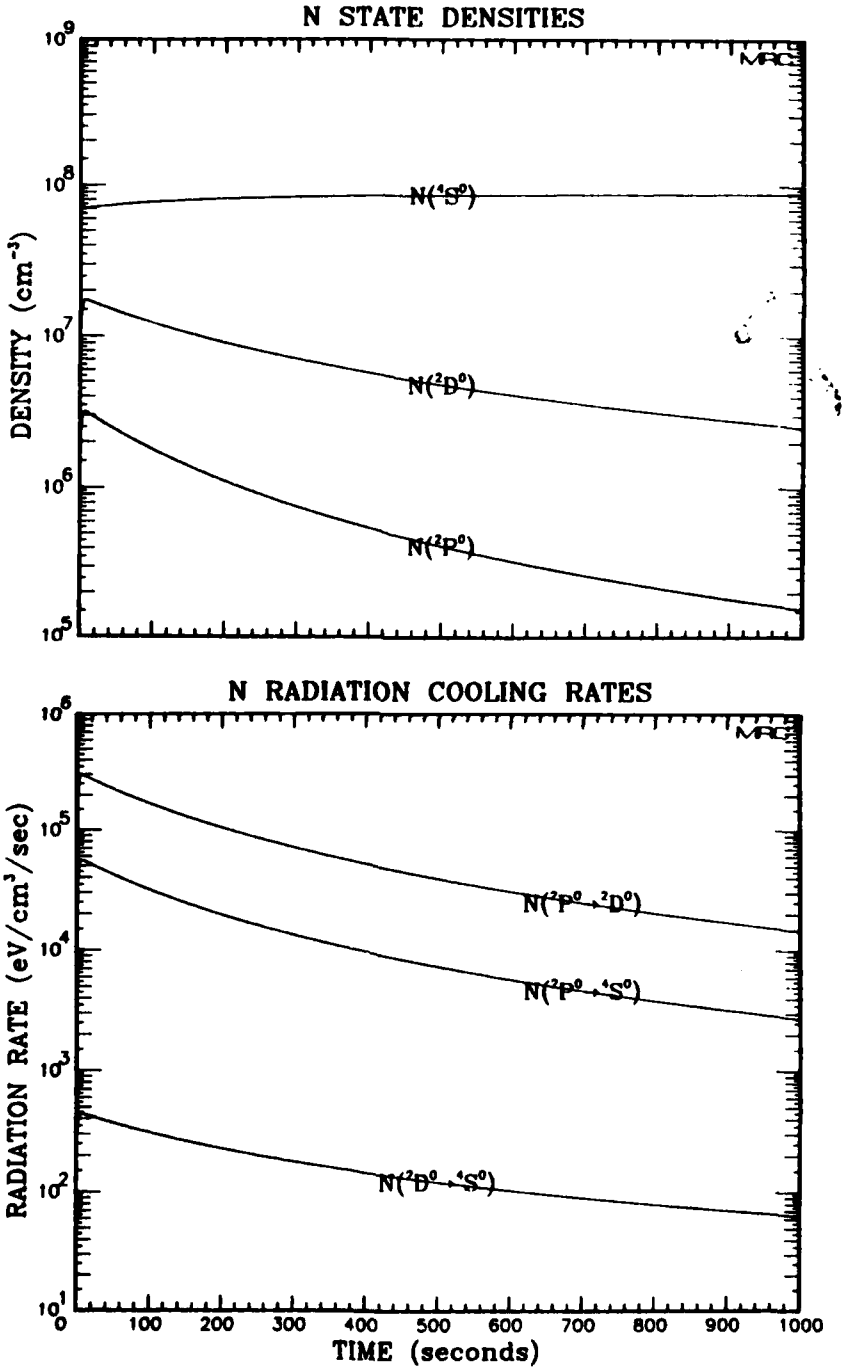

Figure 20 (Continued)

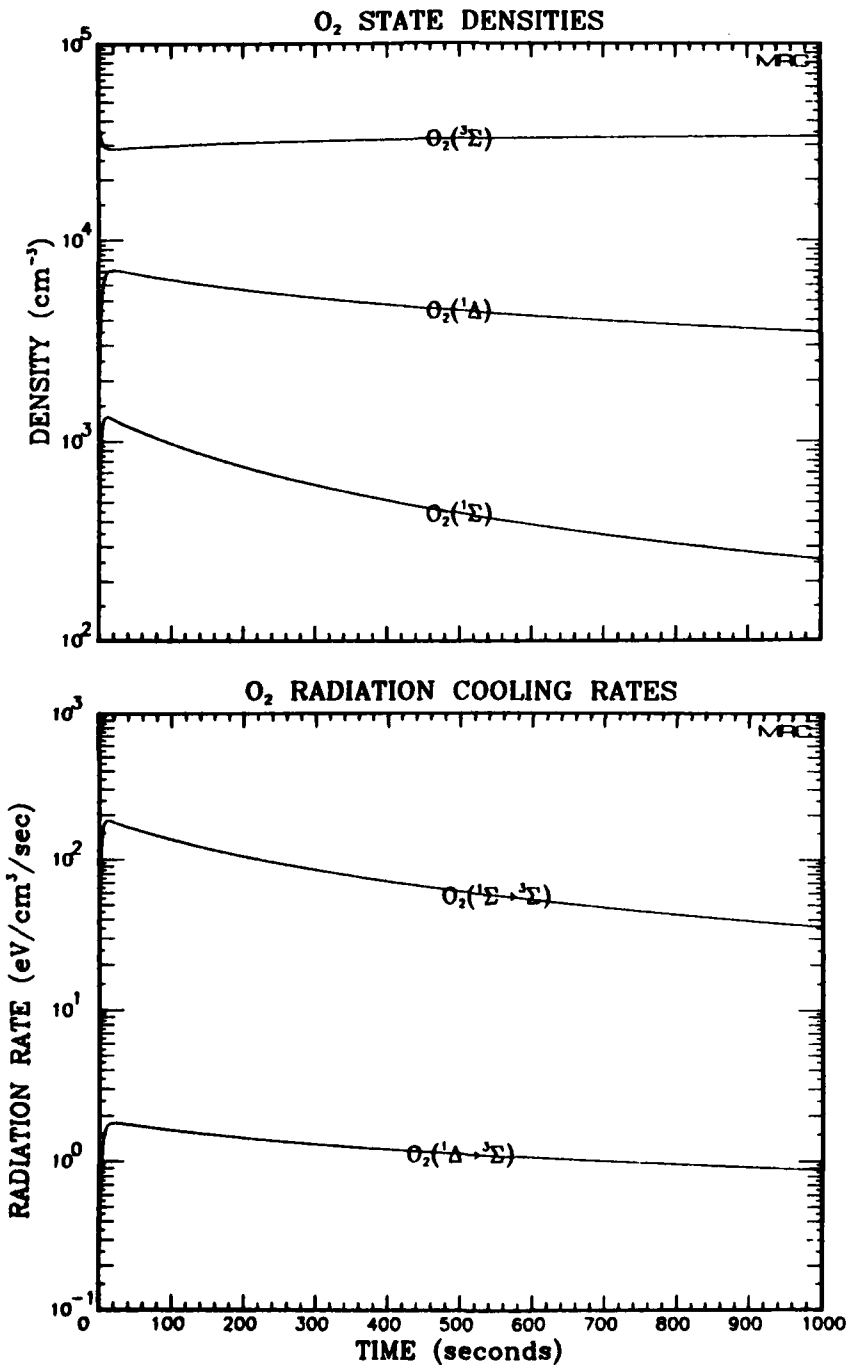

Figure 20 (Continued)

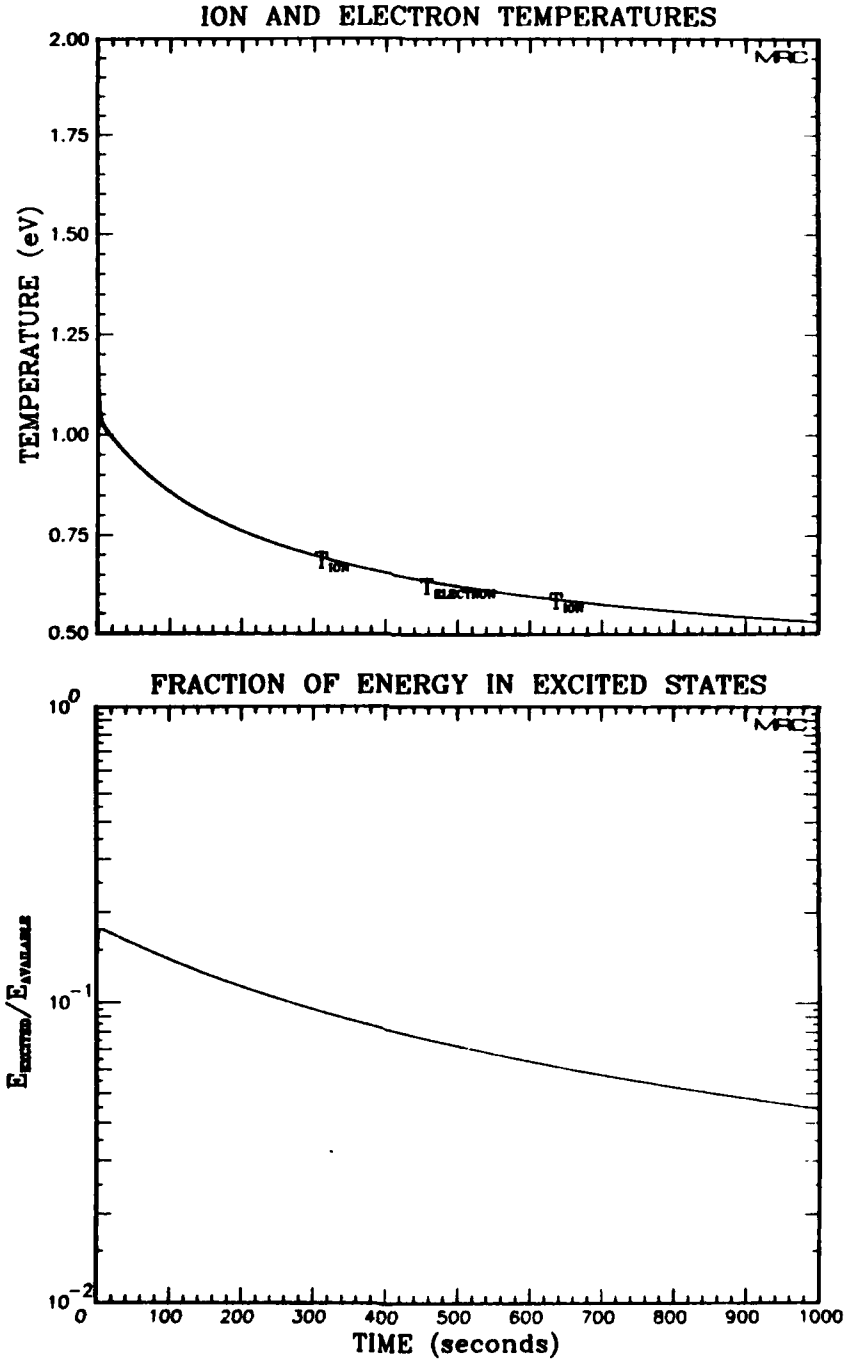

Figure 20 (Continued)

these calculations do not include effects of fluid motion, deionization chemistry, etc. which would act in a complete and self-consistent calculation during the 1000 second span to alter the available thermal energy and, hence, the radiation rate.) Radiation from molecular oxygen is negligible, from the cooling standpoint, because the O_2 density is so low.

In order to investigate radiation cooling and energy partition long after a nuclear detonation, we consider the high altitude environment predicted by a detailed, two-fluid numerical simulation [26] of a megaton-range explosion at 200 km altitude. Calculations depicted in Figure 21 and 22 represent, at time zero, species densities and temperatures extracted from the detailed simulation at 60 minutes after detonation. These radiation computations span almost 3 hours.

The calculation presented in Figure 21 represents the environment at 850 km altitude within a dense portion of the geomagnetic field aligned fireball/plume. As indicated in Table 2, the electron density is slightly above 10^8 cm^{-3}, and the predominant species are ions. Ion and electron temperatures were both initialized to 0.504 eV at the beginning of the radiation cooling calculation. One finds that this system almost instantaneously attains a quasi-steady state with only a bit more than one percent of the available energy associated with excited states. An examination of radiation rate curves reveals that nitrogen ions are the most active radiators. In fact, N^+ transitions radiate, over 10,000 seconds, more energy than all of the other species combined; about 30% of the initial energy is radiated during this interval.

The final case to be considered is shown in Figure 22 and represents conditions extracted from the aforementioned simulation at 60 minutes after detonation. This set of species and temperatures represents the environment at 1000 km altitude in a region within the geomagnetic field aligned fireball/plume plasma but outside of its dense core. Ionic

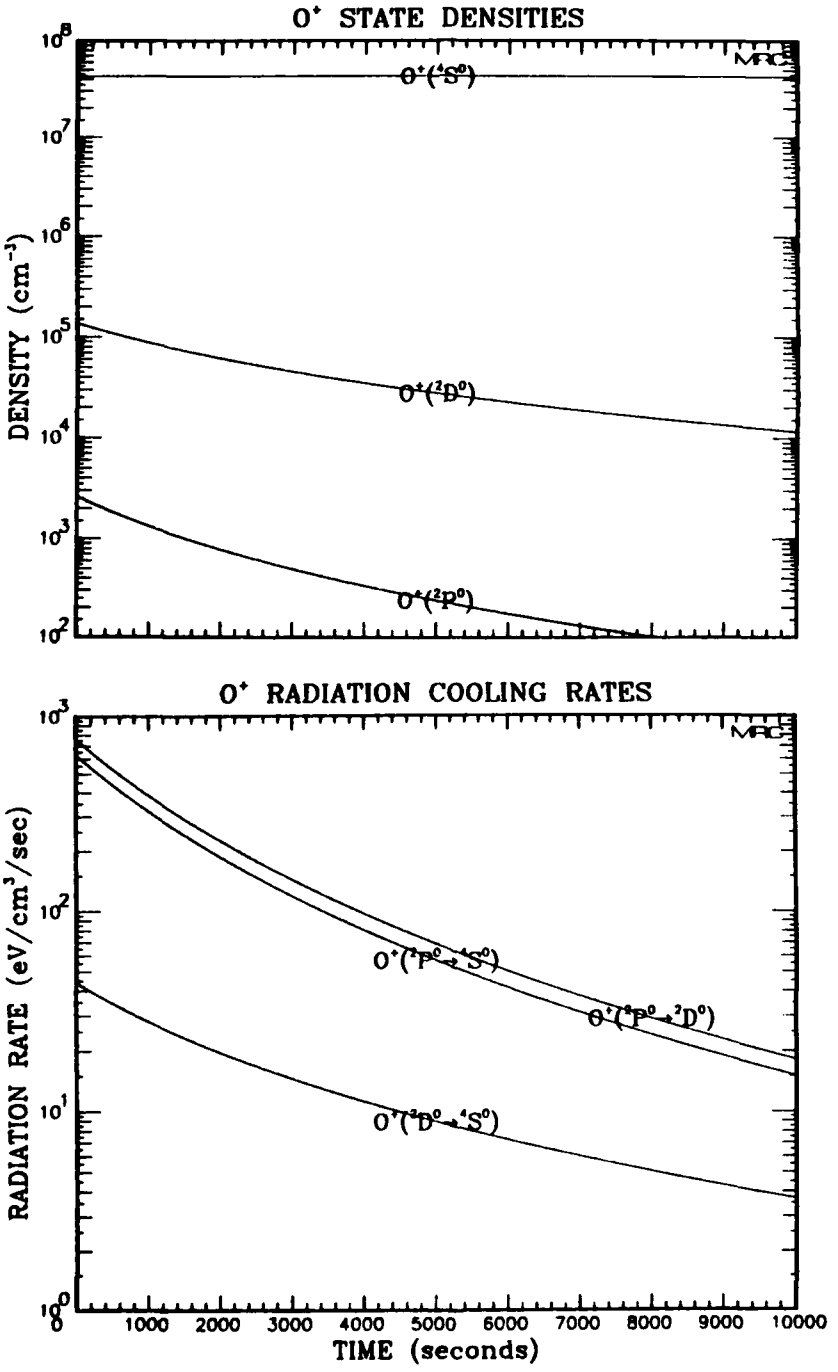

Figure 21. Radiation properties based on the 60 minute environment at 850 km altitude in a calculation of a megaton-range nuclear explosion at 200 km altitude.

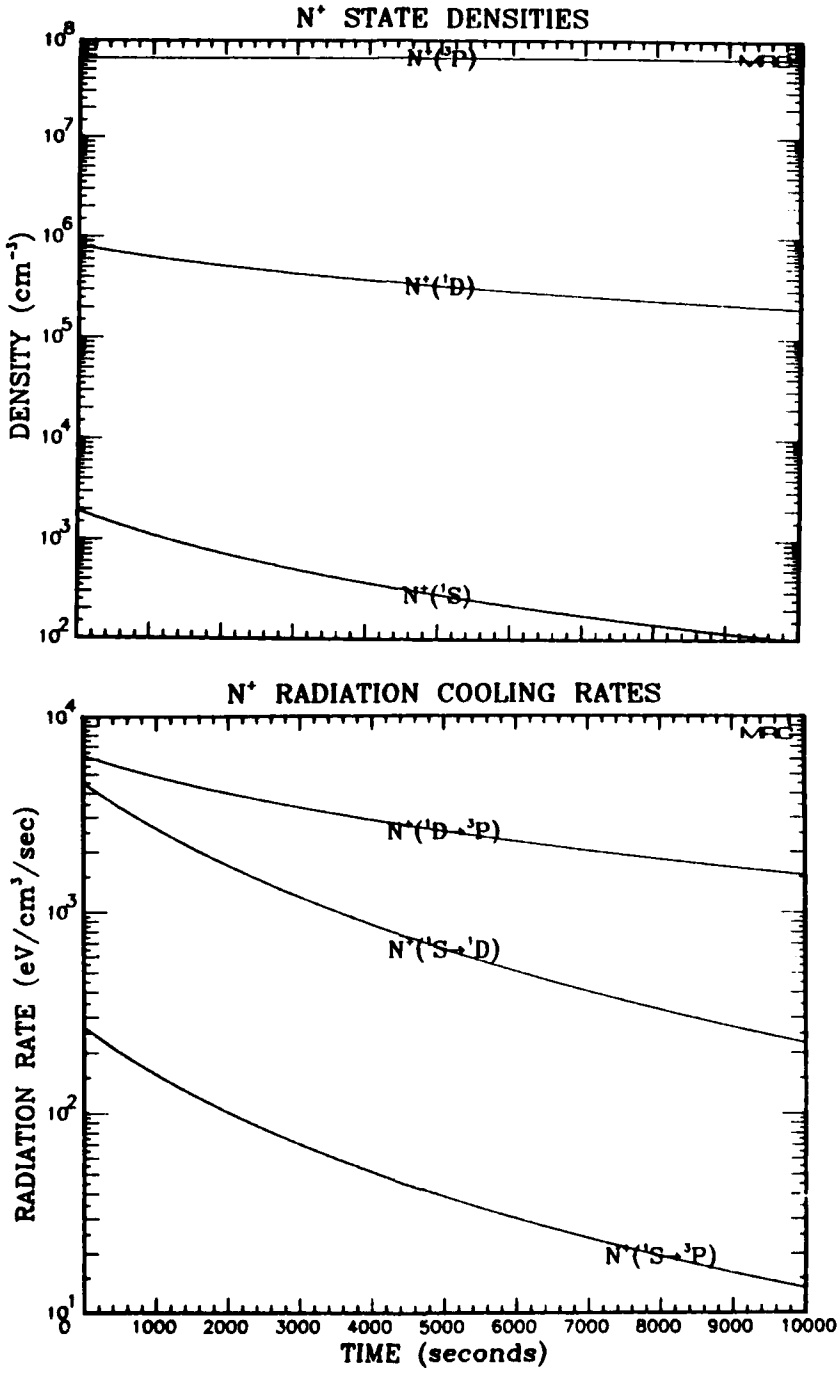

Figure 21 (Continued)

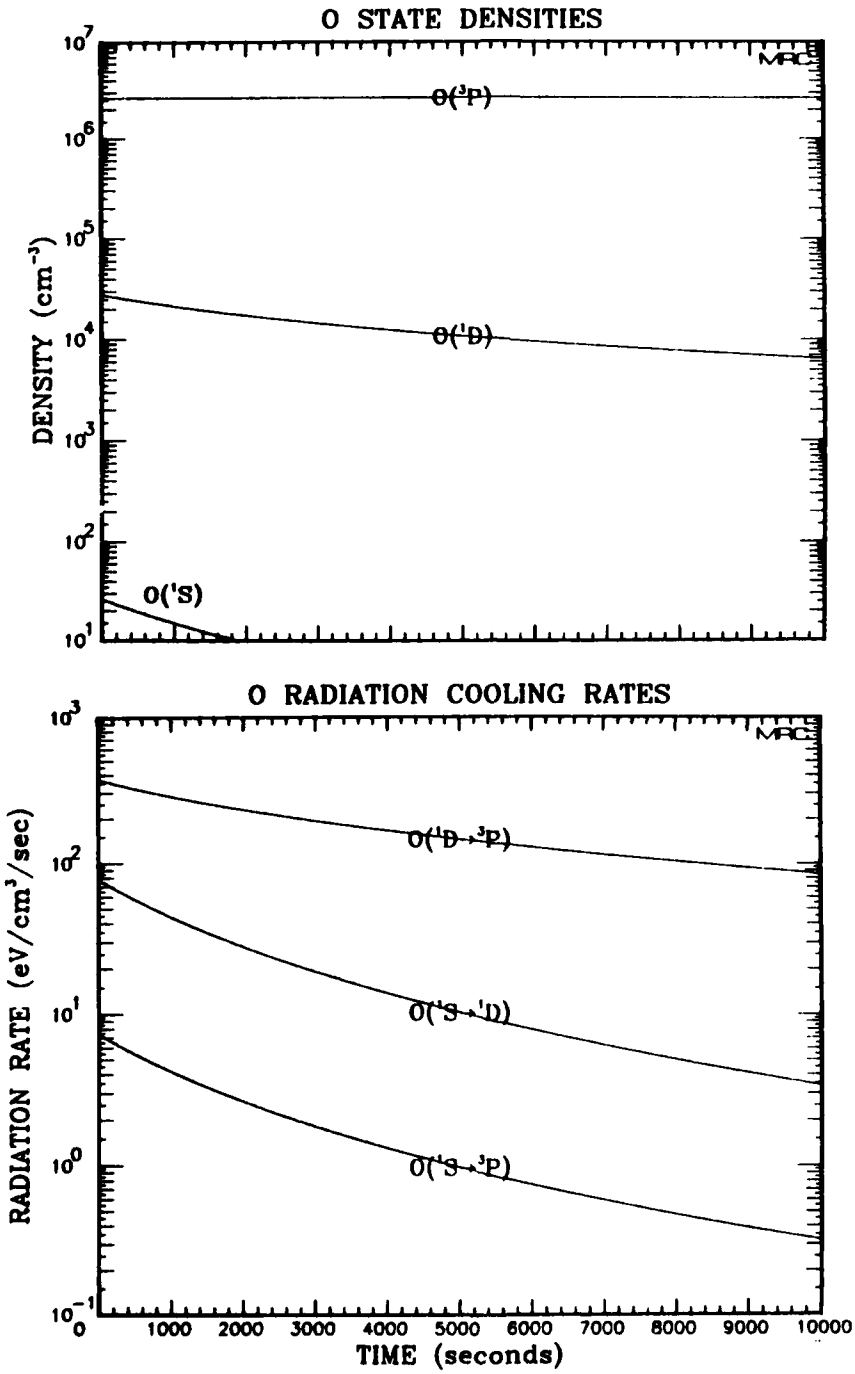

Figure 21 (Continued)

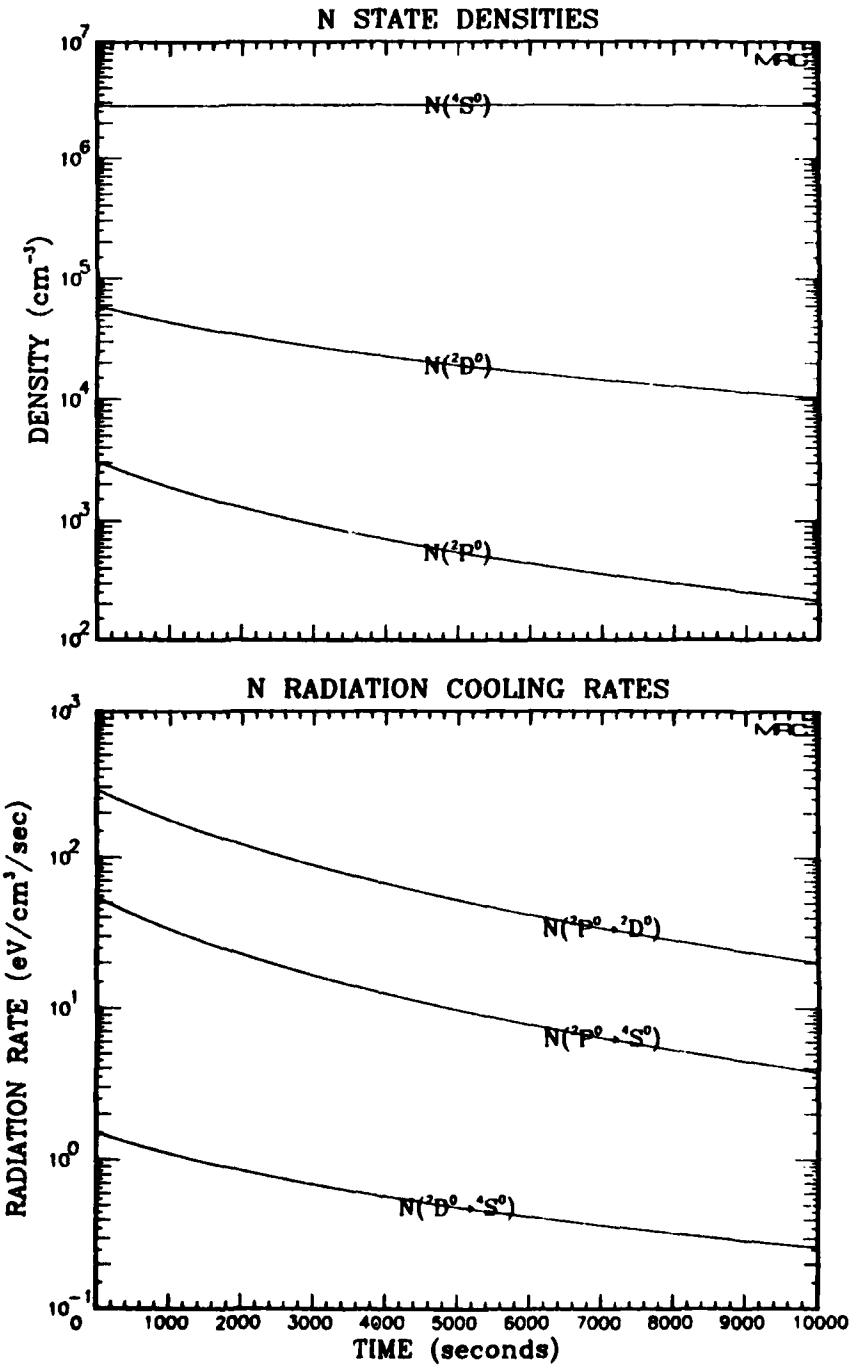

Figure 21 (Continued)

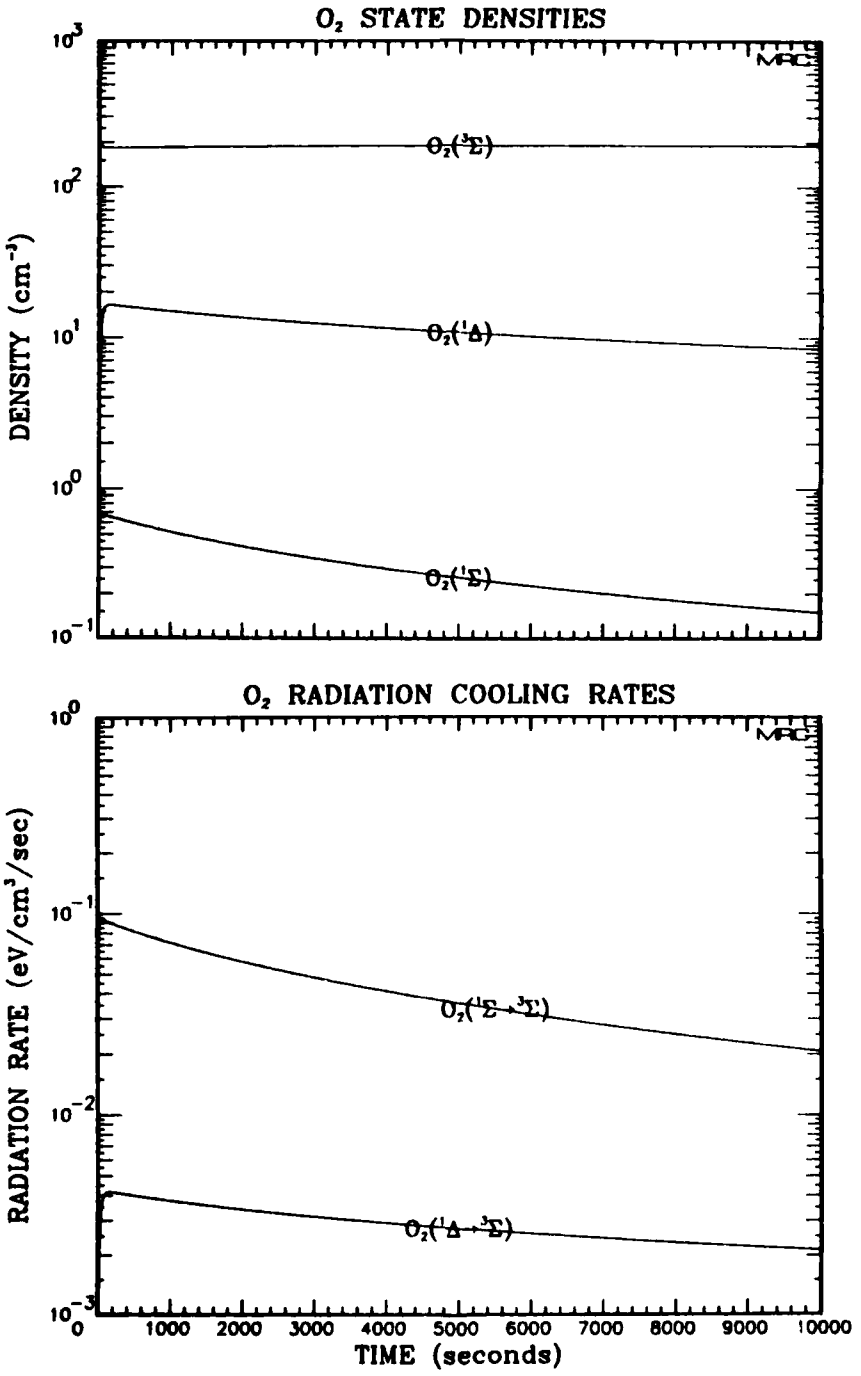

Figure 21 (Continued)

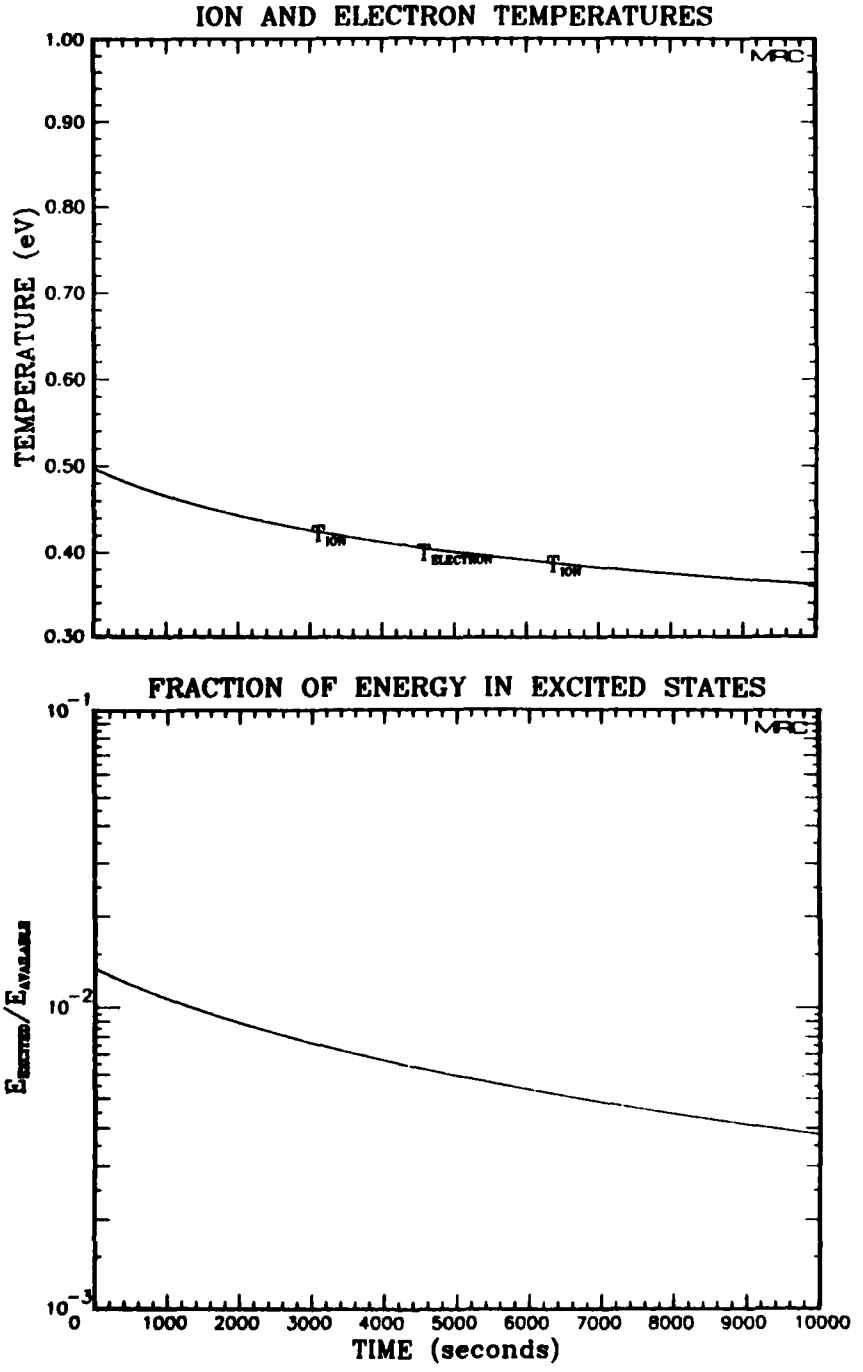

Figure 21 (Continued)

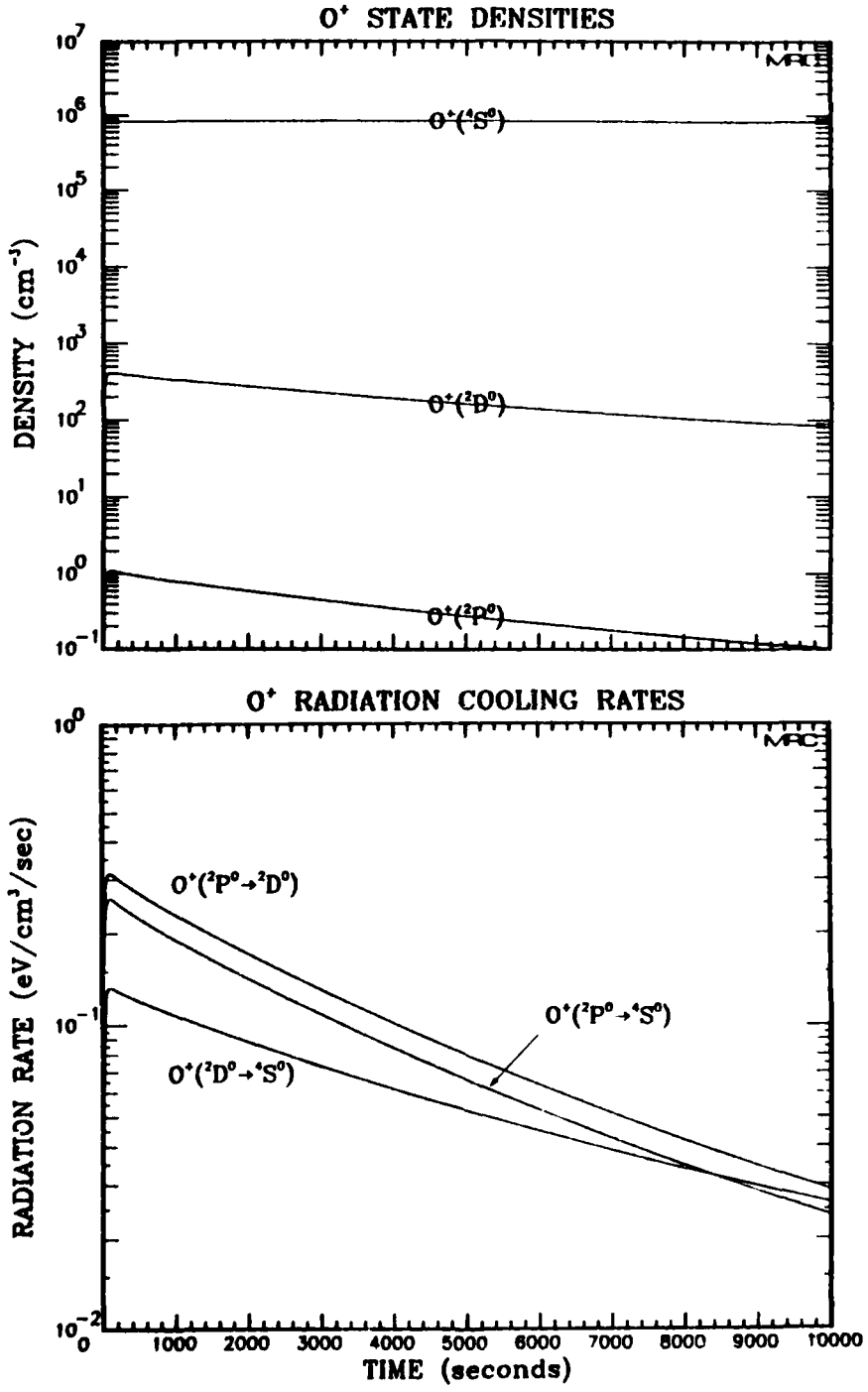

Figure 22. Radiation properties based on the 60 minute environment at 1000 km altitude in a calculation of a megaton-range nuclear explosion at 200 km altitude.

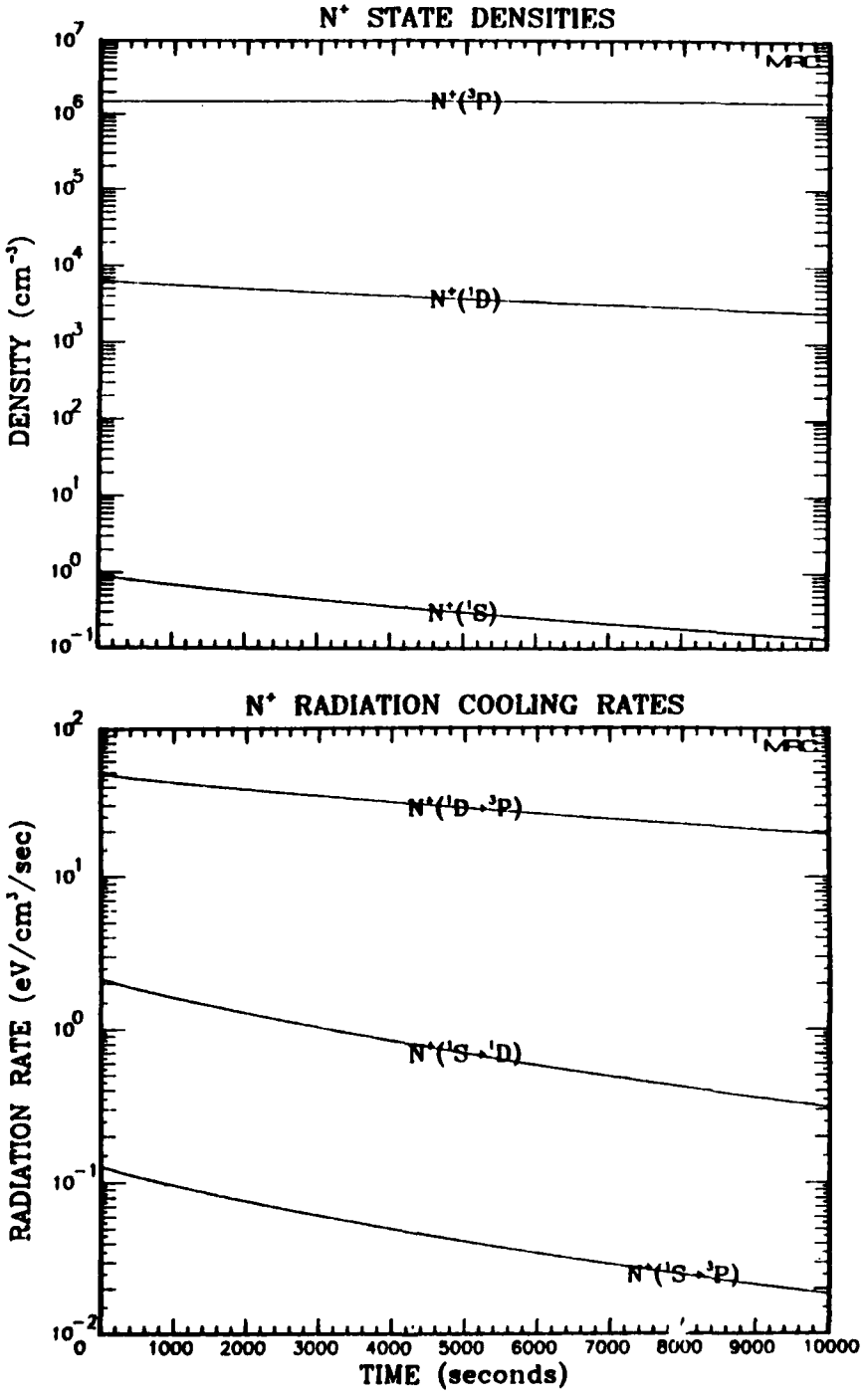

Figure 22 (Continued)

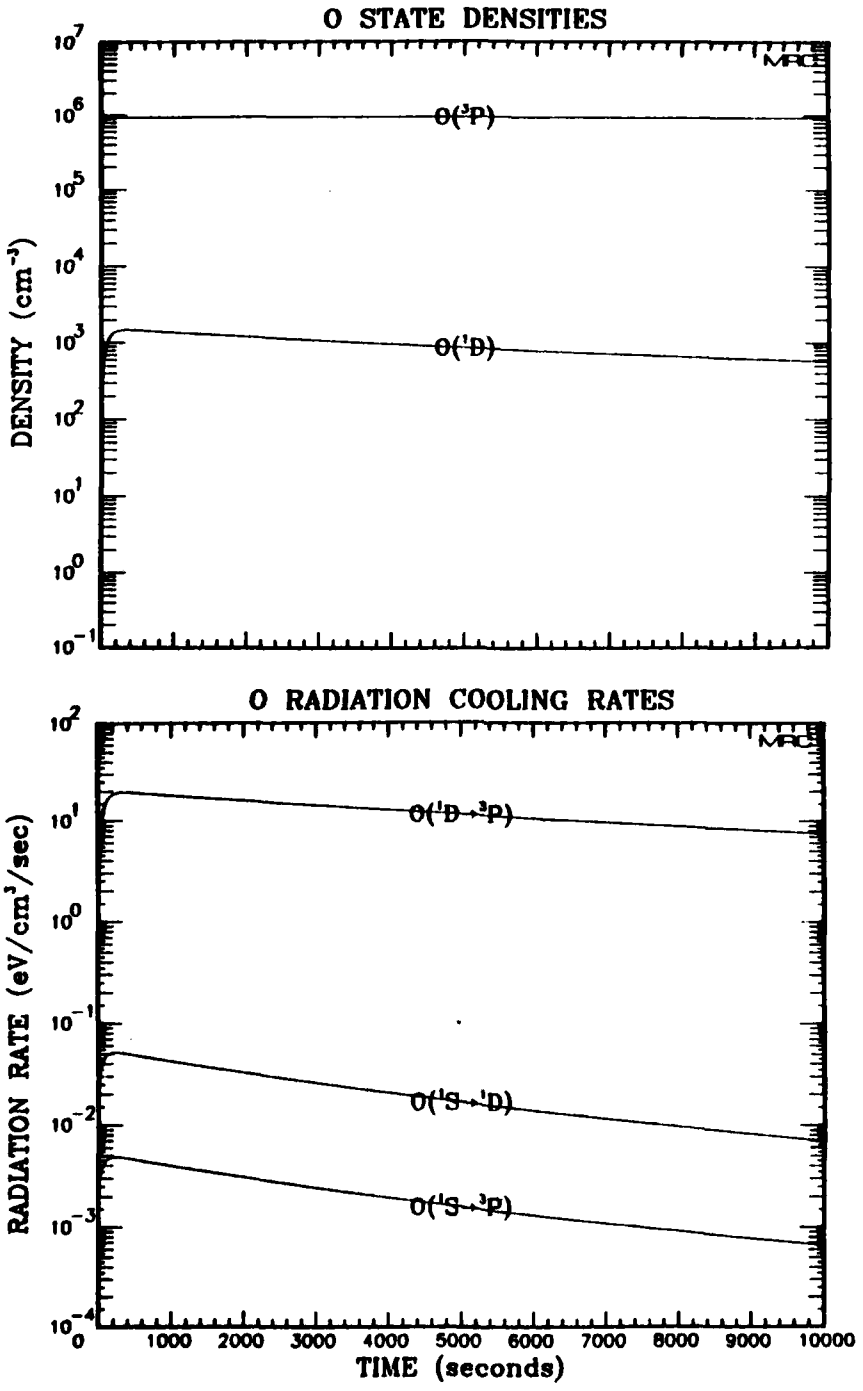

Figure 22 (Continued)

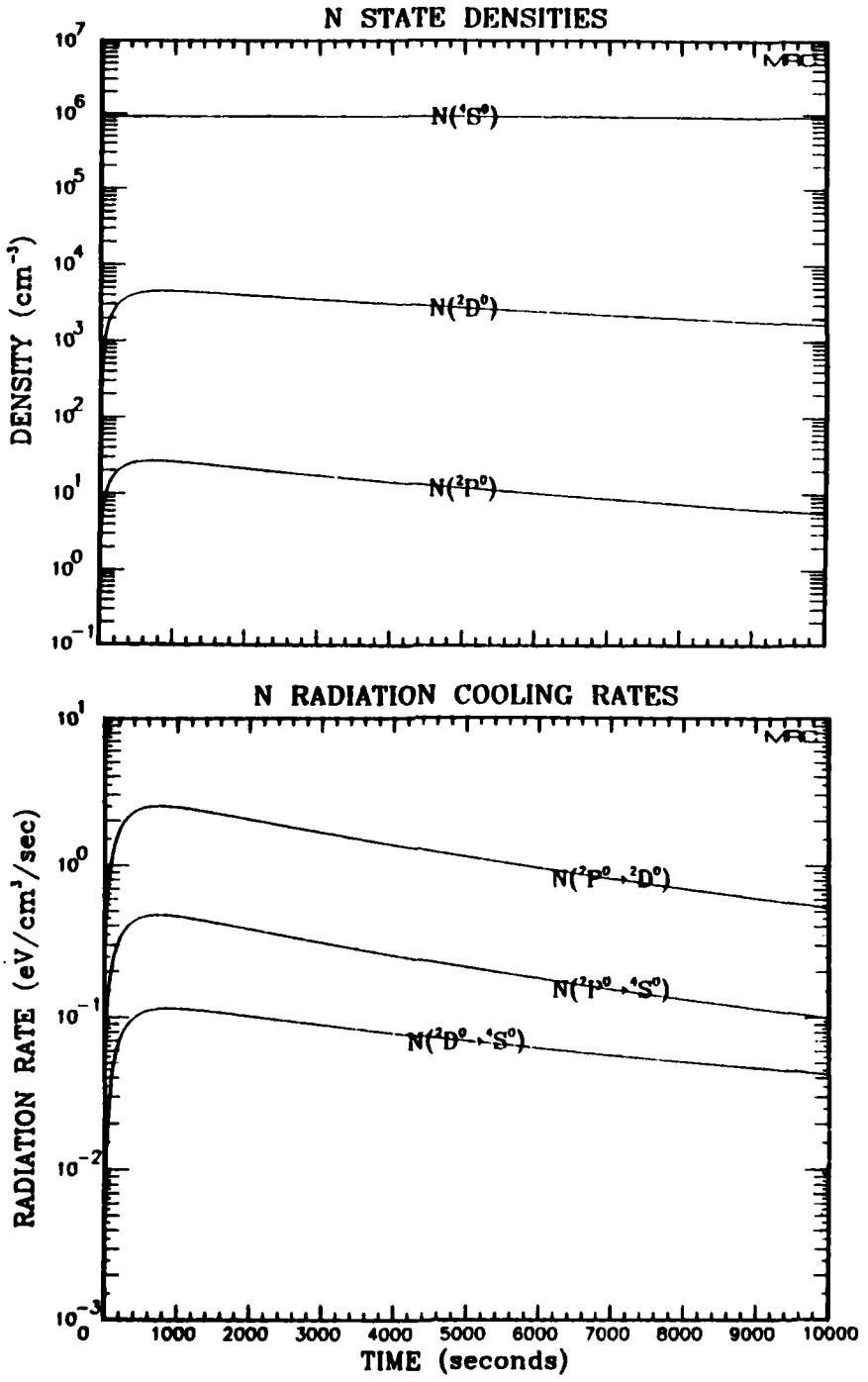

Figure 22 (Continued)

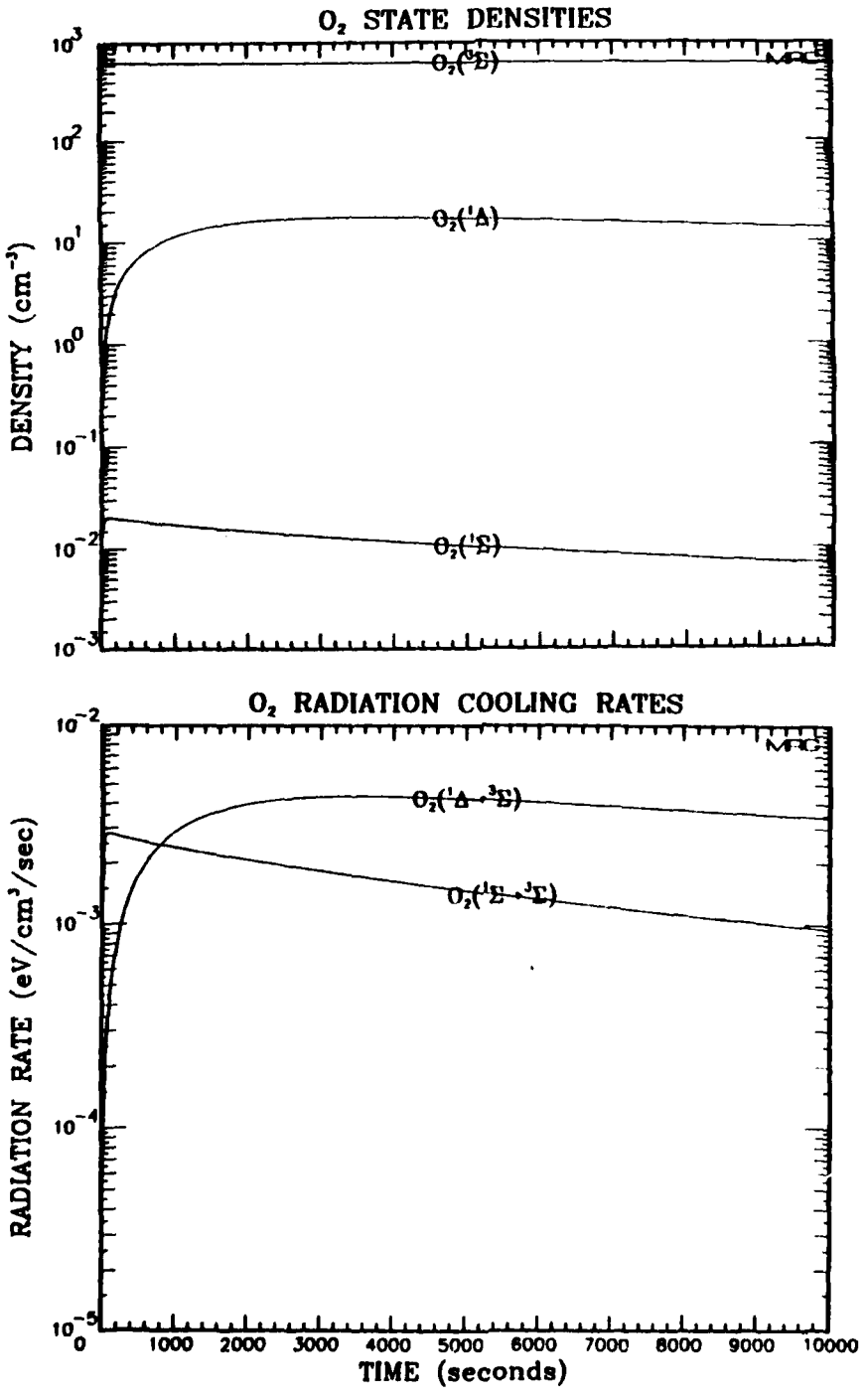

Figure 22 (Continued)

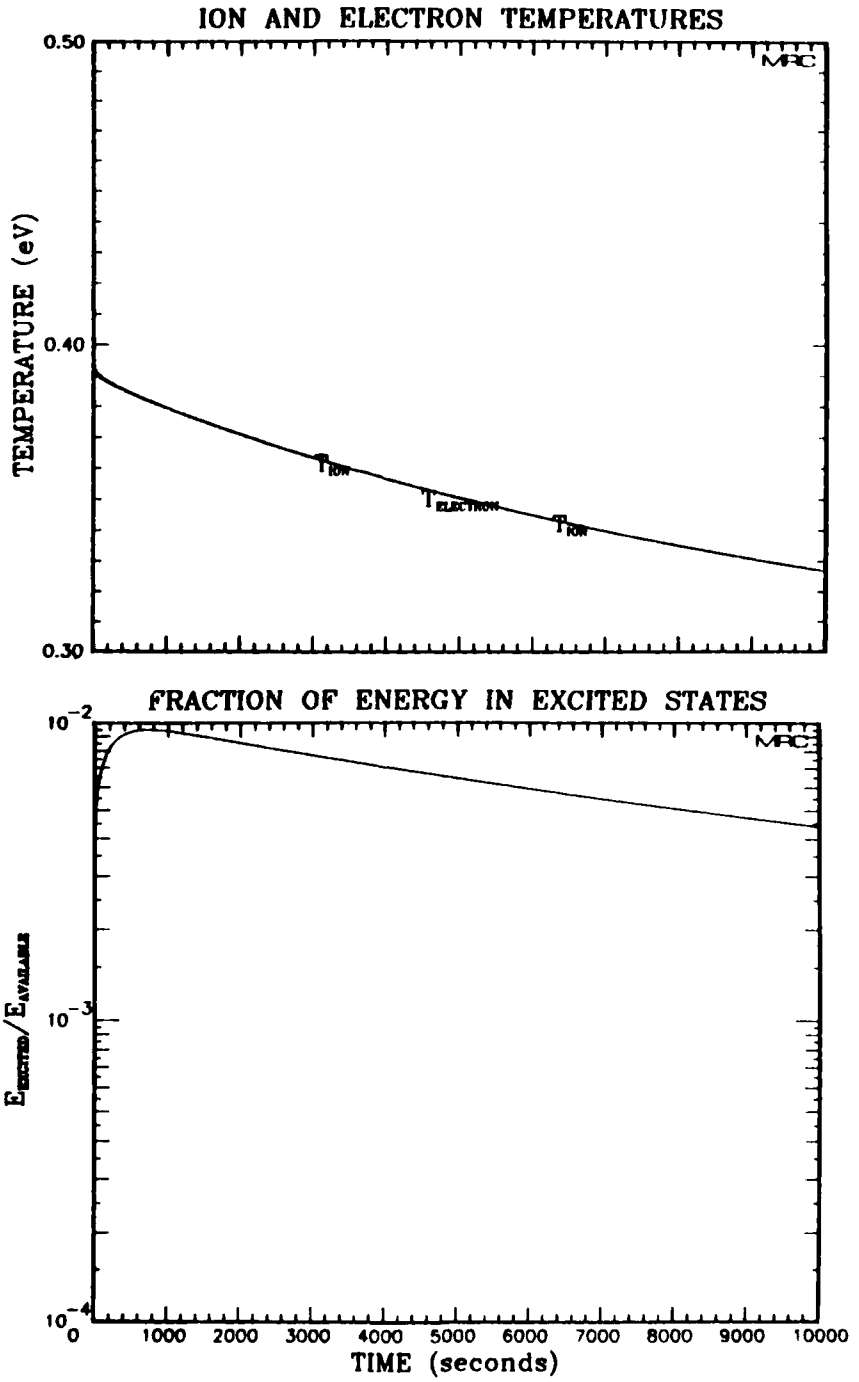

Figure 22 (Continued

AD-A131 266 FORBIDDEN LINE RADIATION COOLING OF HIGH ALTITUDE PLASMAS(U) MISSION RESEARCH CORP SANTA BARBARA CA W W WHITE 19 FEB 82 MRC-R-687 DNA-6125T

2/2

UNCLASSIFIED DNA001-80-C-0096 F/G 18/3 NL

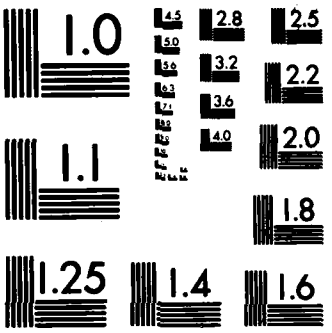

and atomic species all have nearly equal densities of about 10^6 cm^{-3}, and molecular oxygen is present only as a very minor species. The initial ion and electron temperatures have values of 0.393 eV, so this case describes plasma which is initially much cooler than that in previous cases. The radiation cooling curves indicate that, at these low temperatures, nitrogen ions and oxygen atoms are the effective radiators. In both species, it is the red lines which account for the cooling. In view of the low temperatures and approximate equality between electron and radiating species densities, it's not surprising that at most about one precent of the available energy was contained in excited states. The temperature curves indicate that about 17% of the initial energy was radiated over the 10,000 second period.

SECTION 4

DISCUSSION AND CONCLUSIONS

The sample calculations of the preceding section rather conclusively demonstrate that, on a time scale of hours, forbidden line radiation from low lying metastable states of atmospheric constituents can remove substantial fractions of the available thermal energy. From the standpoint of computing the behavior and decay of fireball plasma from a high altitude nuclear explosion, a process, such as radiation cooling, which significantly changes the ion and electron temperatures may be quite important. In addition to altering temperature dependent deionization chemistry rate coefficients and the ion-electron scale height, radiation cooling may result in a reduction in the diamagnetic levitation of a plasma in the geomagnetic field. This last effect derives from the fact that ion-electron thermal energy drives a system of electrical currents within the plasma which interact with the geomagnetic field and cause the plasma to move, transverse to the field, toward a region of reduced field (i.e., generally upward).

The results presented are a bit artificial in the sense that they represent the response of an initially cold system of particles to a delta-function heating pulse at zero time. In a more realistic calculation, the system at some non-zero initial temperature would be subject to non-instantaneous heating (and cooling) as the result of hydrodynamic evolution. Nevertheless, the results provide a basis for estimating e-folding time constants for cooling and for particular forbidden line radiation rates under a variety of conditions. Although most of these forbidden lines are in the visible, a few are in the ultraviolet and short wavelength infrared.

Earlier, in Section 2, it was pointed out that excited state populations and radiation rates do not scale in a simple way with electron density. The mathematical statement of the scaling under quasi-steady conditions was presented in Equation 13, and the computed results nicely demonstrate the variation of excited populations with electron density under more general conditions. The intertwining of temperature dependent excitation and deexcitation rate coefficients and radiative transition probabilities makes it difficult to sort out the significance of individual line radiations relative to the others without doing quite a bit of work.

A very interesting result of the calculations concerns the partition of available energy between excited state and thermal energies. The computations indicate that when the temperature is an electron volt or lower, and when the electron density is comparable to or exceeds the density of radiating species, then the fraction of available energy tied up in excited states is ~10% or less. However, if the radiating species density substantially exceeds the electron density (e.g., far more N or O atoms than electrons), then a large fraction of the available energy may go to producing excited states, even if the temperature is fairly low (<0.4 eV). Under such circumstances, fluid dynamical calculations which compute ion-electron pressures without accounting for thermal energy which would be absorbed in the production of excited states will possibly miscompute pressure gradient forces and diamagnetic effects by perhaps a factor of two. One remedy for this problem would be to carry explicitly excited state populations. However, the present calculations indicate that at electron densities of greatest interest (10^6 cm^{-3} and larger), the quasi-steady state is attained rather rapidly. Therefore, it should be possible, in all but highly dynamic situations, to compute by the quasi-steady approximation the excited state populations without explicitly carrying them. Thus, standard fluid treatments could be improved by computing the energy tied up in excited states and by subtracting this

energy from the thermal energy prior to a calculation of ion electron pressure or temperature.

In summary, it has been determined that high altitude nuclear burst simulations which span substantial time intervals (hours) need to include radiation cooling by forbidden line radiation. The quasi-steady state approximation, which avoids the necessity of carrying excited state densities explicitly, appears to be acceptable for all but highly dynamic problems. Furthermore, it has been shown that failure to account for the partition between excited state and thermal energies can introduce non-trivial errors into pressure and other temperature dependent terms of the magnetized fluid equations.

REFERENCES

1. Hays, P. B., A. F. Nagy, and R. G. Roble, "Interferometric Measurements of the 6300Å Doppler Temperature During a Magnetic Storm," J. Geophys. Res. 74, 4162 (1969).

2. Hernandez, G. and R. G. Roble, "Direct Measurements of Nighttime Thermospheric Winds and Temperatures - 1. Seasonal Variations During Geomagnetic Quiet Periods," J. Geophys. Res. 81, 2065 (1976).

3. Jacka, F., A. R. D. Bower, and P. A. Wilksch, "Thermospheric Temperatues and Winds Derived From OI λ 630 nm Night Airglow Line Profiles," J. Atmos. Terr. Phys. 41, 397 (1979).

4. Rees, M. H. and D. Luckey, "Auroral Electron Energy Derived From Ratio of Spectroscopic Emissions - 1. Model Calculations," J. Geophys. Res. 79, 5181 (1974). (See also note in Ref. 8).

5. Moore, J. G. and E. J. Weber, "OI 6300 and 7774Å Airglow Measurements of Equatorial Plasma Depletions," J. Atmos. Terr. Phys. 43, 851 (1981).

6. Herrero, F. A. and J. W. Meriwether, Jr., "Equatorial Night-time F-region Events: A Survey of 6300Å Airglow Intensity Maps at Arecibo," J. Atmos. Terr. Phys. 43, 859 (1981).

7. Freund, J. T. and F. Jacka, "Structure in the λ 557.7 nm [OI] Airglow," J. Atmos. Terr. Phys. 41, 25 (1979).

8. Gerard, J.-C., "A Review of Optical F-Region Processes in the Polar Atmosphere" in Exploration of the Polar Upper Atmosphere, ed. by C.S. Deehr and J. A. Holtet, D. Reidel Publishing Co. (1981).

9. Tinsley, B. A., "Spectrogram of Artificial Aurora Near Samoa of July 9, 1962, and Associated Lithium Emission in Twilight," Canadian J. Phys. 42, 779 (1964).

10. Markham, T. P., "Artificial Conjugate Auroral and Afterglow Spectra," Planet. Space Sci. 18, 731 (1970).

11. Hoerlin, H., United States High-Altitude Test Experiences, A Review Emphasizing the Impact on the Environment, LA-6405, Los Alamos Scientific Laboratory (1976).

12. Ali, A. W., Electron Impact Rate Coefficients for the Low Lying Metastable States of O, O^+, N, and N^+, NRL Memorandum Report 3371, Naval Research Laboratory (1976).

13. Ali, A. W., R. H. Kummler, F. R. Gilmore, and J. W. McGowan, Upper Atmospheric Excitation Processes, NRL Memorandum Report 3920, Naval Research Laboratory (1979).

14. Stone, E. J. and E. C. Zipf, "Excitation of the OI(^{3}S) and NI(^{4}P) Resonance States by Electron Impact on O and N," Phys. Rev. A 4, 610 (1971).

15. Berrington, K. A. and P. G. Burke, "Effective Collision Strengths for Forbidden Transitions in e-N and e-O Scattering," Planet. Space Sci. 29, 377 (1981).

16. Torr, D. G. and M. R. Torr, "Chemistry of the Thermosphere and Ionosphere," J. Atmos. Terr. Phys. 41, 797 (1979). Also "Determination of the Thermal Rate Coefficient, Products, and Branching Ratios for the Reaction of $O^+(^2D)$ with N_2," J. Geophys. Res. 85, 783 (1980).

17. Wiese, W. L., M. W. Smith, and B. M. Glennon, Atomic Transition Probabilities, Vol. I - Hydrogen Through Neon, NSRDS - NBS 4, National Standard Reference Data Series, National Bureau of Standards (1966).

18. Archer, D. H., private communication.

19. Trajmar, S., D. C. Cartwright, and W. Williams, "Differential and Integral Cross Sections for the Electron Impact Excitation of the $a^1\Delta_g$ and $b^1\Sigma_g^+$ States of O_2," Phys. Rev. A 4, 1482 (1971).

20. Badger, R. M., A. C. Wright, and R. F. Whitlock, "Absolute Intensities of the Discrete and Continuous Absorption Bands of Oxygen Gas at 1.26 and 1.065 μ and the Radiative Lifetime of the $^1\Delta_g$ State of Oxygen," J. Chem. Phys. 43, 4345 (1965).

21. McGowan, J. W., R. H. Kummler, and F. R. Gilmore, "Excitation and Deexcitation Processes," Chapter 20 in Reaction Rate Handbook, 2nd Edition, DNA 1948H, Defense Nuclear Agency (1972). See Table 20-1.

22. Kilb, R. W., R. W. Stagat, and R. E. Stoeckly, Collisional Momentum and Energy Transfer Rates For Two-Fluid Nuclear-Burst Simulations, DNA 3827T (MRC-R-181), Mission Research Corporation (1975).

23. Jacchia, L. G., "Atmospheric Models in the Region From 110 to 2000 km" in CIRA 1972, COSPAR International Reference Atmosphere 1972, Akademie-Verlag, Berlin (1972). See atmosphere table on pages 300-301.

24. Sappenfield, D. S., private communication. Heat transfer coefficent results from Sappenfield's analysis of results of G. J. Schulz, "Vibrational Excitation of N_2, CO, and H_2 by Electron Impact," Phys. Rev. 135. #4A, 988 (1964).

25. Fajen, F. E., private communication.

26. Fajen, F. E., A. W. Gregersen, and W. W. White, private communication.

APPENDIX

The following tables summarize electron impact and deexcitation rate coefficients for O^+, N^+, O, N, and O_2.

TABLE A-1.† DEEXCITATION RATE COEFFICIENTS FOR THE LOW-LYING METASTABLE STATES OF O^+ (T_e in eV)

Transition	Deexcitation Rate Coefficient (cm^3/sec)
$^2D^0 - {}^4S^0$	$1.3 \times 10^{-8} (T_e)^{-1/2}$
$^2p^0 - {}^4S^0$	$6.3 \times 10^{-9} (T_e)^{-1/2}$
$^2p^0 - {}^2D^0$	$2.4 \times 10^{-8} (T_e)^{-1/2}$

† From reference 13.

TABLE A-2.† DEEXCITATION RATE COEFFICIENTS FOR THE LOW-LYING METASTABLE STATES OF N^+ (T_e in eV)

Transition	Deexcitation Rate Coefficient (cm^3/sec)
$^1D - {}^3P$	$4.8 \times 10^{-8} (T_e)^{-1/2}$
$^1S - {}^3P$	$3.2 \times 10^{-8} (T_e)^{-1/2}$
$^1S - {}^1D$	$3.3 \times 10^{-8} (T_e)^{-1/2}$

† From reference 13.

TABLE A-3.† ELECTRON IMPACT EXCITATION AND DEEXCITATION RATE COEFFICIENTS FOR THE LOW-LYING STATES OF ATOMIC OXYGEN.

T_e(eV)	$^3P - {}^1D$	$^3P - {}^1S$	$^1D - {}^1S$
0.1	1.92 (-18)[a]	1.78 (-28)	2.25 (-19)*
	1.1 (- 9)[b]	2.1 (- 9)	2.2 (-13)
0.2	5.28 (-14)	1.96 (-19)	1.76 (-14)
	1.7 (- 9)	2.1 (- 9)	3.9 (-11)
0.3	1.76 (-12)	2.10 (-16)	8.07 (-13)
	2.2 (- 9)	2.1 (- 9)	2.3 (-10)
0.5	3.28 (-11)	6.04 (-14)	1.52 (-11)
	2.9 (- 9)	2.3 (- 9)	8.7 (-10)
0.7	1.21 (-10)	7.25 (-13)	5.4 (-11)
	3.5 (- 9)	2.5 (- 9)	1.5 (- 9)
1.0	3.43 (-10)	4.93 (-12)	1.38 (-10)
	4.4 (- 9)	2.9 (- 9)	2.3 (- 9)
1.2	5.20 (-10)	1.06 (-11)	1.97 (-10)
	4.8 (- 9)	3.1 (- 9)	2.7 (- 9)
1.5	7.94 (-10)	2.32 (-11)	2.76 (-10)
	5.2 (- 9)	3.4 (- 9)	3.1 (- 9)
2.0	1.21 (- 9)	5.15 (-11)	3.98 (-10)
	5.8 (- 9)	3.7 (- 9)	3.6 (- 9)
3.0	1.84 (- 9)	1.16 (-10)	5.30 (-10)
	6.3 (- 9)	4.2 (- 9)	3.9 (- 9)
5.0	2.52 (- 9)	2.21 (-10)	7.16 (-10)
	6.7 (- 9)	4.6 (- 9)	4.5 (- 9)
7.0	2.73 (- 9)	2.8 (-10)	7.76 (-10)
	6.5 (- 9)	4.6 (- 9)	4.6 (- 9)
10.0	2.80 (- 9)	3.3 (-10)	7.5 (-10)
	6.1 (- 9)	4.5 (- 9)	4.2 (- 9)
15.0	2.58 (- 9)	3.8 (-10)	6.9 (-10)
	5.3 (- 9)	4.5 (- 9)	3.7 (- 9)
20.0	2.23 (- 9)	3.7 (-10)	6.4 (-10)
	4.4 (- 9)	4.1 (- 9)	3.4 (- 9)

* Numbers in parenthesis indicate the power of ten by which the enteries are multiplied.
[a] Excitation rate coefficient.
[b] The corresponding deexcitation rate coefficient.
† From reference 13.

TABLE A-4.† ELECTRON IMPACT EXCITATION AND DEEXCITATION RATE COEFFICIENTS FOR THE LOW-LYING STATES OF ATOMIC NITROGEN.

T_e(eV)	$^4S^0 - {}^2D^0$	$^4S^0 - {}^2P^0$	$^2D^0 - {}^2P^0$
0.1	8.0 (-20)[a]	2.6 (-25)	2.10 (-14)*
	6.3 (-10)[b]	5.5 (-10)	5.7 (- 9)
0.2	1.54 (-14)	2.03 (-17)	1.16 (-11)
	8.6 (-10)	7.5 (-10)	7.8 (- 9)
0.3	1.25 (-12)	1.11 (-14)	9.78 (-11)
	1.35 (- 9)	1.1 (- 9)	8.9 (- 9)
0.5	4.2 (-11)	1.47 (-12)	6.0 (-10)
	1.9 (- 9)	1.2 (- 9)	1.0 (- 8)
0.7	1.98 (-10)	1.63 (-11)	1.1 (- 9)
	2.34 (- 9)	1.8 (- 9)	1.0 (- 8)
1.0	6.38 (-10)	8.91 (-11)	2.05 (- 9)
	2.7 (- 9)	2.1 (- 9)	1.1 (- 8)
1.2	1.08 (- 9)	1.73 (-10)	2.56 (- 9)
	3.1 (- 9)	2.29 (- 9)	1.16 (- 8)
1.5	1.52 (- 9)	3.38 (-10)	3.24 (- 9)
	2.9 (- 9)	2.4 (- 9)	1.2 (- 8)
2.0	2.27 (- 9)	6.54 (-10)	4.1 (- 9)
	2.9 (- 9)	2.6 (- 9)	1.2 (- 8)
3.0	3.31 (- 9)	1.23 (- 9)	5.18 (- 9)
	2.9 (- 9)	2.7 (- 9)	1.3 (- 8)
5.0	4.5 (- 9)	1.99 (- 9)	6.2 (- 9)
	2.90 (- 9)	2.7 (- 9)	1.3 (- 8)
7.0	5.26 (- 9)	2.36 (- 9)	6.5 (- 9)
	2.9 (- 9)	2.6 (- 9)	1.3 (- 8)
10.0	5.85 (- 9)	2.4 (- 9)	6.5 (- 9)
	2.9 (- 9)	2.3 (- 9)	1.2 (- 8)
15.0	5.97 (- 9)	2.49 (- 9)	6.1 (- 9)
	2.79 (- 9)	2.1 (- 9)	1.1 (- 8)
20.0	4.96 (- 9)	2.28 (- 9)	5.47 (- 9)
	2.2 (- 9)	1.8 (- 9)	9.7 (- 9)

* Numbers in parenthesis indicate the power of ten by which the enteries are multiplied.

[a] Excitation rate coefficient.

[b] The corresponding deexcitation rate coefficient.

† From reference 13.

TABLE A-5. ELECTRON IMPACT DEEXCITATION RATE COEFFICIENTS FOR LOW-LYING STATES OF MOLECULAR OXYGEN

T_e(eV)	$a^1\Delta_g \rightarrow X^3\Sigma_g^-$	$b^1\Sigma_g^+ \rightarrow X^3\Sigma_g^-$
0.1	2.595 (-11)*	2.058 (-11)
0.2	8.968 (-11)	8.089 (-11)
0.3	1.560 (-10)	1.575 (-10)
0.4	2.241 (-10)	2.433 (-10)
0.5	2.989 (-10)	3.341 (-10)
0.6	3.821 (-10)	4.262 (-10)
0.7	4.733 (-10)	5.171 (-10)
0.8	5.704 (-10)	6.052 (-10)
0.9	6.714 (-10)	6.894 (-10)
1.0	7.742 (-10)	7.690 (-10)
1.2	9.795 (-10)	9.140 (-10)
1.4	1.177 (- 9)	1.040 (- 9)
1.6	1.362 (- 9)	1.149 (- 9)
1.8	1.532 (- 9)	1.242 (- 9)
2.0	1.687 (- 9)	1.322 (- 9)
2.5	2.009 (- 9)	1.474 (- 9)
3.0	2.253 (- 9)	1.574 (- 9)
4.0	2.569 (- 9)	1.680 (- 9)
5.0	2.735 (- 9)	1.712 (- 9)
6.0	2.811 (- 9)	1.706 (- 9)
7.0	2.833 (- 9)	1.679 (- 9)
8.0	2.819 (- 9)	1.641 (- 9)
9.0	2.784 (- 9)	1.596 (- 9)
10.0	2.733 (- 9)	1.548 (- 9)

* Numbers in parenthesis indicate the power of ten by which the entries are multiplied.

DISTRIBUTION LIST

DEPARTMENT OF DEFENSE

Assistant to the Secretary of Defense
Atomic Energy
ATTN: Exec Asst

Command & Control Tech Ctr
ATTN: C-650
ATTN: C-312, R. Mason
ATTN: C-650, G. Jones
3 cy ATTN: C-650, W. Heidig

Defense Communications Agency
ATTN: Code 230
ATTN: Code 205
ATTN: J300 for Yen-Sun Fu

Defense Communications Engineer Ctr
ATTN: Code R410, N. Jones
ATTN: Code R410
ATTN: Code R410, R. Craighill
ATTN: Code R123

Defense Intelligence Agency
ATTN: DB-4C, E. O'Farrell
ATTN: DC-7B
ATTN: DB, A. Wise
ATTN: DT-1B
ATTN: DIR

Defense Nuclear Agency
ATTN: STNA
ATTN: NAFD
ATTN: RAEE
ATTN: NATD
ATTN: RAAE, P. Lunn
3 cy ATTN: RAAE
4 cy ATTN: TITL

Defense Technical Information Ctr
12 cy ATTN: DD

Deputy Under Secretary of Defense
Comm, Cmd, Cont & Intell
ATTN: Dir of Intell Sys

Field Command Defense Nuclear Agency
Det 1
Lawrence Livermore Lab
ATTN: FC-1

Field Command
Defense Nuclear Agency
ATTN: FCPR
ATTN: FCTXE
ATTN: FCTT, W. Summa

Interservice Nuclear Wpns School
ATTN: TTV

Joint Chiefs of Staff
ATTN: C3S
ATTN: C3S, Eval Ofc (HDOO)

Joint Strat Tgt Planning Staff
ATTN: JLA, Threat Appl Div
ATTN: JLTW-2

DEPARTMENT OF DEFENSE (Continued)

National Security Agcy
ATTN: W-32, O. Bartlett
ATTN: R-52, J. Skillman
ATTN: B-3, F. Leonard

Under Secretary of Defense for Rsch & Engrg
ATTN: Strat & Space Sys (OS)
ATTN: Strat & Theater Nuc Forces, B. Stephan

WWMCCS Sys Engrg Org
ATTN: J. Hoff

DEPARTMENT OF THE ARMY

Assistant Chief of Staff for Automation & Comm
ATTN: DAMO-C4, P. Kenny

Atmospheric Sciences Lab
ATTN: DELAS-EO, F. Niles

BMD Advanced Tech Ctr
ATTN: ATC-R, D. Russ
ATTN: ATC-O, W. Davies
ATTN: ATC-R, W. Dickinson
ATTN: ATC-T, M. Capps

BMD Systems Command
ATTN: BMDSC-HLE, R. Webb
2 cy ATTN: BMDSC-HW

Deputy Chief of Staff for Ops & Plans
ATTN: DAMO-RQC, C2 Div

Harry Diamond Labs
ATTN: DELHD-NW-P, 20240
ATTN: DELHD-NW-R, R. Williams, 22000

USA Chemical School
ATTN: ATZN-CM-CS

USA Comm-Elec Engrg Instal Agcy
ATTN: CCC-EMEO-PED, G. Lane
ATTN: CCC-CED-CCO, W. Neuendorf

USA Communications Cmd
ATTN: CC-OPS-W
ATTN: CC-OPS-WR, H. Wilson

USA Communications R&D Cmd
ATTN: DRDCO-COM-RY, W. Kesselman

USA Foreign Science & Tech Ctr
ATTN: DRXST-SD

USA Materiel Dev & Readiness Cmd
ATTN: DRCLDC, J. Bender

USA Nuclear & Chem Agcy
ATTN: Library

USA TRADOC Sys Analysis Actvy
ATTN: ATAA-PL
ATTN: ATAA-TCC, F. Payan, Jr
ATTN: ATAA-TDC

DEPARTMENT OF THE ARMY (Continued)

USA Missile Cmd
ATTN: DRSMI-YSO, J. Gamble

DEPARTMENT OF THE NAVY

Joint Cruise Missiles Proj Ofc
ATTN: JCMG-707

Naval Air Systems Cmd
ATTN: PMA 271

Naval Electronic Systems Cmd
ATTN: PME 117-211, B. Kruger
ATTN: PME 106-13, T. Griffin
ATTN: Code 501A
ATTN: PME 117-20
ATTN: PME 117-2013, G. Burnhart
ATTN: Code 3101, T. Hughes
ATTN: PME 106-4, S. Kearney

Naval Intell Support Ctr
ATTN: NISC-50

Naval Ocean Systems Ctr
ATTN: Code 5322, M. Paulson
ATTN: Code 532
ATTN: Code 5323, J. Ferguson

Naval Research Lab
ATTN: Code 4720, J. Davis
ATTN: Code 4780
ATTN: Code 7500, B. Wald
ATTN: Code 4780, S. Ossakow
ATTN: Code 6700
ATTN: Code 7950, J. Goodman
ATTN: Code 4187
ATTN: Code 4700

Naval Space Surveillance System
ATTN: J. Burton

Naval Surface Wpns Ctr
ATTN: Code F31

Office of Naval Research
ATTN: Code 412, W. Condell
ATTN: Code 414, G. Joiner

Strat Sys Proj Ofc
ATTN: NSP-2141
ATTN: NSP-2722, F. Wimberly
ATTN: NSP-43

Theater Nuc Warfare Proj Office
ATTN: PM-23, D. Smith

DEPARTMENT OF THE AIR FORCE

Aerospace Defense Cmd
ATTN: DC, T. Long

Air Force Geophysics Lab
ATTN: OPR, H. Gardiner
ATTN: OPR-1
ATTN: LKB, K. Champion
ATTN: CA, A. Stair
ATTN: PHY, J. Buchau
ATTN: R. Babcock
ATTN: R. O'Neil

DEPARTMENT OF THE AIR FORCE (Continued)

Air Force Tech Appl Ctr
ATTN: TN

Air Force Weapons Lab
ATTN: SUL
ATTN: NTYC
ATTN: NTN

Air Force Wright Aeronautical Lab
ATTN: A. Johnson
ATTN: W. Hunt

Air Logistics Cmd
ATTN: OO-ALC/MM

Air Univ Library
ATTN: AUL-LSE

Assistant Chief of Staff
Studies & Analyses
ATTN: AF/SASC, C. Rightmeyer
ATTN: AF/SASC, W. Kraus

Ballistic Missile Office
ATTN: ENSN, W. Wilson
ATTN: SYC, Col Kwan

Deputy Chief of Staff
Research, Development, & Acq
ATTN: AFRDS, Space Sys & C3 Dir
ATTN: AFRDSS
ATTN: AFRDSP

Deputy Chief of Staff
Ops & Plans
ATTN: AFXOKCD
ATTN: AFXOKT
ATTN: AFXOKS

Electronic Systems Div
ATTN: SCT-2, J. Clark

Electronic Systems Div
ATTN: OCT-4, J. Deas

Electronic Systems Div
ATTN: SCS-1E
ATTN: SCS-2, LTC Vinkels

Foreign Technology Div
ATTN: NIIS Library
ATTN: TQTD, B. Ballard

Rome Air Development Ctr
ATTN: OCS, V. Coyne
ATTN: TSLD

Rome Air Development Ctr
ATTN: EEP, J. Rasmussen

Space Div
ATTN: YGJB, W. Mercer

Space Div
ATTN: YKM, Maj Alexander
ATTN: YKM, Capt Norton

DEPARTMENT OF THE AIR FORCE (Continued)

Strategic Air Command
ATTN: NRT
ATTN: DCX
ATTN: XPFS
ATTN: ADWATE, B. Bauer
ATTN: DCXT, T. Jorgensen
ATTN: XPFS

OTHER GOVERNMENT AGENCIES

Central Intelligence Agency
ATTN: OSWR/SSD for K Feuerpfetl
ATTN: OSWR/NED

Department of Commerce
National Bureau of Standards
ATTN: Sec Ofc for R. Moore

Department of Commerce
National Oceanic & Atmospheric Admin
ATTN: R. Grubb

Institute for Telecom Sciences
ATTN: L. Berry
ATTN: A. Jean
ATTN: W. Utlaut

NATO

NATO School (SHAPE)
ATTN: US Docs Ofcr

DEPARTMENT OF ENERGY CONTRACTORS

EG&G, Inc
ATTN: D. Wright
ATTN: J. Colvin

University of California
Lawrence Livermore National Lab
ATTN: Tech Info Dept Library
ATTN: L-389, R. Ott
ATTN: L-31, R. Hager

Los Alamos National Lab
ATTN: MS 664, J. Zinn
ATTN: P. Keaton
ATTN: D. Simons
ATTN: MS 670, J. Hopkins
ATTN: T. Kunkle, ESS-5
ATTN: R. Jeffries
ATTN: J. Wolcott
ATTN: C. Westervelt

Sandia National Lab
ATTN: D. Dahlgren
ATTN: Tech Library 3141
ATTN: Space Proj Div
ATTN: D. Thornbrough
ATTN: ORG 1250, W. Brown
ATTN: ORG 4231, T. Wright

Sandia National Labs, Livermore
ATTN: T. Cook
ATTN: B. Murphey

DEPARTMENT OF DEFENSE CONTRACTORS

Aerospace Corp
ATTN: V. Josephson
ATTN: T. Salmi
ATTN: R. Slaughter
ATTN: I. Garfunkel
ATTN: J. Straus
ATTN: D. Olsen

BDM Corp
ATTN: L. Jacobs
ATTN: T. Neighbors

Berkeley Research Assoc, Inc
ATTN: J. Workman
ATTN: S. Brecht
ATTN: C. Prettie

Boeing Aerospace Co
ATTN: MS/87-63, D. Clauson

Boeing Co
ATTN: G. Hall
ATTN: S. Tashird

BR Communications
ATTN: J. McLaughlin

Charles Stark Draper Lab, Inc
ATTN: A. Tetewski
ATTN: J. Gilmore
ATTN: D. Cox

Computer Sciences Corp
ATTN: F. Eisenbarth

Cornell University
ATTN: D. Farley, Jr
ATTN: M. Kelly

Electrospace Systems, Inc
ATTN: H. Logston
ATTN: P. Phillips

EOS Technologies, Inc
ATTN: B. Gabbard

ESL, Inc
ATTN: R. Ibaraki
ATTN: R. Heckman
ATTN: J. Lehman
ATTN: E. Tsui
ATTN: J. Marshall

General Research Corp
ATTN: B. Bennett

Geo-Centers, Inc
ATTN: E. Marram

Harris Corp
ATTN: E. Knick

Honeywell, Inc
ATTN: G. Collyer, Avionics Dept
ATTN: G. Terry, Avionics Dept

DEPARTMENT OF DEFENSE CONTRACTORS (Continued)

Horizons Technology, Inc
ATTN: R. Kruger

HSS, Inc
ATTN: D. Hansen

IBM Corp
ATTN: H. Ulander
ATTN: M. Chuler

Institute for Defense Analyses
ATTN: E. Bauer
ATTN: H. Wolfhard
ATTN: J. Aein
ATTN: H. Gates

JAYCOR
ATTN: J. Sperling

JAYCOR
ATTN: J. Doncarlos

Johns Hopkins University
ATTN: J. Newland
ATTN: T. Evans
ATTN: P. Komiske
ATTN: J. Phillips

Kaman Sciences Corp
ATTN: T. Stephens

Kaman Tempo
ATTN: B. Gambill
ATTN: DASIAC
ATTN: J. Devore
ATTN: W. Knapp
ATTN: K. Schwartz
ATTN: W. McNamara

Litton Systems, Inc
ATTN: B. Zimmer

Lockheed Missiles & Space Co, Inc
ATTN: R. Sears
ATTN: J. Kumer

Lockheed Missiles & Space Co, Inc
ATTN: C. Old
ATTN: D. Churchill
ATTN: Dept 60-12

MIT Lincoln Lab
ATTN: D. Towle

Magnavox Govt & Indus Electronics Co
ATTN: G. White

Martin Marietta Corp
ATTN: R. Heffner

McDonnell Douglas Corp
ATTN: W. Olson
ATTN: Tech Library Svcs
ATTN: R. Halprin
ATTN: H. Spitzer

DEPARTMENT OF DEFENSE CONTRACTORS (Continued)

Mission Research Corp
ATTN: R. Hendrick
ATTN: C. Lauer
ATTN: R. Kilb
ATTN: F. Fajen
ATTN: R. Bigoni
ATTN: G. McCartor
ATTN: F. Guigliano
6 cy ATTN: Tech Library, Doc Con
ATTN: S. Gutsche
ATTN: R. Bogusch
4 cy ATTN: W. White

Mitre Corp
ATTN: A. Kymmel
ATTN: B. Adams
ATTN: G. Harding
ATTN: C. Callahan
ATTN: MS J104, M. Dresp

Mitre Corp
ATTN: W. Hall
ATTN: M. Horrocks
ATTN: W. Foster
ATTN: J. Wheeler

Pacific-Sierra Research Corp
ATTN: F. Thomas
ATTN: E. Field, Jr
ATTN: H. Brode

Pennsylvania State University
ATTN: Ionospheric Res Lab

Photometrics, Inc
ATTN: I. Kofsky

Physical Dynamics, Inc
ATTN: E. Fremouw

R&D Associates
ATTN: R. Lelevier
ATTN: C. Greifinger
ATTN: R. Turco
ATTN: H. Ory
ATTN: W. Wright
ATTN: M. Gantsweg
ATTN: W. Karzas
ATTN: F. Gilmore

R&D Associates
ATTN: B. Yoon

Rand Corp
ATTN: E. Bedrozian
ATTN: C. Crain

Riverside Research Institute
ATTN: V. Trapani

Rockwell International Corp
ATTN: R. Buckner

Rockwell International Corp
ATTN: S. Quilici

DEPARTMENT OF DEFENSE CONTRACTORS (Continued)

Santa Fe Corp
ATTN: D. Paolucci

Science Applications, Inc
ATTN: L. Linson
ATTN: C. Smith
ATTN: E. Straker
ATTN: D. Hamlin

Science Applications, Inc
ATTN: J. Cockayne

SRI International
ATTN: G. Price
ATTN: R. Tsunoda
ATTN: J. Vickrey
ATTN: W. Chesnut
ATTN: R. Livingston
ATTN: D. Neilson
ATTN: J. Petrickes
ATTN: D. McDaniels
ATTN: R. Leadabrand
ATTN: M. Baron
ATTN: A. Burns
ATTN: C. Rino
ATTN: G. Smith
ATTN: V. Gonzales
ATTN: W. Jaye

DEPARTMENT OF DEFENSE CONTRACTORS (Continued)

Stewart Radiance Lab
ATTN: J. Ulwich

Sylvania Systems Group
ATTN: R. Steinhoff

Technology International Corp
ATTN: W. Boquist

Tri-Com, Inc
ATTN: D. Murray

TRW Electronics & Defense Sector
ATTN: G. Kirchner
ATTN: R. Plebuch
ATTN: D. Dee

Utah State University
ATTN: A. Steed
ATTN: D. Burt
ATTN: L. Jensen, Elec Eng Dept
ATTN: K. Baker, Dir Atmos & Space Sci

Visidyne, Inc
ATTN: C. Humphrey
ATTN: O. Shepard
ATTN: W. Reidy
ATTN: J. Carpenter

END

FILMED

9-83

DTIC